THE ACUTE CELLULAR AND BEHAVIORAL RESPONSE TO MECHANICAL NEURONAL INJURY

A Dissertation
Presented to
The Academic Faculty

by

Marcus Christian Lessing

In Partial Fulfillment
of the Requirements for the Degree
Doctor of Philosophy in the
School of Biomedical Engineering

Georgia Institute of Technology
December 2008

THE ACUTE CELLULAR AND BEHAVIORAL RESPONSE TO MECHANICAL NEURONAL INJURY

Approved by:

Dr. Michelle C. LaPlaca, Advisor
School of Biomedical Engineering
Georgia Institute of Technology

Dr. Suzanne G. Eskin
School of Biomedical Engineering
Georgia Institute of Technology

Dr. Andrés J. García
School of Mechanical Engineering
Georgia Institute of Technology

Dr. Marc E. Levenston
Department of Mechanical Engineering
Stanford University

Dr. Edward H. Pettus
Department of Cell Biology
Emory University School of Medicine

Date Approved: November 17, 2008

Mark, Margaret, and Collin deserve all my gratitude and respect.

ACKNOWLEDGEMENTS

I would like to thank my labmates, classmates, and close friends for helping me through the challenges of the past several years and for bringing joy to this experience. I would also like to thank the individuals at Johnson & Johnson Regenerative Therapeutics that welcomed me into their team as an intern in 2006. Finally I thank my colleagues and friends at Georgia Bio that that took a sincere interest in my personal and professional growth.

Regarding the research presented here, Amir Makhmalbaf, Maggie Wolfson, Sarah Stabenfeldt and Chris Wilson provided technical support for Chapter 2, while I worked closely with Kacy Cullen to design, implement, and interpret the study. Deanna Felice provided assistance and Crystal Simon and Gustavo Prado offered technical support and advice for Chapter 3. Liying Zhang provided advice and preliminary FEM data for Chapter 4. Crystal Simon and Shan Sharif were indispensible with their help designing, implementing, and interpreting the study presented in Chapter 5. Through this entire process, Michelle LaPlaca has challenged me to become a better scientist.

TABLE OF CONTENTS

LIST OF TABLES

LIST OF FIGURES

SUMMARY

Traumatic brain injury (TBI) is a major health and socioeconomic concern in the United States and across the globe. Experimental models of TBI are used to study the mechanisms underlying cell dysfunction and death that result from injury, the functional deficits that result from injury, and the potential of various therapies to treat injury. This thesis explores the fundamental mechanical damage associated with brain trauma, investigating the effects of mechanical deformation on neurons at the molecular, cellular, tissue, and animal levels. First, a novel hydrogel system was developed to support 3-D neuronal cultures, and the cultures were studied in an in vitro model of neuronal injury. The dependence of cell viability on hydrogel stiffness and extracellular matrix ligand concentration revealed a role for molecular interactions in the cellular response to injury. Subsequently, in a rat model of TBI neuronal plasma membrane damage was observed coincidentally with cell death within the hippocampus; however not all permeable cells died, suggesting a complex role for plasma membrane damage in neuronal degeneration. The spatial profile of permeable cells in the hippocampus reveals further heterogeneity of neuronal plasma membrane damage, with populations of cells in certain hippocampal subregions exhibiting an increased vulnerability to plasma membrane damage. These observations support recent finite element model predictions of strains in the brain during injury. Finally a system for measuring locomotor disturbances is used for the first time following brain injury. Continued investigation of how neurons deform and fail mechanically will contribute to the understanding of the pathophysiology of brain injury and may help identify potential therapeutic targets.

CHAPTER 1

INTRODUCTION

Traumatic brain injury (TBI) is a major health and socioeconomic concern in the United States and across the globe. Experimental models of TBI are used to study the mechanisms underlying cell dysfunction and death that result from injury, the functional deficits that result from injury, and the potential of various therapies to treat injury. This thesis explores the fundamental mechanical damage associated with brain trauma. A novel cell culture scaffold is established to elucidate the contributions of individual extracellular matrix (ECM) components to the neural response to mechanical trauma *in vitro*. In an *in vivo* model of brain injury, the mechanical trauma causes cellular plasma membrane damage and alterations in locomotor function. Investigation of TBI at the molecular, cellular, animal, and tissue levels will lead to a better understanding of the role of mechanical forces in the pathophysiology of injury and may help identify therapeutic targets.

1.1 Traumatic brain injury

The brain is protected from exposure to external mechanical forces by the skull, and thus cells of the brain do not experience significant deformations under normal physiological conditions. TBI occurs when the brain is exposed to excessive mechanical forces. While causing deformations on the macroscopic level, these mechanical forces can also result in complex loading regimes at the microscopic level and cause cellular

damage. These damaging events may ultimately lead to cellular dysfunction and death, but the mechanisms involved are poorly understood.

Traumatic brain injury is a leading cause of morbidity and mortality in the United States. Nearly 1.5 million Americans sustain a TBI annually, requiring more than 1 million emergency room visits and 235,000 hospitalizations. About 50,000 deaths result annually from TBI. Of those individuals who survive a TBI, it is believed that 80,000 to 90,000 experience permanent disabilities including: memory impairment; attention and mood disorders; impaired problem solving and reasoning skills; and physical disabilities affecting sight, hearing, and coordinated movement. Motor vehicle accidents are the leading cause of TBI related hospitalizations, while falls are responsible for the majority of TBI in young children and the elderly (for reviews, see (Thurman et al. 1999; Langlois et al. 2006)).

1.2 Experimental models of TBI

Experimental models have been developed to study brain injury *in vitro* and *in vivo* (for reviews, see (Gennarelli 1994; Morrison et al. 1998)). Each of these models has its own limitations that must be considered when designing studies and interpreting results. While the diversity of models available provides multiple options, the optimization of different models for studying particular types of deformations or different outcome measures can make the comparison of results between models and labs difficult. Thus model selection must be approached carefully.

1.2.1 *In vitro* models of TBI

In vitro models of neural injury allow investigation of brain injury mechanisms, potentially reducing the need for animal studies. The simplicity of these models allows the direct manipulation of many experimental parameters including cell types, extracellular matrix properties, media formulations, and the mechanics of the injury. These systems also enable direct perturbation of the pathways involved in the injury response and high throughput testing of treatments. Several *in vitro* injury models are available in our lab.

1.2.1.1 Two-dimensional stretch

A two-dimensional (2-D) equibiaxial stretch device was developed to injure neurons cultured on elastic membranes (Geddes and Cargill 2001). Stretch injury caused non-specific calcium influx, energy depletion, and cell death in neurons (Geddes et al. 2003b). A second study with this device showed that stretch injury induced transient plasma membrane damage, the extent of which depended on both strain rate and magnitude (Geddes et al. 2003a). An advantage of this system is that the equibiaxial mechanical loading profile provides the same strain at all points on the culture surface, whereas for other stretch injury systems local strains depend on position on the deforming elastic surface. However the planar orientation of cells and stretch deformation limits the types of forces cells are exposed to.

1.2.1.2 Two-dimensional shear

A second 2-D injury device in the lab is an adaptation of a fluid shear induced injury device developed by LaPlaca et al. (LaPlaca et al. 1997). The current device

consists of a cone and plate setup that imparts a homogeneous shear deformation to neurons cultured on a rigid substrate. An advantage of this device is that cells can be cultured on any rigid substrate, including microelectrode arrays that allow for electrophysiological measurements before, during, and after injury. While plasma membrane disruptions and perturbations in neuronal electrophysiology were detected after injury in this system (Prado et al. 2005), cell death is difficult to induce with this injury model.

1.2.1.3 Three-dimensional shear

The third injury device imparts a shear deformation to three-dimensional (3-D) neural cultures (LaPlaca et al. 2005). This deformation provides a complex loading regime where the types of forces (compression, tension, and shear) experienced at the cellular level is primarily determined by the orientation of the cell within the culture at the time of deformation (Cullen and LaPlaca 2006). This heterogeneous loading profile is likely more similar to the complex deformation profiles cells in the brain experience *in vivo*. While 2-D cultures have interactions with the extracellular matrix (ECM) only on one surface, interactions in 3-D cultures are also more similar to the *in vivo* situation. Consideration of the organization of cell-ECM and cell-cell interactions is critical when studying the effects of cell deformation, as the interactions determine how forces are transferred to cells and initiate the biochemical events that influence cell outcome. These connections between the cell and its surroundings can also be sites of stress concentrations that can lead to failure of the mechanical integrity of the cell. This 3-D model was chosen for the *in vitro* component of this work because of its robustness and increased relevance to *in vivo* injury mechanics compared to other *in vitro* models.

1.2.2 *In vivo* models of TBI

In contrast to *in vitro* models, *in vivo* models of brain injury are needed for their complexity (Cernak 2005). Despite attempts to do so, the complex structural organization of brain cannot be duplicated *in vitro*. The brain is made up of more than just neurons: astrocytes, oligodendrocytes, and microglia also reside in the brain, are susceptible to injury, and play a role in the injury response. Additionally the vasculature of the brain is also vulnerable to injury and when injured can introduce systemic factors from the blood into the otherwise protected environment of the brain. The primary insult causes the primary injury, which includes mechanical damage to cells and blood vessels. The extent of this injury is primarily determined by the biomechanics of the mechanical insult, not only its magnitude and location but also the type of loading (Gennarelli 1994). This primary injury can then act as a secondary insult that leads to a secondary injury (ischemia, edema, excitotoxicity, and free radical production) hours or days after the initial mechanical insult. The functional effects of this tissue damage and cell death can be studied by training the animals to perform tasks that allow measurement of changes in cognitive and motor function (Fujimoto et al. 2004).

1.2.2.1 Impact acceleration and weight drop models

The impact acceleration and weight drop models of TBI involves dropping a weight from a known height onto a metal disc adhered to the skull to produce a closed-head injury (Marmarou et al. 1994). This model generally results in widespread injury throughout the brain including diffuse axonal injury (Foda and Marmarou 1994); however leaving the head unconstrained during injury introduces variability into the injury.

Fluid percussion models of brain injury deliver a fluid pressure pulse through an opening in the skull while leaving the dura intact (Dixon et al. 1987). This injury causes some cortical damage and results in damage to the deeper structures including the brainstem. The biomechanics of the fluid percussion injury are difficult to model, however (Dixon et al. 1991).

1.2.2.2 Controlled cortical impact

Controlled cortical impact (CCI), also called a cortical contusion injury, models acceleration loading of the brain by delivering a rigid impact to the outer layer of the brain called the cortex (Dixon et al. 1991). A craniectomy is performed to remove the skull at the injury site, allowing the experimenter impart a focal injury to a prescribed location on the surface of the brain. While this injury regime causes a necrotic cavity to form in the cortex at the injury site, cell damage is also observed in the cavity penumbra, contrecoup to the injury site, and in other structures of the brain like the hippocampus. These lesions are primarily located in the ipsilateral hemisphere (the side of the brain receiving the injury) but are sometimes evident in the contralateral hemisphere (the opposite side of the brain) as well. CCI is the preferred injury model for the studies in this thesis because its biomechanics are well defined with controllable injury parameters including injury location, size (diameter of impactor tip), depth, velocity, and dwell time.

The positioning of the craniectomy tangent to the sagittal and coronal sutures allows the CCI injury to be delivered directly to the left frontoparietal cortex (Figure 1.1) (Paxinos and Watson 1998), the region of the brain responsible for sensorimotor function. The structure of the brain directly beneath the frontoparietal cortex is the hippocampus, and it is bordered on its anterior, posterior, dorsal, and lateral surfaces by the cortex and

corpus callosum and on its ventral and medial surfaces by the thalamus (Figure 1.1). The hippocampus primarily controls memory and spatial awareness, and it is divided into several subregions including CA1, CA2, CA3, and the dentate gyrus (Figure 1.2).

1.3 Measuring outcomes in experimental TBI

The variety of experimental injury models makes direct comparisons of injury between models difficult. However an emphasis has been placed emphasis has been placed on identifying outcome measures that can be directly compared. Among these are plasma membrane damage, cell death, and alterations in behavior.

1.3.1 Plasma membrane damage

The idea that mechanical deformation can damage the plasma membrane is relatively straight forward. A neuron is morphologically complex, with axons and dendrites and sometimes a particular orientation. If that cell is stretched or sheared by a small amount and slowly enough, it can resist or adapt to the deformation (Smith et al. 1999). However if the magnitude or rate of deformation is increased, the cell may not be able to withstand the deformation and will experience structural failure. Failure of the plasma membrane, which forms a protective between the intracellular and extracellular domains, may have dire implications for cell survival following injury (Farkas and Povlishock 2007). Molecules that reseal a damaged plasma membrane, such as polyethylene glycol and Poloxamer 188, have been shown to reduce production of reactive oxygen species, reduce cell loss, improve motor function, and reduce activation of pro-apoptotic kinases in experimental models of traumatic brain and spinal cord injury

(Shi and Borgens 1999; Shi and Borgens 2000; Luo et al. 2002; Koob et al. 2005; Serbest et al. 2005; Serbest et al. 2006; Koob et al. 2008).

1.3.1.1 Mechanisms of pore formation

While it is known that cellular plasma membrane damage occurs during TBI, it remains unclear exactly how and where on the membrane this damage happens. Traumatic axonal injury occurs when the mechanical force of the injury tears the axonal projections of neurons in the brain, resulting in plasma membrane and cytoskeletal damage that is evident as axonal retraction balls that precede Wallerian degeneration (Pettus et al. 1994; Pettus and Povlishock 1996; Buki and Povlishock 2006; Kelley et al. 2006). This damage could occur at any point along the length of the axon or at morphological features such as axonal branches or the hillock. Plasma membrane damage could also presumably occur at the soma or along dendrites.

The plasma membrane itself is a heterogeneous structure whose composition, which supports its structure and function, may predispose it to mechanical damage. The bulk of its composition is the phospholipid bilayer, two layers of amphipathic phospholipids arranged with their hydrophilic heads facing the aqueous intracellular and extracellular domains while the hydrophobic tails associate together inside the membrane away from the surrounding aqueous environment (Alberts 1994). The selectively permeable bilayer allows small uncharged or lipid soluble molecules to freely diffuse across the membrane, while other molecules must travel through pores or channels to cross the membrane. Proteins serve as these channels and the receptors that allow communication between the extracellular and intracellular environments and as such play a prominent role in the function of the plasma membrane. Transmembrane proteins span

the thickness of the plasma membrane while other proteins may only be associated with either the intracellular or extracellular faces of the plasma membrane. The hydrophobic domains of these proteins associate with the hydrophobic tail groups of the phospholipid bilayer and anchor the proteins to the plasma membrane, and some of these proteins also associate with the cytoskeleton. Other families of molecules in the plasma membrane include cholesterols, steroids, and carbohydrates (including glycoproteins and glycolipids). The plasma membrane and its components are held together by non-covalent hydrophobic interactions, and the fluid mosaic model of the plasma membrane suggests these molecules can move relatively freely within the membrane (Singer and Nicolson 1972). However with thermodynamics rather than covalent interactions being the driving force for plasma membrane integrity, a mechanically loaded plasma membrane may fail at the interface between its components; an example of this interface is where the hydrophobic domain of a transmembrane receptor passes through the hydrophobic portion of the plasma membrane.

Lipid raft microdomains, which are cholesterol rich components of the plasma membrane (Brown and London 1998), may also play a role in determining how mechanical forces are transferred to neurons during injury. The fluidity of these lipid raft microdomains is different from the surrounding membrane: it lies somewhere between the fluidity of the purely fluid-mosaic model bilayer and that of a membrane in its gel state (Brown and London 1998; Simons and Toomre 2000). The presence of cholesterol may contribute to this reduced fluidity and is known to increase membrane stiffness (Needham and Nunn 1990). Clustering of separate rafts is also known to occur (Simons and Toomre 2000), potentially giving rise to local inhomogeneities in the plasma

membrane. Finally, lipid rafts are not necessarily free-floating structures but are rather anchored to the actin cytoskeleton (Itoh et al. 2002; Hering et al. 2003). In neurons it was first believed that lipid rafts were concentrated at axons (Simons and Ikonen 1997), but recent studies have shown that lipid rafts exist in the post-synaptic domains of dendrites as well (Hering et al. 2003). The biomechanical role of lipid rafts in brain injury has not been discussed in the literature, possibly because technical and biophysical limitations have made the identification and isolation of lipid rafts difficult (Simons and Toomre 2000). However given this evidence it is conceivable that lipid rafts play a role in force transfer to neurons and plasma membrane damage during mechanical deformation.

Studies by McNeil and colleagues suggest that while thermodynamics are responsible for the integrity of the unperturbed plasma membrane, thermodynamic stability does not cause the membrane to spontaneously reseal. In fact they have shown that repair of transient pores formed by a traumatic insult is an active molecular process, requiring energy, calcium-activated enzymes, and vesicle recruitment and fusion (McNeil et al. 2003; Miyake and McNeil 2003; McNeil and Kirchhausen 2005; McNeil et al. 2006; Mellgren et al. 2007).

1.3.1.2 Dye exclusion assay

Dye exclusion assays are commonly used to identify cells with plasma membrane breaches. When a dye is introduced into the extracellular space, it is excluded from the intracellular space by the plasma membrane; however if the plasma membrane damage results in holes forming, the membrane impermeable dye can flood the intracellular space and freely diffuse along its concentration gradient (Figure 1.3). These permeability markers can be dyes or non-dye molecules (Table 1.1). Dyes are generally identified

directly using microscopy, while non-dyes such as horseradish peroxidase (HRP) and lactate dehydrogenase (LDH) require extra processing. The HRP enzyme is identified within the cell by the addition of a chromogenic substrate or by immunohistochemistry. The LDH method is more accurately a dye inclusion assay. LDH is a naturally produced cytosolic enzyme that is released into the extracellular space after plasma membrane damage, where it can be detected by its enzymatic activity.

Plasma membrane damage has been observed using the dye exclusion method in *in vitro* and *in vivo* models of brain injury. A summary of these studies is provided in Table 1.2. A recent study showed that plasma membrane damage can be transient, permanent, or delayed (Farkas et al. 2006), and these three types of permeability are illustrated in Figure 1.4. Delivery of the permeability marker before injury captures cells that are damaged at the moment of injury. Delivery of the permeability marker after injury, however, may identify permeable cells that remain damaged from moment of injury as well as cells that have a delayed onset of permeability. The dynamic nature of plasma membrane damage in the first 24 hours following injury is revealed in Table 1.3.

The size of a dye may affect its ability to cross a damaged membrane, shown previously *in vitro* in a study where the extent of dye uptake depended not only on the mechanics of the injury (strain magnitude and rate) but also the size of the permeability marker (Geddes et al. 2003a). Furthermore it was shown that injured cells were permeable to smallest dyes for at least five minutes post injury while dextran-based dyes 10 kDa or larger could only enter cells at the moment of the mechanical insult. Another study suggests the charge of the dye may also affect its ability to enter an injured cell, with neutral or uncharged dyes entering the cell more easily than a negatively charged

dye (Eddleman et al. 1998). The conjugation method used by Molecular Probes to attach fluorescent labels to dextrans generally yields anionic markers (the Texas Red dextran conjugates are an exception and have a neutral charge) (Invitrogen 2006). Whereas these dyes can be combined with cell culture media and introduced directly to cells *in vitro*, the size and charge of a permeability marker may also affect its ability to diffuse throughout the brain tissue *in vivo*. Thus when selecting a permeability marker for this work we considered both permeability marker size and charge, deciding the properties of the 3 kDa anionic dextran-tetramethylrhodamine were best suited for our injury model and allowed comparison to previous studies of plasma membrane damage.

1.3.2 Cell dysfunction and death

Neuronal dysfunction following traumatic brain injury is evident in multiple cellular processes. Cell signaling pathways, especially ones regulating cell survival like the Bcl-2 genes, the MAP kinases, and the caspase family of proteases, also change their activation states following injury (Raghupathi 2004). Brain injury induced plasma membrane damage also disrupts ion homeostasis, allowing the charged molecules that drive action potentials (sodium, potassium, and calcium) to diffuse freely into the cell rather than through channels in the normal tightly regulated fashion. This causes alterations in the electrochemical balance in neurons, leading to functional changes within the brain without causing cell death (Cohen et al. 2007). The mechanical forces of the injury itself can also cause axons to rupture and disconnect from their synaptic targets (Singleton et al. 2002; Stone et al. 2004; Buki and Povlishock 2006; Kelley et al. 2006).

Altered global cerebral metabolism is evident following clinical and experimental TBI (Hillered et al. 2006; Marklund et al. 2006) and may be due to several cellular,

subcellular, and molecular factors. Mitochondrial damage is observed in neurons after brain injury (Pettus et al. 1994; Lifshitz et al. 2003), reducing cellular capacity for energy production. Ischemia from reduced blood flow to the head reduces cerebral oxygen levels and also leads to energy depletion (White et al. 2000). Following ischemia, reperfusion of the brain introduces reactive oxygen species that cause oxidative damage to the lipids, proteins, and nucleic acids of neurons (Lewen et al. 2000; White et al. 2000).

Increased release of neurotransmitters results in excitotoxicity within the brain following injury, resulting in abnormal NMDA receptor activation and increased intracellular calcium (Weber 2004). Extracellular calcium can also enter neurons through mechanically induced holes or tears in the plasma membrane (LaPlaca and Thibault 1998; Geddes and Cargill 2001). This non-specific influx of calcium following plasma membrane damage raises intracellular calcium levels and activates calcium-dependent proteases and endonucleases associated with neuronal cell death. An example is calpain which is activated by free cytoplasmic calcium to digest spectrin in the neuron cytoskeleton during apoptosis.

In fact, many of the events described in the previous paragraphs can be triggered by plasma membrane damage and lead to cell dysfunction or even cell death (Figure 1.5). Thus plasma membrane damage may play an important role in cell death via necrosis and apoptosis, both of which are observed in the brain following a traumatic injury (Colicos and Dash 1996). Apoptosis, or programmed cell death, is an active process that is associated with plasma membrane damage as described above. Necrosis in neurons is identified by plasma membrane rupture and cell lysis; several standard viability assays

(including ethidium homodimer and propidium iodide uptake or lactate dehydrogenase release) identify dead cells by their loss of plasma membrane integrity.

1.3.3 Behavioral outcomes

Physical manifestations of brain injury can include altered neurological cognitive and motor function (for a thorough review, see (Fujimoto et al. 2004)). Plasma membrane damage can disrupt electrophysiology on the cellular level and can lead to reduced or increased excitability of neurons in critical pathways in the brain (Cohen et al. 2007). Similarly, significant cell death in these neuronal pathways can permanently alter the connectivity of the network. If these disturbances occur in critical pathways, the alterations in cognitive or motor function can be measured. Gait-related motor impairments have been observed using open field locomotor tasks that measure exploratory behavior and general movement (Koob et al. 2006) and footprint analysis of gait parameters like stride width and length (Gonzalez-Pina et al. 2005). Motor coordination and balance can also be measured using the rotarod (Hamm et al. 1994), beam walk (Dixon et al. 1999), and grid walk tasks (Baskin et al. 2003). Deficits in memory and learning can be measured using a cognitive task like the Morris water maze (Dixon et al. 1999).

1.4 Thesis overview

Current *in vitro* neuronal culture systems and injury models allow limited control over the mechanical and molecular properties of the culture scaffold. These limitations are addressed in Chapter 2 with a novel hydrogel system with controllable stiffness and extracellular matrix presentation that was developed to support 3-D neuronal cultures and

in vitro injury. The dependence of the cell viability on extracellular matrix ligand concentration in this study reveals a role for receptor-ligand interactions in the cellular response to injury.

Plasma membrane damage may contribute to cell dysfunction and death following brain injury, and the objective of Chapter 3 is to investigate hippocampal cell plasma membrane damage in a rat model of TBI. After injury most degenerating neurons in the hippocampus show evidence of plasma membrane damage, but it is shown here that only a subset of neurons with plasma membrane damage is degenerating. Additionally a tissue-level finite element model of brain injury predicts peak strains in the subregions where the greatest level of plasma membrane damage is observed.

Cognitive and locomotor behavioral changes are observed after injury, and behavioral tasks can be used to measure these functional deficits at the animal level in experimental injury models. Many locomotor tasks qualitatively assess gross motor function but do not allow for direct measurement of individual gait parameters. A new locomotor task called the CatWalk system, however, is capable of these measurements, and it is described in Chapter 4 to characterize locomotor dysfunction for the first time following traumatic brain injury.

Finally the specific contributions of this work to the existing literature and implications for therapy are discussed in Chapter 5. The overall goal of this thesis is to study traumatic brain injury by investigating the effects of mechanical deformation on neurons at the molecular, cellular, tissue, and animal levels. This work is significant because improved understanding of how neurons deform and fail mechanically will lead to new opportunities for therapeutic intervention.

Table 1.1: List of permeability markers

Abbreviation	Marker	Molecular weight
CBF	Carboxyfluorescein	380
EB	Ethidium bromide	394
LY	Lucifer yellow	457
A488	Alexa 488 hydrazide	570
Calcein	Calcein	623
PI	Propidium iodide	668
YOYO-1	YOYO-1	1,323
D3	Dextran	3,000
D10	Dextran	10,000
D40	Dextran	40,000
HRP	Horseradish peroxidase	40,000
D70	Dextran	70,000
LDH	Lactate dehydrogenase	140,000
D150	Dextran	150,000
D464	Dextran	464,000

Table 1.2: Plasma membrane disruption model systems

Model	Permeability marker	Marker delivery	Reference
In vitro			
Biaxial shear	CBF	B/A	(Geddes-Klein et al. 2006)
Equibiaxial shear	CBF, Calcein, D10, D40, D70, D150	B/A	(Geddes et al. 2003a)
Fluid shear	Calcein	B/A	(Prado et al. 2005)
Fluid shear	D464	B	(Prado 2004)
Fluid shear	LDH	-	(LaPlaca et al. 1997) (LaPlaca and Thibault 1997) (Serbest et al. 2005)
White matter strip compression	EB, HRP, LDH	A/-	(Luo et al. 2002)
White matter strip compression	HRP	A	(Shi and Borgens 2000)
White matter strip transection	HRP	A	(Shi and Pryor 2000)
White matter strip transection	HRP	A	(Shi and Borgens 2000)
White matter strip transection	HRP	A	(Shi et al. 2000)
White matter strip stretch	HRP	A	(Shi and Pryor 2002)
Uniaxial stretch	A488	B	(Smith et al. 1999)
In vivo: brain injury models			
Controlled cortical impact (mouse)	PI, YOYO-1	B/A	(Whalen et al. 2007)
Controlled cortical impact (rat)	LY	B	(Prado 2004)
Controlled cortical impact (rat)	D3	B	(Lessing and LaPlaca 2008)
Fluid percussion (cat)	HRP	B	(Pettus et al. 1994) (Pettus and Povlishock 1996) (Okonkwo et al. 1998)
Fluid percussion (rat)	D10, D40, HRP	B	(Singleton and Povlishock 2004)
Fluid percussion (rat)	D10	B	(Kelley et al. 2006)
Impact acceleration (rat)	EB, HRP	A	(Koob et al. 2005)
Impact acceleration (rat)	D3, D10, D40	B	(Stone et al. 2004)
Impact acceleration (rat)	D10	B/A	(Farkas et al. 2006)

B: marker delivered before injury
A: marker delivered after injury
- : intracellular molecule release served as marker

Table 1.3: Time course of plasma membrane damage observations

Permeability marker	Time elapsed before permeability observation				
	$0 < t \leq 5$ min	$5 < t \leq 15$ min	$15 < t \leq 60$ min	$1 < t \leq 6$ hr	$6 < t \leq 24$ hr	24 hr < t
CBF	*Geddes et al. 2003*	*Geddes-Klein et al. 2006*				
EB	*Luo et al. 2002*	*Luo et al. 2002*	*Luo et al. 2002*		Koob et al. 2005	
LY		Prado 2004				
A488		*Smith et al. 1999*				
Calcein	*Geddes et al. 2003* *Prado et al. 2005*	*Prado et al. 2005*				
PI	Whalen et al. 2007		Whalen et al. 2007	Whalen et al. 2007	Whalen et al. 2007	Whalen et al. 2007
YOYO-1			Whalen et al. 2007		Whalen et al. 2007	
D3	Stone et al. 2004	Lessing et al. 2008		Stone et al. 2004		Lessing et al. 2008
D10	*Geddes et al. 2003* Singleton et al. 2004 Stone et al. 2004	Kelley et al. 2006	Kelley et al. 2006	Farkas et al. 2006 Kelley et al. 2006 Singleton et al. 2004 Stone et al. 2004	Farkas et al. 2006 Singleton et al. 2004	
D40	*Geddes et al. 2003* Stone et al. 2004		Stone et al. 2004	Singleton et al. 2004 Stone et al. 2004	Singleton et al. 2004	
HRP	*Shi et al. 2000a* *Shi et al. 2000b* *Shi et al. 2002* *Luo et al. 2002* Pettus et al. 1994 Pettus et al. 1996	*Luo et al. 2002* Okonkwo et al. 1998 Pettus et al. 1994 Pettus et al. 1996	*Luo et al. 2002* *Shi et al. 2000a* *Shi et al. 2000c* Pettus et al. 1994 Pettus et al. 1996	*Shi et al. 2000b* Okonkwo et al. 1998 Pettus et al. 1994 Pettus et al. 1996 Singleton et al. 2004	Koob et al. 2005 Singleton et al. 2004	
D70	*Geddes et al. 2003*					
LDH	*LaPlaca et al. 1997a* *LaPlaca et al. 1997b* *Serbest et al. 2005*	*Luo et al. 2002* *Serbest et al. 2005*	*LaPlaca et al. 1997b* *Luo et al. 2002*	*LaPlaca et al. 1997b*	*LaPlaca et al. 1997a* *LaPlaca et al. 1997b*	
D150	*Geddes et al. 2003*					
D464	*Prado 2004*					

in vitro study; in vivo study

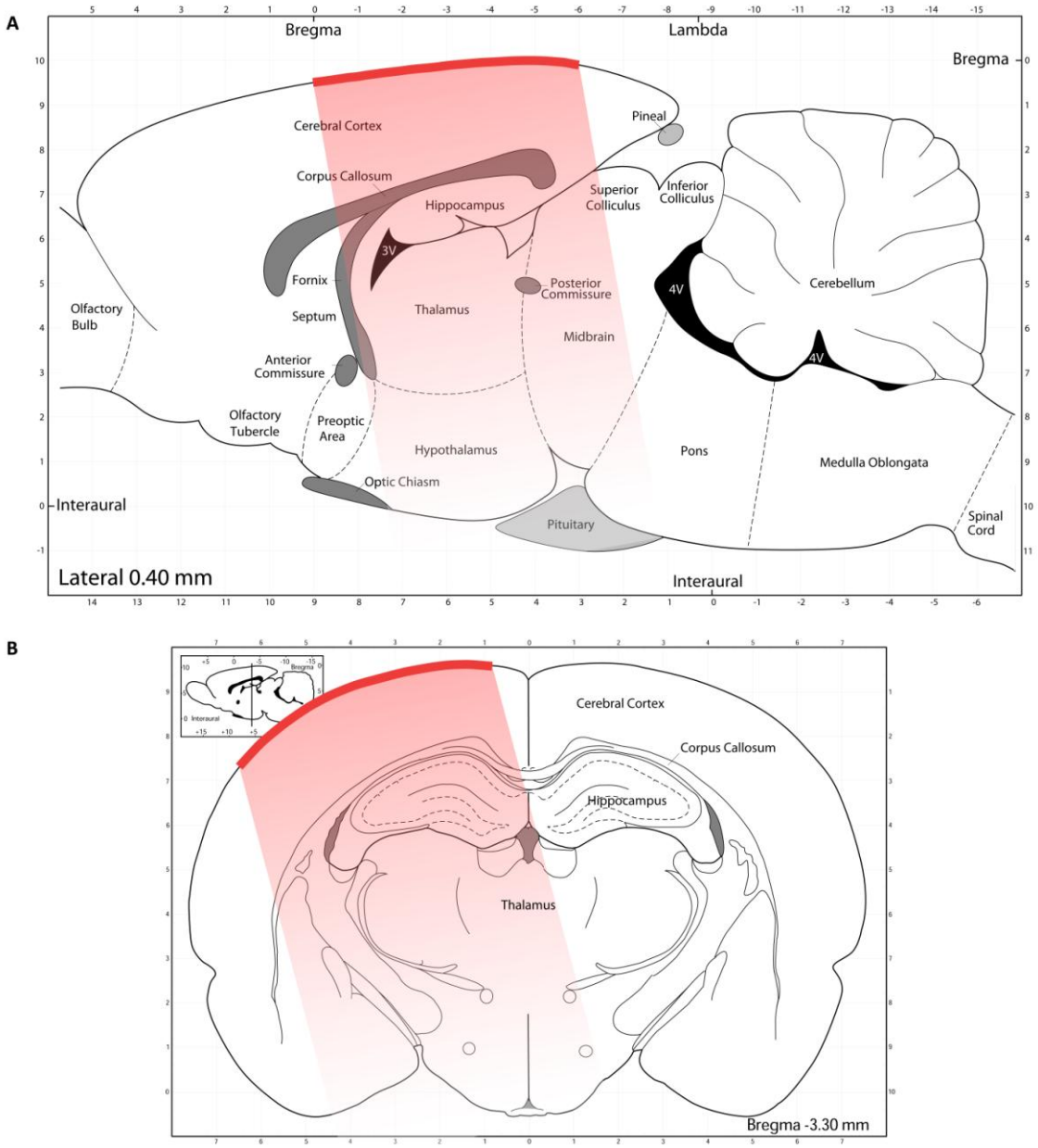

Figure 1.1: Location of controlled cortical impact injury

(A) The lateral view of the rat brain shows the orientation of the hippocampus. The thick red line indicates where the impactor makes contact with the surface of the brain. To ensure even contact at injury, this top surface of the brain is oriented to be perpendicular to the axis of the impactor; the red shadow shows the region directly beneath the injury site. (B) A coronal section of the rat brain with the injury site and the

region directly beneath it marked. The impactor is angled at 15° from vertical in the coronal plane. The schematics of the brain are adapted from Paxinos and Watson (1998).

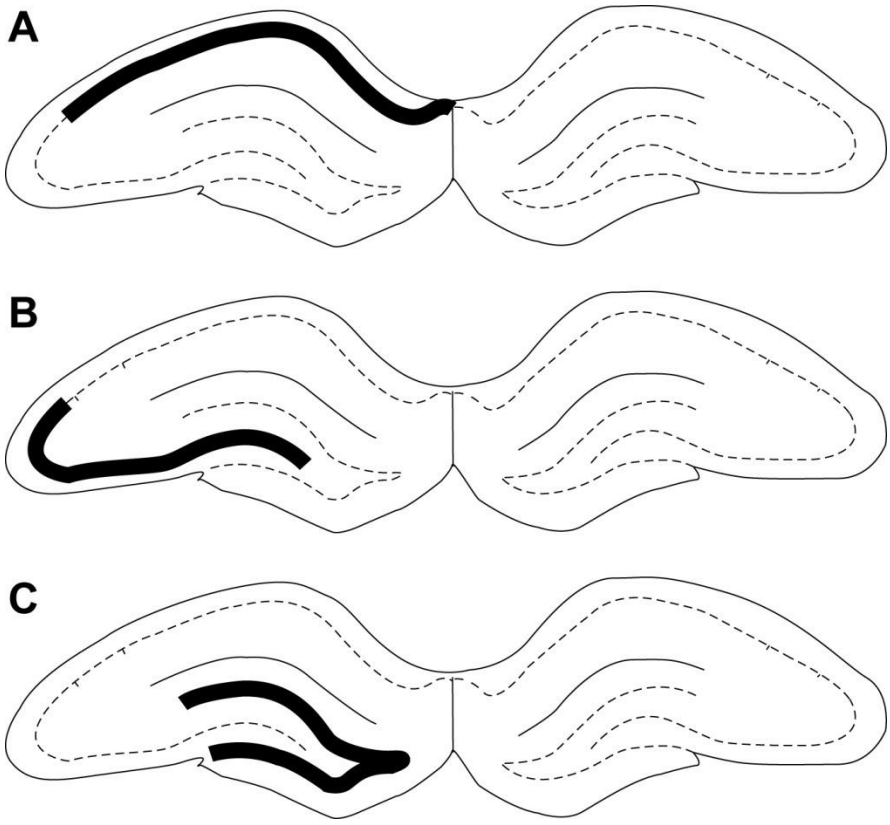

Figure 1.2: Subregions of the hippocampus

The following subregions of the hippocampus are indicated by a solid black line: CA1/CA2 (A), CA3 (B), and the dentate gyrus (C). The schematic is adapted from Paxinos and Watson (1998).

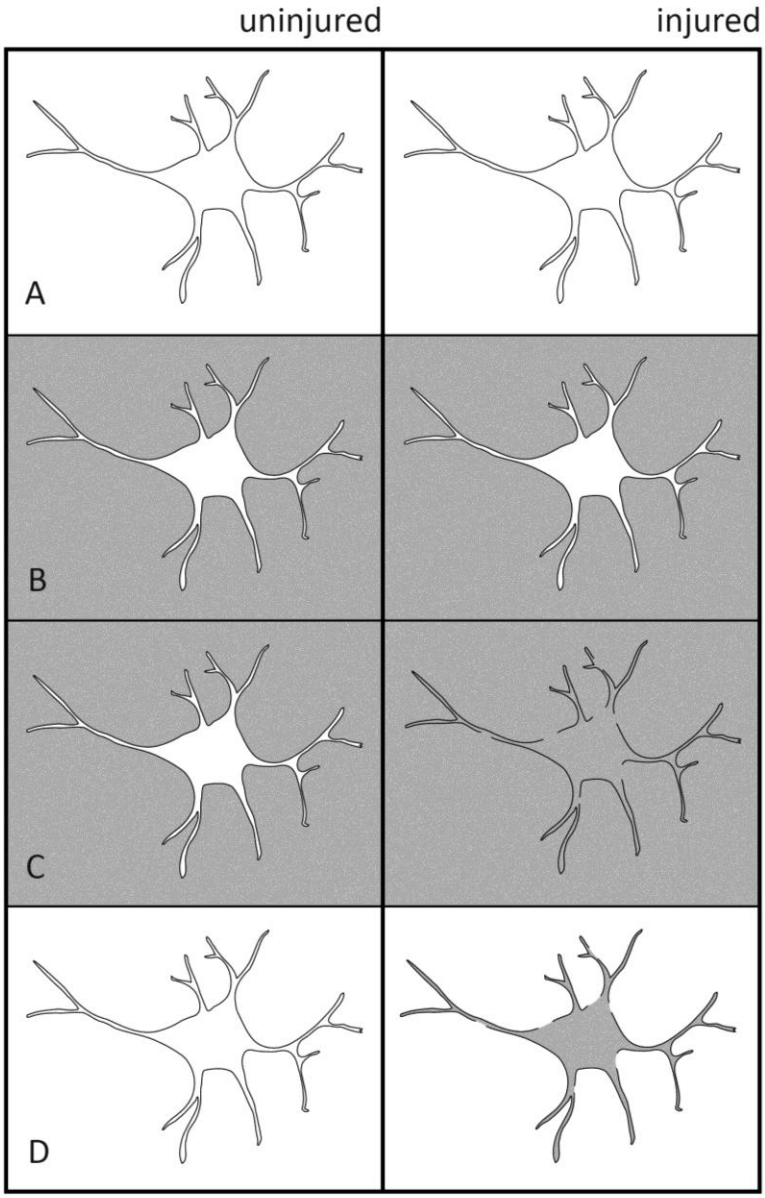

Figure 1.3: Dye exclusion assay

Before injury, cells have intact plasma membranes (A). Dye is introduced into the extracellular space (B). A mechanical insult causes plasma membrane damage, allowing dye to flood the intracellular space of the injured cell (C). Extracellular dye is rinsed away, leaving dye within the injured cell (D).

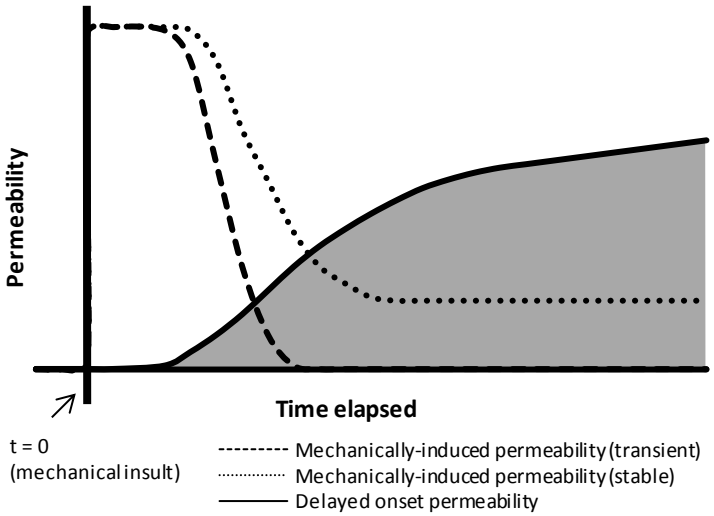

Figure 1.4: Time course of plasma membrane damage

Three categories of plasma membrane disruptions have been observed (Farkas et al. 2006). Transient pores are caused by the primary mechanical insult but reseal completely in the acute period following injury. Stable pores are also caused by the primary mechanical insult but do not reseal completely. A third category of pores, caused by secondary injury mechanisms rather than the primary mechanical insult, forms in the post-acute period following injury.

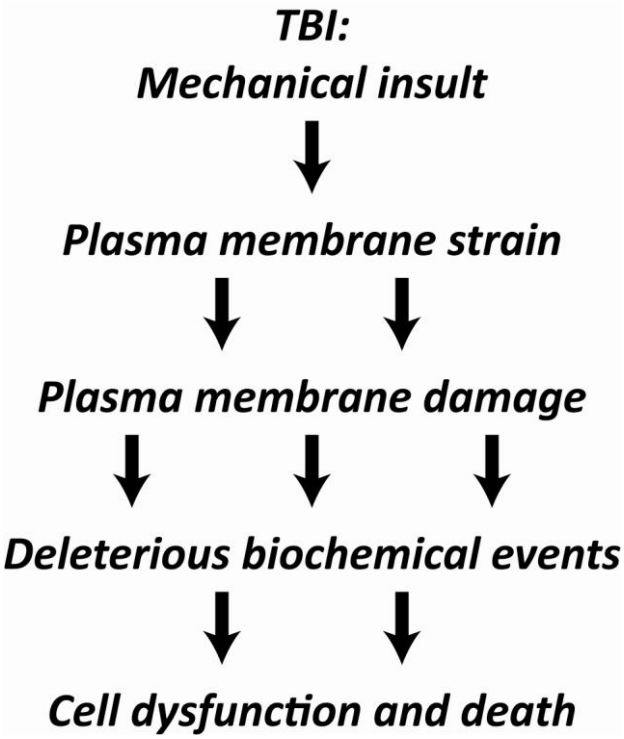

Figure 1.5: Plasma membrane damage leads to cell death

It is hypothesized that traumatic brain injury (TBI) causes deformation of the plasma membrane that results in damage to the membrane. This damage triggers biochemical events that ultimately lead to neuronal dysfunction and cell death.

1.5 Works cited

Alberts, B. (1994). Molecular biology of the cell. New York, Garland Pub.

Baskin, Y. K., W. D. Dietrich and E. J. Green (2003). "Two effective behavioral tasks for evaluating sensorimotor dysfunction following traumatic brain injury in mice." Journal Of Neuroscience Methods **129**(1): 87-93.

Brown, D. A. and E. London (1998). "Functions of lipid rafts in biological membranes." Annual Review Of Cell And Developmental Biology **14**(1): 111-136.

Buki, A. and J. T. Povlishock (2006). "All roads lead to disconnection?--Traumatic axonal injury revisited." Acta Neurochirurgica **148**(2): 181-93; discussion 193-4.

Cernak, I. (2005). "Animal models of head trauma." Neurorx: The Journal Of The American Society For Experimental Neurotherapeutics **2**(3): 410-22.

Cohen, A. S., B. J. Pfister, E. Schwarzbach, M. S. Grady, P. B. Goforth and L. S. Satin (2007). "Injury-induced alterations in CNS electrophysiology." Prog Brain Res **161**: 143-69.

Colicos, M. A. and P. K. Dash (1996). "Apoptotic morphology of dentate gyrus granule cells following experimental cortical impact injury in rats: possible role in spatial memory deficits." Brain Research **739**(1-2): 120-131.

Cullen, D. K. and M. C. LaPlaca (2006). "Neuronal response to high rate shear deformation depends on heterogeneity of the local strain field." Journal Of Neurotrauma **23**(9): 1304-1319.

Dixon, C. E., G. L. Clifton, J. W. Lighthall, A. A. Yaghmai and R. L. Hayes (1991). "A controlled cortical impact model of traumatic brain injury in the rat." Journal Of Neuroscience Methods **39**(3): 253-62.

Dixon, C. E., M. F. Kraus, A. E. Kline, X. Ma, H. Q. Yan, R. G. Griffith, B. M. Wolfson and D. W. Marion (1999). "Amantadine improves water maze performance without affecting motor behavior following traumatic brain injury in rats." Restor Neurol Neurosci **14**(4): 285-294.

Dixon, C. E., B. G. Lyeth, J. T. Povlishock, R. L. Findling, R. J. Hamm, A. Marmarou, H. F. Young and R. L. Hayes (1987). "A fluid percussion model of experimental brain injury in the rat." Journal Of Neurosurgery **67**(1): 110-119.

Eddleman, C. S., M. E. Smyers, A. Lore, H. M. Fishman and G. D. Bittner (1998). "Anomalies associated with dye exclusion as a measure of axolemmal repair in vertebrate axons." Neuroscience Letters **256**(3): 123-126.

Farkas, O., J. Lifshitz and J. T. Povlishock (2006). "Mechanoporation induced by diffuse traumatic brain injury: an irreversible or reversible response to injury?" The

Journal Of Neuroscience: The Official Journal Of The Society For Neuroscience **26**(12): 3130-40.

Farkas, O. and J. T. Povlishock (2007). "Cellular and subcellular change evoked by diffuse traumatic brain injury: a complex web of change extending far beyond focal damage." Progress In Brain Research **161**: 43-59.

Foda, M. A. and A. Marmarou (1994). "A new model of diffuse brain injury in rats. Part II: Morphological characterization." J Neurosurg **80**(2): 301-13.

Fujimoto, S. T., L. Longhi, K. E. Saatman, V. Conte, N. Stocchetti and T. K. McIntosh (2004). "Motor and cognitive function evaluation following experimental traumatic brain injury." Neurosci Biobehav Rev **28**(4): 365-78.

Geddes-Klein, D. M., K. B. Schiffman and D. F. Meaney (2006). "Mechanisms and consequences of neuronal stretch injury in vitro differ with the model of trauma." Journal Of Neurotrauma **23**(2): 193-204.

Geddes, D. M. and R. S. Cargill, 2nd (2001). "An in vitro model of neural trauma: device characterization and calcium response to mechanical stretch." Journal Of Biomechanical Engineering **123**(3): 247-255.

Geddes, D. M., R. S. Cargill, 2nd and M. C. LaPlaca (2003a). "Mechanical stretch to neurons results in a strain rate and magnitude-dependent increase in plasma membrane permeability." Journal Of Neurotrauma **20**(10): 1039-49.

Geddes, D. M., M. C. LaPlaca and R. S. Cargill (2003b). "Susceptibility of hippocampal neurons to mechanically induced injury." Experimental Neurology **184**(1): 420-427.

Gennarelli, T. A. (1994). "Animate models of human head injury." Journal Of Neurotrauma **11**(4): 357-68.

Gonzalez-Pina, R., A. Bueno-Nava, S. Montes, A. Alfaro-Rodriguez, A. Gonzalez-Maciel, R. Reynoso-Robles and F. Ayala-Guerrero (2005). "Pontine norepinephrine content after motor cortical ablation in rats." Proc West Pharmacol Soc **48**: 73-6.

Hamm, R. J., B. R. Pike, D. M. O'Dell, B. G. Lyeth and L. W. Jenkins (1994). "The rotarod test: an evaluation of its effectiveness in assessing motor deficits following traumatic brain injury." Journal Of Neurotrauma **11**(2): 187-196.

Hering, H., C.-C. Lin and M. Sheng (2003). "Lipid Rafts in the Maintenance of Synapses, Dendritic Spines, and Surface AMPA Receptor Stability." J. Neurosci. **23**(8): 3262-3271.

Hillered, L., L. Persson, P. Nilsson, E. Ronne-Engstrom and P. Enblad (2006). "Continuous monitoring of cerebral metabolism in traumatic brain injury: a focus on cerebral microdialysis." Current Opinion In Critical Care **12**(2): 112-8.

Invitrogen (2006). Molecular Probes Dextran Conjugates Product Information, MP 01800.

Itoh, K., M. Sakakibara, S. Yamasaki, A. Takeuchi, H. Arase, M. Miyazaki, N. Nakajima, M. Okada and T. Saito (2002). "Cutting edge: negative regulation of immune synapse formation by anchoring lipid raft to cytoskeleton through Cbp-EBP50-ERM assembly." Journal Of Immunology (Baltimore, Md : 1950) **168**(2): 541-4.

Kelley, B. J., O. Farkas, J. Lifshitz and J. T. Povlishock (2006). "Traumatic axonal injury in the perisomatic domain triggers ultrarapid secondary axotomy and Wallerian degeneration." Experimental Neurology **198**(2): 350-60.

Koob, A. O., J. Cirillo and C. F. Babbs (2006). "A novel open field activity detector to determine spatial and temporal movement of laboratory animals after injury and disease." Journal Of Neuroscience Methods **157**(2): 330-6.

Koob, A. O., J. M. Colby and R. B. Borgens (2008). "Behavioral recovery from traumatic brain injury after membrane reconstruction using polyethylene glycol." Journal Of Biological Engineering **2**(1): 9.

Koob, A. O., B. S. Duerstock, C. F. Babbs, Y. Sun and R. B. Borgens (2005). "Intravenous Polyethylene Glycol Inhibits the Loss of Cerebral Cells after Brain Injury." Journal Of Neurotrauma **22**(10).

Langlois, J. A., W. Rutland-Brown and M. M. Wald (2006). "The epidemiology and impact of traumatic brain injury: a brief overview." J Head Trauma Rehabil **21**(5): 375–378.

LaPlaca, M. C., D. K. Cullen, J. J. McLoughlin and R. S. Cargill, 2nd (2005). "High rate shear strain of three-dimensional neural cell cultures: a new in vitro traumatic brain injury model." Journal of Biomechanics **38**(5): 1093-1105.

LaPlaca, M. C., V. M. Y. Lee and L. E. Thibault (1997). "An in vitro model of traumatic neuronal injury: Loading rate-dependent changes in acute cytosolic calcium and lactate dehydrogenase release." Journal of Neurotrauma **14**(6): 355-368.

LaPlaca, M. C. and L. E. Thibault (1997). "An in vitro traumatic injury model to examine the response of neurons to a hydrodynamically-induced deformation." Annals of Biomedical Engineering **25**(4): 665-677.

LaPlaca, M. C. and L. E. Thibault (1998). "Dynamic mechanical deformation of neurons triggers an acute calcium response and cell injury involving the N-methyl-D-aspartate glutamate receptor." Journal of Neuroscience Research **52**(2): 220-229.

Lessing, M. C. and M. C. LaPlaca (2008). Traumatic brain injury causes plasma membrane damage and cell death in the hippocampus of rats. National Neurotrauma Symposium. Orlando, FL.

Lewen, A., P. Matz and P. H. Chan (2000). "Free radical pathways in CNS injury." Journal Of Neurotrauma **17**(10): 871-90.

Lifshitz, J., H. Friberg, R. W. Neumar, R. Raghupathi, F. A. Welsh, P. Janmey, K. E. Saatman, T. Wieloch, M. S. Grady and T. K. McIntosh (2003). "Structural and functional damage sustained by mitochondria after traumatic brain injury in the rat: evidence for differentially sensitive populations in the cortex and hippocampus." Journal Of Cerebral Blood Flow And Metabolism: Official Journal Of The International Society Of Cerebral Blood Flow And Metabolism **23**(2): 219-31.

Luo, J., R. Borgens and R. Shi (2002). "Polyethylene glycol immediately repairs neuronal membranes and inhibits free radical production after acute spinal cord injury." J Neurochem **83**(2): 471-80.

Marklund, N., K. Salci, G. Ronquist and L. Hillered (2006). "Energy metabolic changes in the early post-injury period following traumatic brain injury in rats." Neurochemical Research **31**(8): 1085-93.

Marmarou, A., M. A. Foda, W. van den Brink, J. Campbell, H. Kita and K. Demetriadou (1994). "A new model of diffuse brain injury in rats. Part I: Pathophysiology and biomechanics." J Neurosurg **80**(2): 291-300.

McNeil, A. K., U. Rescher, V. Gerke and P. L. McNeil (2006). "Requirement for annexin A1 in plasma membrane repair." The Journal Of Biological Chemistry **281**(46): 35202-7.

McNeil, P. L. and T. Kirchhausen (2005). "An emergency response team for membrane repair." Nature Reviews Molecular Cell Biology **6**(6): 499-505.

McNeil, P. L., K. Miyake and S. S. Vogel (2003). "The endomembrane requirement for cell surface repair." Proc Natl Acad Sci U S A **100**(8): 4592-7.

Mellgren, R. L., W. Zhang, K. Miyake and P. L. McNeil (2007). "Calpain is required for the rapid, calcium-dependent repair of wounded plasma membrane." The Journal Of Biological Chemistry **282**(4): 2567-75.

Miyake, K. and P. L. McNeil (2003). "Mechanical injury and repair of cells." Crit Care Med **31**(8 Suppl): S496-501.

Morrison, B., 3rd, K. E. Saatman, D. F. Meaney and T. K. McIntosh (1998). "In vitro central nervous system models of mechanically induced trauma: a review." J Neurotrauma **15**(11): 911-28.

Needham, D. and R. S. Nunn (1990). "Elastic deformation and failure of lipid bilayer membranes containing cholesterol." Biophys. J. **58**(4): 997-1009.

Okonkwo, D. O., E. H. Pettus, J. Moroi and J. T. Povlishock (1998). "Alteration of the neurofilament sidearm and its relation to neurofilament compaction occurring with traumatic axonal injury." Brain Res **784**(1-2): 1-6.

Paxinos, G. and C. Watson (1998). The rat brain in stereotaxic coordinates. San Diego, Academic Press.

Pettus, E. H., C. W. Christman, M. L. Giebel and J. T. Povlishock (1994). "Traumatically induced altered membrane permeability: its relationship to traumatically induced reactive axonal change." Journal Of Neurotrauma **11**(5): 507-22.

Pettus, E. H. and J. T. Povlishock (1996). "Characterization of a distinct set of intra-axonal ultrastructural changes associated with traumatically induced alteration in axolemmal permeability." Brain Research **722**(1-2): 1-11.

Prado, G. R. (2004). Neuronal Plasma Membrane Disruption in Traumatic Brain Injury. Biomedical Engineering. Atlanta, GA, Georgia Institute of Technology. **Doctor of Philosophy**.

Prado, G. R., J. D. Ross, S. P. DeWeerth and M. C. LaPlaca (2005). "Mechanical trauma induces immediate changes in neuronal network activity." Journal Of Neural Engineering **2**(4): 148-58.

Raghupathi, R. (2004). "Cell death mechanisms following traumatic brain injury." Brain Pathology (Zurich, Switzerland) **14**(2): 215-22.

Serbest, G., J. Horwitz and K. Barbee (2005). "The effect of poloxamer-188 on neuronal cell recovery from mechanical injury." J Neurotrauma **22**(1): 119-32.

Serbest, G., J. Horwitz, M. Jost and K. Barbee (2006). "Mechanisms of cell death and neuroprotection by poloxamer 188 after mechanical trauma." The FASEB Journal **20**(2): 308-310.

Shi, R., T. Asano, N. C. Vining and A. R. Blight (2000). "Control of Membrane Sealing in Injured Mammalian Spinal Cord Axons." Journal Of Neurophysiology **84**(4): 1763-1769.

Shi, R. and R. B. Borgens (1999). "Acute repair of crushed guinea pig spinal cord by polyethylene glycol." Journal Of Neurophysiology **81**(5): 2406-14.

Shi, R. and R. B. Borgens (2000). "Anatomical repair of nerve membranes in crushed mammalian spinal cord with polyethylene glycol." Journal Of Neurocytology **29**(9): 633-43.

Shi, R. and J. D. Pryor (2000). "Temperature dependence of membrane sealing following transection in mammalian spinal cord axons." Neuroscience **98**(1): 157-66.

Shi, R. and J. D. Pryor (2002). "Pathological changes of isolated spinal cord axons in response to mechanical stretch." Neuroscience **110**(4): 765-77.

Simons, K. and E. Ikonen (1997). "Functional rafts in cell membranes." Nature **387**(6633): 569-572.

Simons, K. and D. Toomre (2000). "Lipid rafts and signal transduction." Nature Reviews. Molecular Cell Biology **1**(1): 31-39.

Singer, S. J. and G. L. Nicolson (1972). "The fluid mosaic model of the structure of cell membranes." Science **175**(23): 720-31.

Singleton, R. H. and J. T. Povlishock (2004). "Identification and characterization of heterogeneous neuronal injury and death in regions of diffuse brain injury: evidence for multiple independent injury phenotypes." The Journal Of Neuroscience: The Official Journal Of The Society For Neuroscience **24**(14): 3543-53.

Singleton, R. H., J. P. Zhu, J. R. Stone and J. T. Povlishock (2002). "Traumatically induced axotomy adjacent to the soma does not result in acute neuronal death." Journal of Neuroscience **22**(3): 791-802.

Smith, D. H., J. A. Wolf, T. A. Lusardi, V. M. Y. Lee and D. F. Meaney (1999). "High Tolerance and Delayed Elastic Response of Cultured Axons to Dynamic Stretch Injury." Journal of Neuroscience **19**(11): 4263.

Stone, J. R., D. O. Okonkwo, A. O. Dialo, D. G. Rubin, L. K. Mutlu, J. T. Povlishock and G. A. Helm (2004). "Impaired axonal transport and altered axolemmal permeability occur in distinct populations of damaged axons following traumatic brain injury." Experimental Neurology **190**(1): 59-69.

Thurman, D. J., C. Alverson, K. A. Dunn, J. Guerrero and J. E. Sniezek (1999). "Traumatic brain injury in the United States: A public health perspective." J Head Trauma Rehabil **14**(6): 602-15.

Weber, J. T. (2004). "Calcium Homeostasis Following Traumatic Neuronal Injury." Current Neurovascular Research **1**(2): 151-171.

Whalen, M., T. Dalkara, Z. You, J. Qiu, D. Bermpohl, N. Mehta, B. Suter, P. Bhide, E. Lo, M. Ericsson and M. Moskowitz (2007). "Acute plasmalemma permeability and protracted clearance of injured cells after controlled cortical impact in mice." J Cereb Blood Flow Metab **28**(3): 490-505.

White, B. C., J. M. Sullivan, D. J. DeGracia, B. J. O'Neil, R. W. Neumar, L. I. Grossman, J. A. Rafols and G. S. Krause (2000). "Brain ischemia and reperfusion: molecular

mechanisms of neuronal injury." Journal Of The Neurological Sciences **179**(S 1-2): 1-33.

CHAPTER 2

COLLAGEN-DEPENDENT NEURITE OUTGROWTH AND RESPONSE TO DYNAMIC DEFORMATION IN THREE-DIMENSIONAL NEURONAL CULTURES

2.1 Abstract

In vitro models of brain injury that use thick 3-D cultures and control extracellular matrix constituents allow evaluation of cell-matrix interactions in a more physiologically relevant configuration than traditional 2-D cultures. Accordingly, a 3-D cell culture system consisting of primary rat cortical neurons distributed throughout thick (> 500 μm thickness) gels consisting of type IV collagen (Col) conjugated to agarose has been developed. Neuronal viability and neurite outgrowth were examined for a range of agarose (AG) percentages (1.0 - 3.0%) and initial collagen concentrations ($[Col]_i$; 0 - 600 μg/mL). In unmodified AG, 1.5% gels supported viable cultures with significant neurite outgrowth, which was not found at lower (≤ 1.0%) concentrations. Varying $[Col]_i$ in 1.25% AG revealed the formation of dense, 3-D neurite networks at $[Col]_i$ of 300 μg/mL, while neurons in unmodified AG and at higher $[Col]_i$ (600 μg/mL) exhibited significantly less neurite outgrowth, although neuronal survival did not vary with $[Col]_i$. The effect of $[Col]_i$ on acute neuronal response following high magnitude, high rate shear deformation (0.50 strain, 30 s^{-1} strain rate) was evaluated in 1.5% AG for $[Col]_i$ of 30, 150, and 300 μg/mL, which supported cultures with similar baseline viability and neurite outgrowth.

Conjugation of Col to AG also increased the complex modulus of the hydrogel. Following high rate deformation, neuronal viability significantly decreased with increasing $[Col]_i$, implicating cell-matrix adhesions in acute mechanotransduction events associated with traumatic loading. These results suggest interrelated roles for matrix mechanical properties and receptor-mediated cell-matrix interactions in neuronal viability, neurite outgrowth, and transduction of high rate deformation. This model system may be further exploited for the elucidation of mechanotransduction mechanisms and cellular pathology following mechanical insult.

2.2 Introduction

Traumatic brain injury (TBI) is caused by a physical insult to the head and may result in prolonged or permanent loss of sensory, motor, and/or cognitive functions (Adelson et al. 2000; Povlishock and Katz 2005), representing a major health and socioeconomic problem (Thurman et al. 1999; Langlois et al. 2004). A rapid insult to the brain produces diffuse strain patterns, which may lead to cell death if strain thresholds are surpassed. However, sublethal strain regimes may lead to persistent alterations in cellular signaling and function. The underlying mechanisms that translate bulk tissue deformation to cellular dysfunction remain poorly understood, but may be dictated by cell orientation, cell-cell connections, as well as cell-extracellular matrix (ECM) interactions.

Receptor-mediated cell-ECM interactions, in particular, are crucial in many homeostatic cellular processes including proliferation, migration, and differentiation (De Arcangelis and Georges-Labouesse 2000; Danen and Sonnenberg 2003), and may be affected during various pathological states (Wehrle-Haller and Imhof 2003; Jin and Varner 2004). However, the role of cell-ECM adhesions in acute and chronic responses

following traumatic neural loading is currently not known. Cell-ECM interactions serve as the direct mechanical linkages between the cell and its extracellular environment, transmitting external mechanical stimulation to the interior of the cell. Traumatic mechanical stimulation may lead to cellular damage including plasma membrane rupture and cytoskeletal collapse.

However in many non-neural systems, cells communicate with their immediate physical environment through such interactions and alter intracellular biochemical signaling in response to mechanical cues, a process referred to as mechanotransduction (Ingber 1997; Alenghat and Ingber 2002; Kamm and Kaazempur-Mofrad 2004). Transmembrane proteins such as integrins transduce mechanical stimuli from the ECM to the cytoskeleton and activate intracellular signaling molecules regulating the activity of enzymes (e.g. proteases, phosphatases, kinases) that can modify cytoskeletal organization and may result in changes in gene expression (Roskelley et al. 1994; Sjaastad et al. 1994; Hamill and Martinac 2001; Ko and McCulloch 2001; Alenghat and Ingber 2002; Cavalcanti-Adam et al. 2005). However, the mechanisms involved in transduction of non-physiological mechanical deformation are not fully understood. Non-homeostatic (i.e., pathological) mechanotransduction may play a role in cellular dysfunction in response to mechanical forces through integrin-mediated signaling events, increasing intracellular Ca^{2+} concentration, causing membrane disruption via protein phosphorylation, and/or activating cytoskeletal-cleaving enzymes; components of the secondary sequelae associated with TBI (Raghupathi 2004). Central nervous system (CNS) neurons are normally protected from high rate strain and may not have inherent mechanisms to homeostatically transduce mechanical stimuli that other cells (e.g.,

vascular smooth muscle cells, osteoblasts) possess and may therefore have a high sensitivity to mechanical forces, causing abnormal biochemical responses leading to cell dysfunction and possibly death.

The study of mechanotransduction under both physiologic and pathologic states requires the use of experimental systems that mimic the cytoarchitecture and microenvironment found *in vivo*. Fundamental differences exist between cells cultured in planar (i.e., two-dimensional or 2-D) versus three-dimensional (3-D) configurations, such as the distribution of cell-cell and cell-ECM interactions, which can alter cell morphology and subsequent signaling and function (Gumbiner and Yamada 1995; Cukierman et al. 2001; Cukierman et al. 2002; Schmeichel and Bissell 2003; Yamada et al. 2003). Cells cultured in 3-D have been found to exhibit more *in vivo*-like viability, growth, proliferation, response to biochemical stimuli, gene expression, and differentiation (Masi et al. 1992; Hoffman 1993; Fawcett et al. 1995; Granet et al. 1998). Models consisting of neurons distributed throughout a 3-D matrix material have previously been developed (Bellamkonda et al. 1995a; Bellamkonda et al. 1995b; Woerly et al. 1996; O'Connor et al. 2000; O'Connor et al. 2001). Dorsal root ganglia (DRG) extend neurites through hydrogel matrices in a manner dependent on the physical properties (e.g., agarose pore size (Dillon et al. 1998) and stiffness (Balgude et al. 2001)), ligand concentration (e.g., collagen (Willits and Skornia 2004) and RGD peptides in fibrin (Schense and Hubbell 2000)), and substrate geometry (Yu and Shoichet 2005). Embryonic cortical neurons have been plated within 3-D matrices of collagen and various hydrogels (e.g., poly[*N*-(2-hydroxypropyl)-methacrylamide] (Woerly et al. 1996), poly(acrylate) (O'Connor et al. 2000), and agarose (O'Connor et al. 2001)). Enhanced survival and neurite outgrowth was observed in

collagen (0.4 - 0.5 mg/mL) as compared to hydrogels lacking ECM ligands, which produced varying degrees of cell viability and a paucity of neurite outgrowth, together indicating that growth and survival of primary cortical neurons are improved by specific cell-matrix interactions (Woerly et al. 1996; O'Connor et al. 2000; O'Connor et al. 2001).

Most *in vitro* models developed to study the response of neural cells to mechanical deformation utilize planar cell culture, and include mechanical stretch (Ellis et al. 1995; Smith et al. 1999; Geddes and Cargill 2001) and hydrodynamic shear stress (LaPlaca et al. 1997; Nakayama et al. 2001) systems. Differences in cell morphology and the spatial distribution of cell-cell/cell-ECM interactions in planar versus 3-D cultures may be important, especially in models of traumatic cellular injury as bulk deformation is translated to cells through physical coupling, which may be unrealistically represented in 2-D culture. Furthermore, models amenable to systematic control of cell culture parameters (e.g., cell composition, matrix constituents) provide a framework for the elucidation of the roles of specific factors in deformation transfer to cells and associated acute responses. Accordingly the 3-D Cell Shearing Device (CSD), a custom electro-mechanical device capable of reproducibly imparting variable rate and magnitude shear deformation to 3-D cell-containing matrices, was previously developed and characterized (LaPlaca et al. 2005).

The overall goal of this study was to investigate the roles of matrix mechanical properties and composition in neuronal survival, neurite outgrowth, and the response to traumatic loading. Therefore a bioactive scaffold was engineered by controlling matrix mechanical properties and ligand density to find optimal ranges for neuronal survival and

neurite outgrowth. This cell culture model was then used to study the response to high rate bulk shear deformation.

2.3 Materials and methods

2.3.1 Preparation of protein-conjugated agarose gels

Agarose was chosen as the matrix backbone for this system because it lacks cell surface receptor binding domains, its physical properties may be tailored based on concentration (Balgude et al. 2001; Yu and Bellamkonda 2001), and procedures have been established for the controlled coupling of bioactive ligands (Bellamkonda et al. 1995a; Dodla and Bellamkonda 2006). Collagen has previously been used for successful 3-D cortical neuronal culture (O'Connor et al. 2000; O'Connor et al. 2001), integrin receptors that recognize collagen have been demonstrated for a range of neuronal sub-types (Tomaselli 1991; Arregui et al. 1994; Carmeliet et al. 1994; Bradshaw et al. 1995; Li et al. 2000; Anderson and Ferreira 2004), and it is a major component in the positive control matrix, Matrigel (Kleinman et al. 1986). Collagen Type IV (Col) (Sigma, St. Louis, MO) was suspended at 2 mg/mL in 0.25 % acetic acid. A heterobifunctional amine reactive and photoreactive crosslinker, sulfosuccinimidyl (perfluoroazidobenzamido) ethyl-1,3-dithiopropionate (SFAD) (Pierce, Rockford, IL), was added (1:100 molar ratio) and the protein/crosslinker solution was incubated in the dark at room temperature for four hours, followed by dilution in ultrapure water to obtain a range of protein concentrations. SeaPrep agarose (BioWhittaker Molecular Applications, Rockland, ME) was prepared at 4% (w/v) in ultrapure water. Equal volumes of protein-crosslinker solution and molten agarose solution were combined, which yielded a 2% stock agarose gel with appropriate collagen concentrations to yield the desired initial collagen

concentrations ($[Col]_i$) of 30, 150, 300, and 600 μg/mL. Mixtures of agarose and protein-crosslinker were gelled at 4°C for 20 minutes, after which they were exposed to UV light (306 nm, 25 watts, 6300 mW/cm^2) for 20 minutes to mediate the photocrosslinking reaction and to sterilize the gels. Resulting gels were rinsed in sterile phosphate buffered saline (PBS, pH = 7.4) for four days to remove unreacted crosslinker and uncoupled protein. For control gels, Col was mixed with agarose according to the same procedures described, without the addition of SFAD.

Photoimmobilization of Col was verified via immunocytochemistry. Briefly, Col presence in Col-coupled agarose gels (referred to as "Col-AG"; n = 7) and agarose gels mixed with Col without crosslinker (referred to as "Col+AG"; n = 6) were compared to unmodified, agarose-only gels (referred to as "AG"; n = 8). Both Col+AG and Col-AG were at a concentration of 300 μg Col/mL, and where then exposed to the UV immobilization procedure and subsequently rinsed in PBS for four days. To assess the remaining Col in the agarose, samples were incubated with an antibody recognizing Col IV (AB748, 1:20, Chemicon, Temecula, CA) and then a fluorescently conjugated secondary antibody (Alexa 488, 1:500, Molecular Probes). Fluorescent intensity readings were collected using a microplate reader and were normalized to background readings attained from the AG samples. One-way ANOVA was performed followed by Tukey's pair-wise comparisons ($p < 0.05$ required for significance)

2.3.2 Rheological characterization

The complex moduli of AG, Col-AG, and Matrigel (referred to as "MG") were determined using a Bohlin CVO rheometer (East Brunswick, NJ). AG and Col-AG gels were cast and punched into discs (12 mm diameter x 1 mm thick) and loaded onto the

rheometer. MG was added to the rheometer when fluid-like (~4°C), and the base plate temperature was then increased to 37°C to permit gelation. The viscous and elastic moduli were determined for AG (1.0% - 4.0%), Col-AG (1.5% AG at $[Col]_i$ = 30, 150, and 300 μg/mL), and MG (7.5 mg/mL in Neurobasal medium) under low oscillatory shear strain (0.005) in a parallel plate configuration at 37°C in an humidified environment. The stress response was measured, and the complex modulus was determined through a frequency sweep of 0.01 to 3.20 Hz (corresponding to the linear response range of the hydrogel). Matrix rheological properties were determined for AG (1.0%, n = 4; 1.5%, n = 11; 2.0%, n = 4; 2.5%, n = 4; 3.0%, n = 3; 4.0%, n = 3), Col-AG (1.5% AG at $[Col]_i$ = 30, 150, and 300 μg/mL; n = 4, 7, 8, respectfully), and MG (7.5 mg/mL; n = 4). General linear model ANOVA was performed with agarose percentage, collagen concentration, and frequency as independent variables and complex modulus as the dependent variable, followed by Tukey's pair-wise comparisons ($p < 0.05$ required for significance).

2.3.3 Harvest and dissociation of primary cortical neurons

All procedures involving animals conformed to guidelines set forth in the NIH Guide for the Care and Use of Laboratory Animals and were approved by the Institutional Animal Care and Use Committee of the Georgia Institute of Technology. All cell reagents were obtained from Invitrogen (Carlsbad, CA) or Sigma (St. Louis, MO) unless otherwise noted. Cortical neurons were harvested from Sasco Sprague-Dawley rat dams (Charles River, Wilmington, MA) at embryonic day 17. Following anesthesia with halothane (Fisher Scientific, Pittsburgh, PA) and decapitation, fetuses were removed by Caesarian section, and the cerebral cortices were isolated and rinsed in sterile Ca^{2+}- and

Mg^{2+}-free Hanks Balanced Salt Solution (HBSS). Trypsin (0.25%, + 1 mM EDTA) was added for ten minutes at 37 °C, then cortices were rinsed, and DNase (0.15 mg/mL with $MgSO_4$ (0.25 mg/mL) in HBSS) was added. The tissue was agitated using a vortex for 30 seconds, centrifuged at 1000 rpm for three minutes, and the pelleted cells were resuspended in culture medium (Neurobasal medium + 2 % B-27 + 500 μM L-glutamine). Cell concentration and initial viability were determined using a hemocytometer and evaluating the exclusion of trypan blue.

2.3.4 3-D Primary cortical neuronal cultures

Neurons were cultured in 3-D within either unmodified agarose (AG), collagen-conjugated agarose (Col-AG), or Matrigel (MG) in custom cell culture chambers consisting of a glass coverslip base with lateral PDMS containment (Dow Corning, Midland, MI). Agarose gels (AG or Col-AG) were heated to 50 °C for 30 minutes to melt the agarose. Col heated to this temperature has previously been shown to return to physiological conformation upon returning to 37 °C (Dolz et al. 1988). The gels were then cooled to 37 °C and the appropriate volume of cell suspension was added to yield 5000 cells/mm^3. After gentle mixing, the cell and agarose mixture was transferred to each well and evenly spread out to create 500 - 750 μm thick cultures. Cultures were placed at –20°C for 60 seconds and then at 4°C for 15 minutes to ensure rapid and complete agarose gelation and 3-D cell entrapment, after which 0.5 mL of pre-warmed medium was added and each culture was placed in a tissue culture incubator (37 °C, 5 % CO_2, 95 % humidified air). MG cultures were plated by combining MG solution and cell suspension to yield 5000 cells/mm^3 in 7.5 mg/mL MG. After gentle mixing, the cell and

MG mixture was transferred to each well and evenly spread out to create 500 - 750 μm thick cultures, and then placed in tissue culture incubator (37 °C, 5 % CO_2, 95 % humidified air) for 30 minutes to allow gelation of the MG, after which pre-warmed medium was added (0.5 mL/culture) and the chambers were returned to a tissue culture incubator. For AG, AG-Col, and MG cultures, half of the medium was replaced every 2 - 3 days *in vitro* (DIV).

Culture viability was assessed using fluorescent probes for distinguishing live and dead cells (LIVE/DEAD Viability/Cytotoxicity Kit; Molecular Probes, Eugene, OR). Cell cultures were incubated with 2 μM calcein AM and 4 μM ethidium homodimer-1 at 37 °C for 30 min and rinsed in PBS. After viability/cytotoxicity staining, cells were viewed using a Laser Scanning Confocal Microscope (Zeiss 510; Zeiss, Oberkochen, Germany). For each culture, three to five z-stacks (460 μm x 460 μm x ≥ 100 μm thick) were acquired from randomly selected regions. Confocal images were viewed using LSM 5 Image Browser (Zeiss). Culture viability was assessed by quantifying the number of live and dead cells. Neurite outgrowth was calculated by counting the number of neurites (≥ 10 μm in length) departing the somas from 12-24 randomly selected live neurons per culture.

Neuronal cultures were plated in unmodified AG and viability was assessed at 1 DIV (1.0%, n = 4; 1.5%, n = 4; 2.0%, n = 4; 3.0%, n = 3) and 8 DIV (1.0%, n = 4; 1.5%, n = 4). Using separate cultures, viability and neurite outgrowth were assessed at 2 DIV in neuronal cultures in AG (1.25%, n = 3), Col-AG (1.25%; $[Col]_i$ = 300 μg/mL or 600 μg/mL, n = 3 each), and MG (7.5 mg/mL, n = 3). Culture thickness was measured; viability was quantified as a function of depth into the matrix (based on 100 μm thick

sections from the top, middle, and bottom). The number of neurites per neuron and the percentage of live neurons extending neurites were counted. In other cultures, viability and neurite outgrowth were assessed at 7 – 8 DIV in AG (1.25%, n = 4), Col-AG (1.25%; $[Col]_i$ = 300 μg/mL or 600 μg/mL, n = 3 and 4 respectively), and MG (7.5 mg/mL, n = 6). General linear model ANOVA was performed followed by Tukey's pair-wise comparisons when appropriate ($p < 0.05$ required for significance).

2.3.5 Three-dimensional in vitro model of TBI

Neuronal cultures in Col-AG or MG were mechanically loaded using the 3-D Cell Shearing Device (CSD), a custom electro-mechanical device capable of reproducibly subjecting 3-D cell-containing matrices to high rate, simple shear deformation (LaPlaca et al. 2005). Cultures were plated in custom deformable cell culture chambers designed to interface with the 3-D CSD, and were deformed by the linear displacement of the chamber top plate with respect to the fixed cell reservoir base (Figure 2.1A). Bulk shear strains up to 0.50 (45° shear angle) at strain rates up to 30 s^{-1} simulate the spatial and temporal strain patterns associated with inertial TBI (Margulies and Thibault 1992), and result in heterogeneous 3-D strain fields throughout the cell-containing matrices dependent upon the initial cellular orientation within the matrix (LaPlaca et al. 2005).

Neurons were plated in Col-AG (1.5%; $[Col]_i$ = 30, 150, or 300 μg/mL) or MG (7.5 mg/mL). At 7 DIV, cultures were subjected to high rate loading (Col-AG: n = 5, 6, 7, respectively; MG: n = 8) or static control conditions (Col-AG: n = 4 each; MG: n = 11). At the time of loading, cell culture medium was removed from the culture, the top plate was gently mounted above the cell-containing matrices, and the chambers were loaded into the device. Neuronal cultures were coupled to the 3-D CSD and subjected to high

rate deformation using symmetric trapezoidal input (0.50 strain, 30 s^{-1} strain rate, 16.7 ms rise time, 5 ms hold time) (Figure 2.1C-D) or left as static controls (0.00 strain, 0 s^{-1} strain rate; Figure 2.1B). After the deformation (or control conditions) was applied, the top plate was removed, fresh medium was added (0.5 mL/well), and the cultures returned to the tissue culture incubator. Culture viability was assessed at 24 hours post-insult. Using two-way ANOVA, matrix and loading condition were independent variables and viability was the dependent variable, followed by Tukey's pair-wise comparisons ($p < 0.05$ for significance).

2.4 Results

2.4.1 Col-AG matrix characterization

The ability to chemically conjugate Col to an agarose backbone was assessed by evaluating the presence of Col in SFAD-conjugated agarose (Col-AG) in comparison to the presence of Col mixed with agarose without crosslinker (Col+AG). Immunostaining following the rinsing period revealed a statistically significant increase in the amount of Col present in the Col-AG versus the Col+AG samples ($p < 0.05$) (Figure 2.2). This demonstrated the effectiveness of the Col crosslinking reaction in coupling the Col to the agarose backbone. Additionally, the complex modulus was determined for AG (as a function of AG percentage), Col-AG (as a function of $[Col]_i$), and MG (7.5 mg/mL) under oscillatory shear strain for a range of frequencies where the material properties were linear. In agarose-only gels, the complex modulus increased proportionally with the AG percentage (data not shown), with values similar to those previously reported (Balgude et al. 2001; Yu and Bellamkonda 2001). For a fixed AG percentage (1.5%), the

complex modulus was determined based on $[Col]_i$ (ranging from 30 – 300 μg/mL), revealing that complex modulus increased as a function of $[Col]_i$, with significant differences between all groups with the exception of the Col(30 μg/mL)-AG versus AG, which were not statistically different. Thus, over the frequency range evaluated, the order of complex moduli was Col(300 μg/mL)-AG > Col(150 μg/mL)-AG > Col(30 μg/mL)-AG = AG, thus revealing a dependence between $[Col]_i$ and complex modulus within the range of [Col] evaluated. Furthermore, the complex moduli were greater in all agarose hydrogels (AG and Col-AG) compared to Matrigel ($p < 0.001$) (Figure 2.3).

2.4.2 Cell culture characterization

Baseline characterization of cortical neuronal culture development in unmodified agarose was performed to gain insight into the requisite physical properties permitting survival and neurite outgrowth. This analysis was performed at 1 and 8 DIV in order to assess the immediate and longer-term effects of AG concentration, and hence physical properties, on cortical neuronal survival. Over the range of AG concentrations evaluated (1.0 - 3.0%), neuronal viability at 1 DIV depended significantly on agarose percentage (viability was 37 ± 4.5% for 1.0% AG; 60 ± 23% for 1.5% AG; 68 ± 14% for 2.0% AG; 82 ± 8% for 3.0% AG). Higher concentration, and hence stiffer, gels resulted in increased survival (1.0% AG vs. 3.0% AG, $p < 0.01$; 1.0% AG vs. 2.0% AG, $p < 0.05$). Additionally, a subset of these parameters were evaluated at 8 DIV, revealing that agarose concentrations ≤ 1.0 % continued to yield minimal neurite outgrowth and poor survival (< 50%), whereas agarose concentrations of 1.5% resulted in viable cultures (~80%) with significant neurite outgrowth by this time point (not shown). While early viability was maximal with the highest AG%, subsequent studies revealed that higher

percentage agarose gels (> 2.0%) were not suitable for 3-D neurite outgrowth as the cortical neurons maintained a spherical morphology over longer time-points (data not shown). Thus, there was a range of matrix mechanical properties, based on a convergence of hydrogel pore size (constrictivity) and sufficient mechanical integrity (increasing complex modulus), where cortical neurons were found to thrive in unmodified agarose. Based on these findings, AG percentages in the range of 1.25 – 1.50 % were chosen for studies to optimize neuronal survival and neurite outgrowth as a function of $[Col]_i$.

Accordingly, neuronal viability and neurite outgrowth were evaluated in unmodified AG and Col-AG ($[Col]_i$ = 300 and 600 μg/mL) gels in comparison to a positive control MG matrix at 2 DIV (Figure 2.4A-D). Viability did not vary based on z-position or based on collagen presence or concentration (Figure 2.5); however, there were statistically significant increases in the percentage of neurons extending neurites as well as the mean number of neurites per neuron in MG and Col(300 μg/mL)-AG versus AG ($p < 0.05$), indicating that neurite outgrowth in 3-D cultures is dependent on $[Col]_i$ at certain agarose concentrations (Figure 2.6A-B). Furthermore, neurite outgrowth and neuronal viability were also evaluated at 7 – 8 DIV (Figure 2.4E-H). At this time point, neurite outgrowth in Col(300 μg/mL)-AG was not statistically different from that of MG in terms of the percentage of neurons extending neurites and the mean number of neurites per neuron ($p > 0.50$) (Figure 2.6A-B). However, neurite outgrowth was significantly reduced in AG ($p < 0.001$) and in Col(600 μg/mL)-AG ($p < 0.05$) compared to MG. It was also observed that the majority of somas in AG or Col-AG maintained a near-spherical morphology, regardless of whether or not they extended neurites. Conversely, neurons cultured in MG developed a range of complex (non-spherical) morphologies

with virtually all live neurons extending neurites. Neuronal survival, however, did not vary between Col(300 μg/mL)-AG, Col(600 μg/mL)-AG, and AG, and the viability in all these groups was statistically lower than that in MG ($p < 0.001$) (Figure 2.7).

2.4.3 Response to mechanical loading

To assess the roles of matrix mechanical properties and ligand density on the neuronal response to high rate deformation, 3-D neuronal cultures were plated in Col-AG ($[Col]_i$ = 30, 150, or 300 μg/mL) or MG and, at 7 DIV, mechanically loaded using the 3-D CSD (0.50 strain, 30 s^{-1} rate) or subjected to static control conditions. Culture viability was assessed at 24 hours post-insult (Figure 2.8). Neurite outgrowth and cell viability were similar in neuronal cultures over the range of $[Col]_i$ used; however, the viability in static control cultures was statistically lower in the Col-AG versus MG cultures ($p < 0.001$). Post-insult neuronal viability depended on the matrix type ($p < 0.05$), mechanical loading ($p < 0.001$), and interactions between these factors ($p < 0.001$). Following loading in the MG cultures, there was a significant decrease in neuronal viability versus MG static controls ($p < 0.001$). However, the response in the Col-AG cultures was dependent upon $[Col]_i$, as the viability in mechanically loaded cultures decreased as $[Col]_i$ increased. Specifically, the neuronal viability did not decrease relative to the respective static control at the lowest $[Col]_i$ evaluated (30 μg/mL); however, the viability was reduced compared to respective static controls for $[Col]_i$ of 150 μg/mL ($p < 0.05$) and 300 μg/mL ($p < 0.01$). The post-loading neuronal viability was similar in the Col(300 μg/mL)-AG and the MG cultures, potentially indicating a limit in injury-induced neuronal death based on the bulk loading parameters and time post-insult. Also, in order to account for differences in the baseline viability of the different static control groups,

this analysis was repeated with the post-loading viability normalized to viability of their respective static control. The normalized post-insult viabilities of MG, Col(150 µg/mL)-AG, and Col(300 µg/mL)-AG groups did not statistically vary ($p > 0.2$); however, the normalized viability of Col(30 µg/mL)-AG was statistically higher than the other groups ($p < 0.05$). Thus, the post-insult reduction in culture viability was equivalent in MG compared to agarose cultures with higher $[Col]_i$, but not low $[Col]_i$.

2.5 Discussion

A 3-D culture system was developed that can be exploited to analyze the effects of controlled matrix composition and bulk matrix mechanical properties on neuronal viability, neurite outgrowth, and the neuronal response to high rate deformation. This neurobiological system demonstrates the dependence of culture environment and architecture on neuronal function and has implications for the development of tissue equivalents for both *in vitro* and *in vivo* applications. Neuronal viability and neurite outgrowth were evaluated over a range of agarose and collagen concentrations in order to optimize culture parameters in this 3-D engineered system. In the acute period following cell seeding, AG concentration, and hence matrix complex modulus, dictated neuronal viability with softer AG gels resulting in reduced survival. The collagen content of Col-AG matrices significantly influenced the matrix complex modulus, and in these matrices at 2 DIV for a fixed AG percentage, neuronal survival did not vary based on $[Col]_i$, but neurite outgrowth was found to be enhanced at the mid-range $[Col]_i$ assayed. This trend continued at 7 DIV, with neurite outgrowth demonstrating a non-linear relationship with respect to $[Col]_i$, but survival not being influenced by $[Col]_i$. These results suggest that neuronal viability and neurite outgrowth in 3-D depend on interrelated biochemical and

physical properties, with initial neuronal survival dependent on matrix complex modulus and neurite outgrowth varying with ligand density. Overall, optimized agarose percentages (1.25 – 1.50%) with a photoimmobolized ECM ($[Col]_i$ = 30 - 300 μg/mL) permitted development of thick, 3-D neuronal cultures with a network of interconnecting neurites throughout all spatial dimensions, with neurite outgrowth, but not survival, similar to a positive control matrix.

It is desirable for 3-D culture development and tissue engineering applications to have a fundamental understanding of interactions between physical and biochemical matrix properties in the ability to support the viability and growth of cells. Parameters of neurite outgrowth such as growth rate and neurite branching depend on matrix mechanical properties (in 3-D and 2-D) (Balgude et al. 2001; Flanagan et al. 2002) as well as ligand presence/density (Krewson et al. 1994; Bellamkonda et al. 1995a; Bellamkonda et al. 1995b; Schense and Hubbell 2000; Willits and Skornia 2004). Neuronal survival and neurite outgrowth in 3-D matrices may be influenced by intrinsic (e.g., neuronal maturation, receptor expression) as well as extrinsic (e.g., matrix mechanical properties, ligand concentration) signals. For example, the effects of agarose concentration on DRG neurite outgrowth revealed matrix stiffness and pore size differentially influence the rate and degree of neurite extension, with maximal neurite outgrowth occurring in low concentration (<1.00%) gels (Bellamkonda et al. 1995b; Dillon et al. 1998; Balgude et al. 2001). However, low concentration hydrogels have been shown to be unsuitable for the survival and neurite outgrowth of cortical neurons in the present study as well as previous work (O'Connor et al. 2001), underscoring that different intrinsic mechanisms exist between different neuronal sub-types, and thus engineered

systems must be optimized for a particular neuronal population. DRG neurite outgrowth was studied in collagen matrices of varying concentrations, and hence stiffness, finding that neurite extension was maximized in lower (0.6 mg/mL) rather than higher (2 mg/mL) concentration gels (Willits and Skornia 2004). Taken together, these studies suggest that matrix stiffness may be a good predictor of neurite outgrowth in the absence of ligand presence (Balgude et al. 2001). However, the addition of significant ligand binding revealed a non-linear relationship between ligand concentration and neurite outgrowth in the present study, as well as previous work demonstrating intermediate ligand densities resulted in maximal DRG neurite extension with higher densities inhibiting outgrowth (Schense and Hubbell 2000). Thus, optimized neurite outgrowth and survival for a particular neuronal sub-type may require a specific range of ligand density, matrix complex modulus, and pore size, with optimized ranges for one factor potentially related to the state of other factors. This model system is advantageous in that it is relatively simple and increasing levels of complexity (including other ECM ligands and additional cell types) can systematically be added to further manipulate culture properties.

Another consideration is the use of neurons harvested from embryonic rats for comparison to adult models of brain injury. The use of embryonic neurons is a matter of necessity: cell harvests from adult rat brains typically yield a heterogeneous cell population with low neuronal viability. The primary cortical neuron harvest from embryonic day 17-18 rats however yields a mostly neuronal population with high viability. Culturing these neurons allows for them to mature, developing a branched and interconnected morphology within a week of plating. Spontaneous electrophysiological activity begins by 10 to 14 days, and a previous study shows few differences between the

electrophysiology of neurons harvested from embryonic and adult rats (Evans et al. 1998). For these reasons neurons from embryonic sources have been accepted for use in this and other culture systems.

Neuronal cultures in optimized Col-AG ranges were utilized to investigate the effects of matrix mechanical properties and ligand density on acute mechanotransduction events associated with high rate shear deformation (0.50 strain, 30 s^{-1} strain rate). This 3-D model of traumatic neural loading may be suitable for the investigation of defined strain transfer to individual neurons and analysis of the roles of specific parameters in the subsequent pathology with a temporal and spatial resolution not currently possible *in vivo*. Specifically, given morphological and force transduction alterations between cells cultured in 2-D and 3-D, this system may better recreate complex, 3-D cellular biomechanics associated with traumatic loading *in vivo*, and may be more appropriate to model the effects of specific receptor-mediated interactions in acute mechanotransduction events and subsequent intracellular signaling following a defined mechanical input. The bulk mechanical properties of brain tissue varies based on the type of sample and the testing parameters, but it should be noted that the stiffness of the hydrogels presented in this study are comparable to that of native brains (Gefen et al. 2003).

In the current study, the post-loading viability in Col-AG neuronal cultures decreased with increasing $[Col]_i$ and with increasing complex modulus, indicating that both factors may work in concert to translate bulk shear deformation to cells. The physical properties of the matrix material, including complex modulus and pore characteristics (e.g., the mean pore size for 1.5% AG is 150 nm (Bellamkonda et al. 1995b)) influence the degree to which cells were contained within the matrix material,

and as such they may dictate whether forces deforming the gel (i.e. bulk shear deformation) were translated to and thus deform the cells within the gel. Additionally, receptor-mediated cell-matrix interactions may also influence the translation of forces from bulk matrix deformation to cellular deformation. Cell-ECM adhesions may increase the fidelity of deformation transfer from matrix to cellular deformation, and serve as areas where forces are acutely translated to create local stress concentrations. This stress distribution may influence the probability of structural failure, and resulting biophysical disruptions of the plasma membrane, for example, may alter ionic homeostasis (LaPlaca et al. 1997; Geddes et al. 2003b), initiating abnormal neuronal signaling and leading to cell death (Raghupathi 2004). Additionally, cell surface receptor-mediated mechanotransduction may contribute to biochemical alterations following high rate deformation, possibly initiating neuronal dysfunction and/or death. While mechanotransduction is generally considered in a homeostatic context (e.g., cells relying on mechanical stimulation to sense environmental cues), it may also contribute to neuronal dysfunction by altering the balance of phosphatase/kinase activity (Genis et al. 2000; Dash et al. 2002; Mori et al. 2002) and activating Ca^{2+}-dependent proteases that degrade cytoskeletal elements (Fitzpatrick et al. 1998; Huh et al. 2002; Volbracht et al. 2005). Future studies will aim to determine the contribution of specific receptor-mediated cell-ECM interactions to altered, and potentially detrimental, intracellular signaling events following high rate loading.

With plasma membrane damage being the focus of Chapter 3 of this thesis, measurement of plasma membrane damage following injury *in vitro* was attempted with this model. By replicating *in vitro* the plasma membrane damage observed *in vivo*, the *in*

vitro injury model could have been used to elucidate a strain threshold for plasma membrane damage and investigate the pathways by which plasma membrane damage leads to neuronal dysfunction and death. However numerous attempts to measure plasma membrane damage using the dye exclusion assay with a fluorescent dextran were unsuccessful. The dye exclusion assay is dependent on adequate contrast between intracellular and extracellular dye, but in this system it was not possible to sufficiently rinse away extracellular dye from the hydrogel to identify permeable cells, potentially because of the thickness of the cultures or an affinity between the dye and the culture scaffold. As such, permeable cells were of the same fluorescent intensity as background when visualized using both fluorescent and laser scanning confocal microscopy techniques. To work around this limitation, the cultures were frozen and sectioned into thin sections. This improved the contrast between permeable cells and background, but the thin cryosections reduced the number of cells visible for quantification.

Alternatively, using ethidium homodimer or propidium iodide may have allowed improved visualization of permeable cell bodies, as the fluorescence of the molecules increase when they bind DNA. This methodology was not pursued for several reasons. First, the intention was to compare the permeability profile of injured neurons *in vitro* with the *in vivo* study in Chapter 3. However with molecular weights of 857 Da and 668 Da respectively, ethidium homodimer and propidium iodide are significantly smaller than the 3000 Da dextran used for the *in vivo* study. Molecular weight and charge affect how a molecule can diffuse, and previous studies have shown that permeability marker size and charge determine the extent of its uptake (Eddleman et al. 1998; Geddes et al. 2003a). Second, one of the assets of this *in vitro* injury model is that local cellular strains (rather

than the bulk deformation of the entire culture) are dependent on the orientation of the cells in 3-D within the culture (Cullen and LaPlaca 2006). Using a nuclear dye limits visualization of permeable cells to their somata and neglects their extensions, preventing any determination of cell orientation; thus inferences of correlation between cell level strains and observed permeability would not have been possible. Finally, use of molecule like ethidium or propidium iodide that bind DNA could potentially affect cell function, precluding the studies of the mechanisms of cell death that were desired by replicating plasma membrane damage *in vitro*. Thus attempts to characterize plasma membrane damage *in vitro* using this model were unsuccessful.

This is the first report of a ligand concentration-dependent response to high rate mechanical loading in a 3-D configuration, demonstrating that both the biochemical and physical properties of the culture environment are important considerations. This 3-D cellular model of neural trauma is capable of systematically evaluating the role of cell-ECM interactions in the response to a well-defined deformation. An increased understanding of deleterious biochemical pathways initiated by acute mechanotransduction events may uncover potential therapeutic targets for prevention of widespread cellular dysfunction, death, and neurodegeneration following neural trauma. Furthermore, this system has several applications in neurobiology and tissue engineering, both of which require control over the extracellular culture configuration and related interactions in order to better mimic tissue composition and properties.

2.6 Note

Please note the text of this chapter was adapted from work originally published in the Annals of Biomedical Engineering in 2007 with co-first authors Cullen and Lessing

contributing equally to the manuscript (Cullen et al. 2007). Reference: Cullen, D. K., M. C. Lessing, M. C. LaPlaca. (2007). "Collagen-dependent neurite outgrowth and response to dynamic deformation in three-dimensional neuronal cultures." Annals Of Biomedical Engineering 35(5): 835-46.

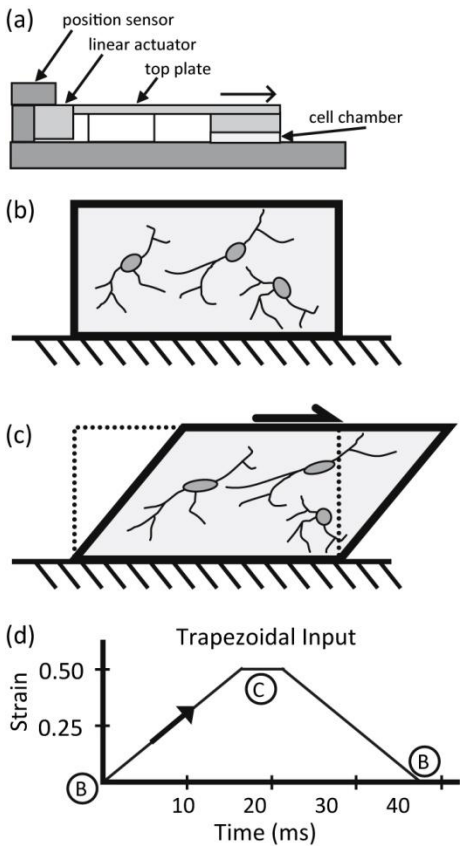

Figure 2.1: 3-D *in vitro* injury model

Schematic of the custom-built electro-mechanical 3-D Cell Shearing Device (CSD) interfacing with neuronal cultures (A). Side view showing an undeformed 3-D neuronal cell culture in the cell chamber (B). High rate deformation was imparted to the 3-D cell-containing matrices through the horizontal motion of the cell culture top plate while the culture base was held fixed (C). Mechanical loading of the 3-D cell-containing matrices followed a symmetrical trapezoidal input to 0.50 shear strain at a 30 s^{-1} strain rate, resulting in a 16.7 ms rise time and 5 ms hold time for the deformation (D). The points of no deformation (B) and peak deformation (C) are indicated on the loading profile.

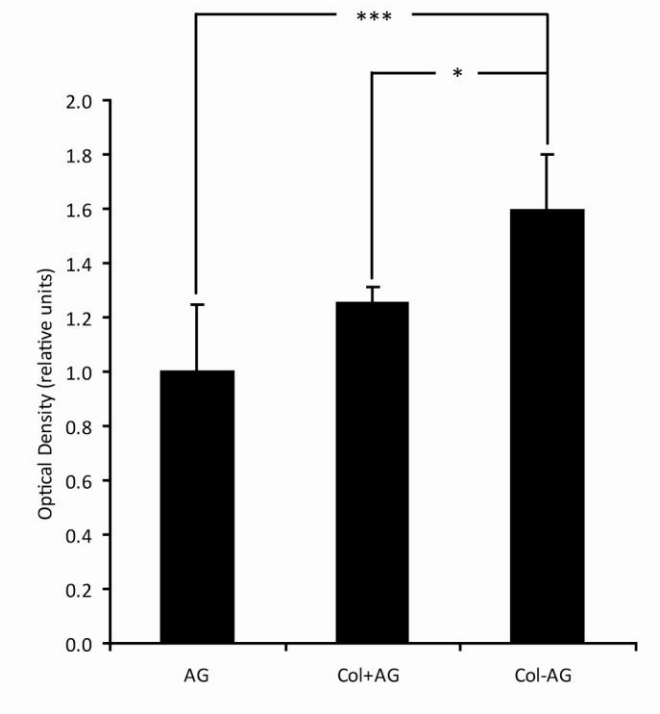

Figure 2.2: Confirmation of crosslinking reaction

Efficacy of the collagen-agarose crosslinking reaction was confirmed by comparing the presence of fluorescently-labeled collagen in SFAD-conjugated agarose (Col-AG) to the presence of fluorescently-labeled collagen mixed with agarose without crosslinker (Col+AG). There was a statistically significant increase in the fluorescence intensity in the Col-AG group versus the Col+AG group (*, $p < 0.05$) and the AG group (***, $p < 0.001$). Data were normalized to background reading attained from unmodified AG (no Col) gels; data presented as mean ± standard deviation.

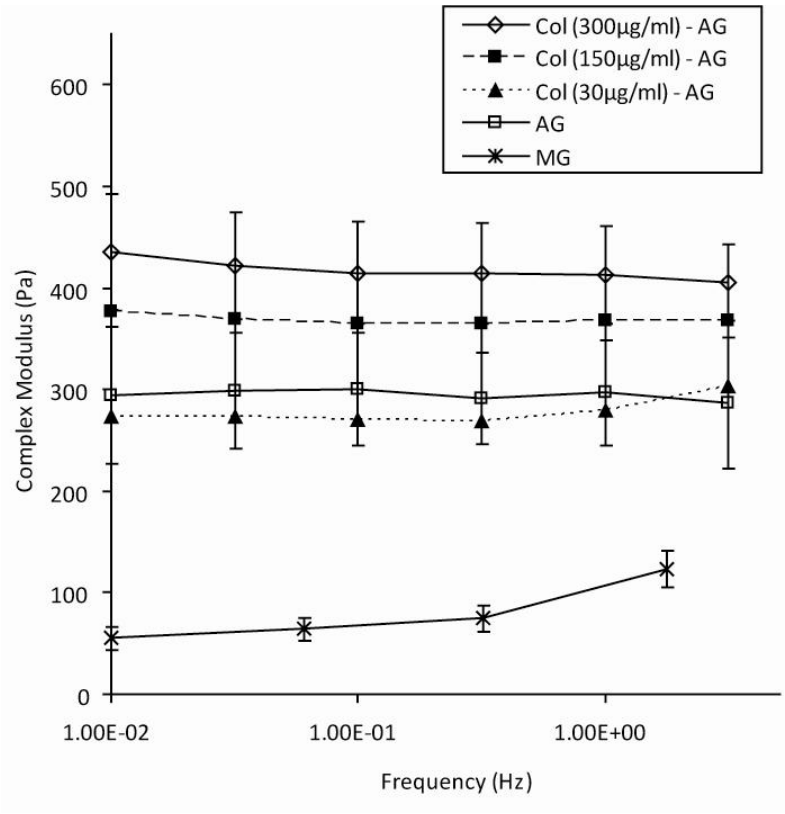

Figure 2.3: Mechanical properties of agarose gel

The complex modulus was determined for Matrigel (MG), unmodified agarose (AG), and collagen-conjugated agarose (Col-AG) hydrogels. There were statistically significant differences between all groups with the exception of the Col(30 µg/mL)-AG and AG. The complex moduli were greater in all agarose hydrogels (AG and Col-AG) compared to Matrigel ($p < 0.001$). In Col-AG samples, there was a correlation between increasing $[Col]_i$ and increasing complex modulus within the range of $[Col]_i$ evaluated. Data presented as mean ± standard deviation.

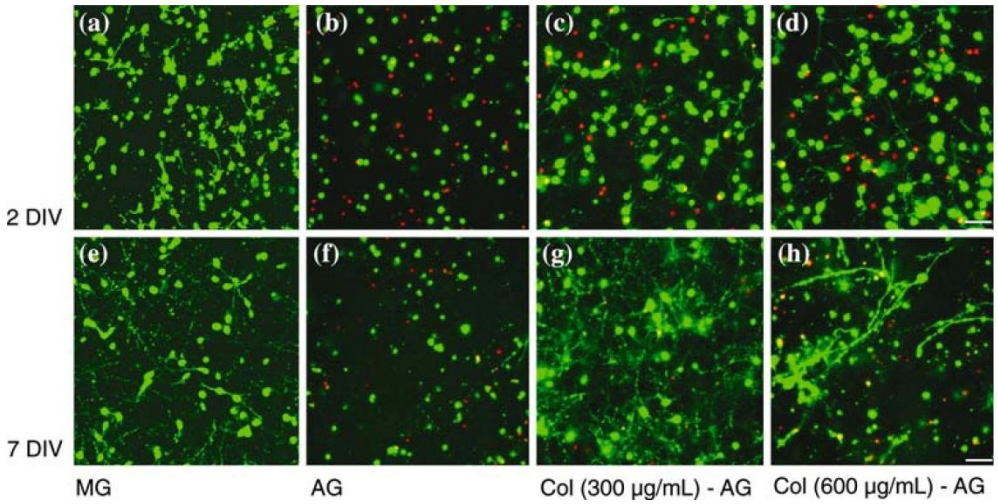

Figure 2.4: Cultures in Col-AG hydrogels

Neuronal viability was evaluated neuronal cultures in MG (A, E), AG (B, F), Col(300 µg/mL)-AG (C, G), and Col(600 µg/mL)-AG (D, H) at 2 DIV (A-D) and 7 DIV (E-H) by staining with calcein-AM (live cells stained green) and ethidium homodimer (dead cells stained red). (scale bar = 50 µm)

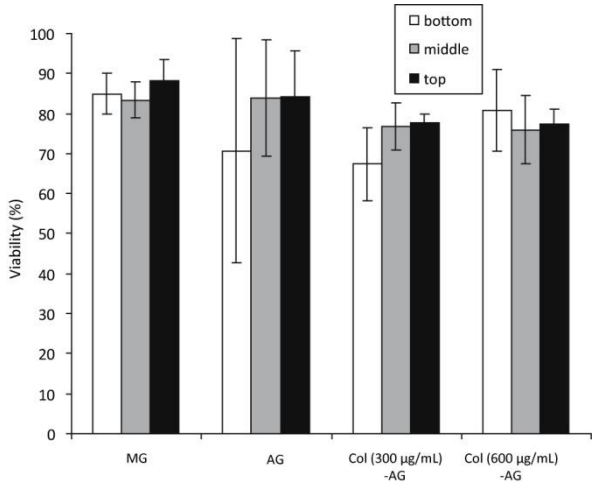

Figure 2.5: Neuronal viability at 2 days

Viability of neuronal cultures in MG, AG, Col(300 µg/mL)-AG, and Col(600 µg/mL)-AG did not vary at 2 DIV based on z-position or based on collagen presence or concentration. ($p > 0.05$)

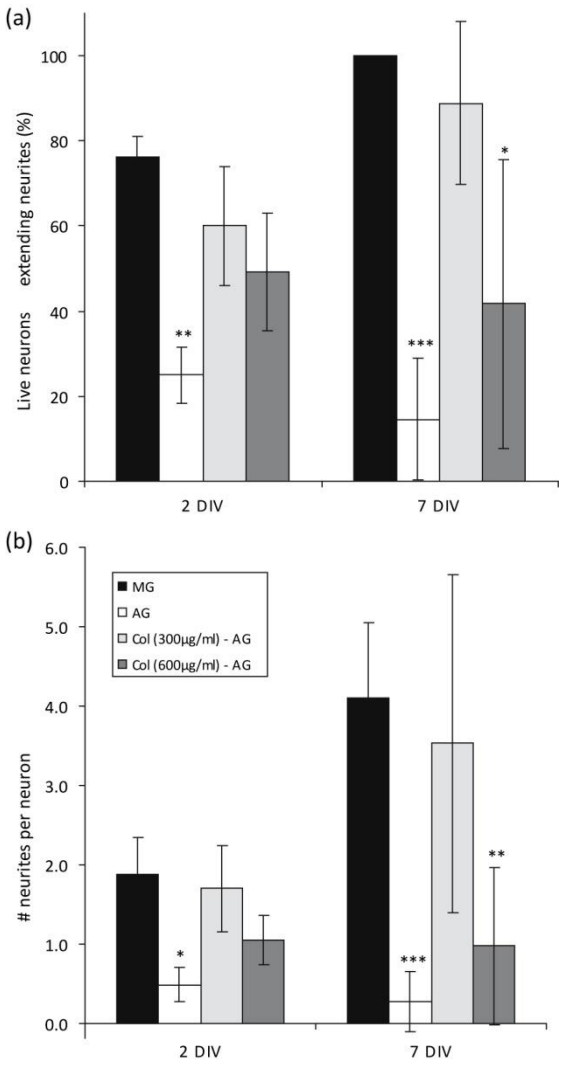

Figure 2.6: Neurite outgrowth in Col-AG hydrogels

Neurite outgrowth in neuronal cultures in MG, AG, Col(300 μg/mL)-AG, and Col(600 μg/mL)-AG varies with Col content. At 2 DIV there were statistically significant decreases in the (A) percentage of live neurons extending neurites and (B) the number of neurites per neurons in AG and compared to MG (**, $p < 0.01$; *, $p < 0.05$); statistically there was no difference between MG, Col(300 μg/mL)-AG, and Col(600 μg/mL)-AG. At 7 DIV the (A) percentage of neurons extending neurites and (B) the number of neurites per neuron were statistically less than MG for cultures in AG (***, $p < 0.001$) and Col(600 μg/mL)-AG (*, $p < 0.05$; **, $p < 0.01$); statistically there was no difference in

neurite outgrowth between MG and Col(300 μg/mL)-AG ($p > 0.05$). Data presented as mean ± standard deviation.

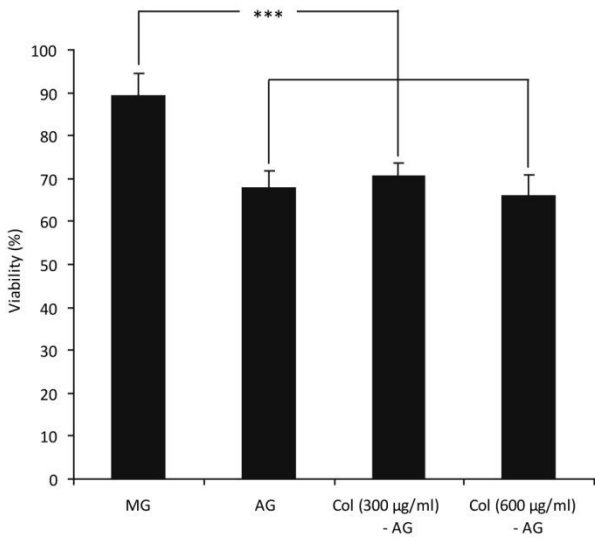

Figure 2.7: Neuronal viability after 7 days

The viability of 3-D neuronal cultures in MG, AG, Col(300 µg/mL)-AG, and Col(600 µg/mL)-AG was quantified at 7 DIV. There were no statistical differences in neuronal survival in between AG, Col(300 µg/mL)-AG, and Col(600 µg/mL)-AG cultures. However, the AG and Col-AG groups had significantly lower neuronal viability than MG cultures (***, $p < 0.001$). Data presented as mean ± standard deviation.

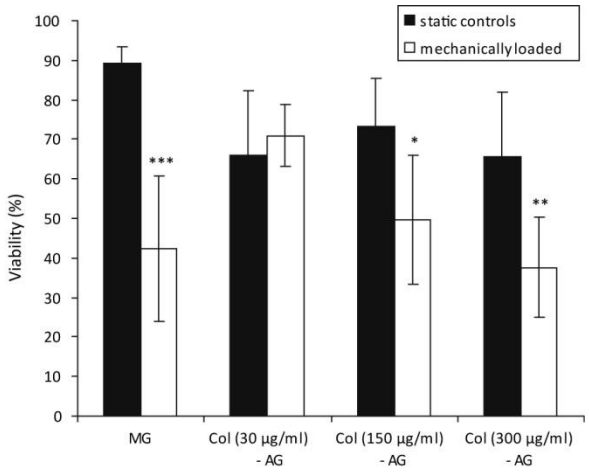

Figure 2.8: Neuronal viability after injury

The response to high-rate deformation of 3-D neuronal cultures in Col-AG ($[Col]_i$ = 30, 150, and 300 µg/mL) was compared to the response in MG cultures. At 7 DIV, 3-D neuronal cultures were either subjected to static control conditions (0.00 strain, 0 s^{-1} strain rate) or mechanically loaded (0.50 strain, 30 s^{-1} strain rate), and culture viability was determined 24 hrs post-loading. The viability of static controls in Col-AG was statistically lower than in MG static controls ($p < 0.001$). Following high rate deformation, there was a significant reduction in culture viability in MG (***, $p < 0.001$) as well as in the Col(150 µg/mL)-AG (*, $p < 0.05$) and the Col(300 µg/mL)-AG (**, $p < 0.01$) cultures. However, in the lowest $[Col]_i$, Col(30 µg/mL)-AG, there was not a statistically significant decrease in viability following high rate deformation. Data presented as mean ± standard deviation.

2.7 Works cited

Adelson, P. D., C. E. Dixon and P. M. Kochanek (2000). "Long-term dysfunction following diffuse traumatic brain injury in the immature rat." J Neurotrauma **17**(4): 273-82.

Alenghat, F. J. and D. E. Ingber (2002). "Mechanotransduction: all signals point to cytoskeleton, matrix, and integrins." Sci STKE **2002**(119): PE6.

Anderson, K. L. and A. Ferreira (2004). "alpha1 Integrin activation: a link between beta-amyloid deposition and neuronal death in aging hippocampal neurons." J Neurosci Res **75**(5): 688-97.

Arregui, C. O., S. Carbonetto and L. McKerracher (1994). "Characterization of neural cell adhesion sites: point contacts are the sites of interaction between integrins and the cytoskeleton in PC12 cells." J Neurosci **14**(11 Pt 2): 6967-77.

Balgude, A. P., X. Yu, A. Szymanski and R. V. Bellamkonda (2001). "Agarose gel stiffness determines rate of DRG neurite extension in 3D cultures." Biomaterials **22**(10): 1077-1084.

Bellamkonda, R., J. P. Ranieri and P. Aebischer (1995a). "Laminin oligopeptide derivatized agarose gels allow three-dimensional neurite extension in vitro." J Neurosci Res **41**(4): 501-9.

Bellamkonda, R., J. P. Ranieri, N. Bouche and P. Aebischer (1995b). "Hydrogel-based three-dimensional matrix for neural cells." J Biomed Mater Res **29**(5): 663-71.

Bradshaw, A. D., K. M. McNagny, D. B. Gervin, G. M. Cann, T. Graf and D. O. Clegg (1995). "Integrin alpha 2 beta 1 mediates interactions between developing embryonic retinal cells and collagen." Development **121**(11): 3593-602.

Carmeliet, G., B. Himpens and J. J. Cassiman (1994). "Selective increase in the binding of the alpha 1 beta 1 integrin for collagen type IV during neurite outgrowth of human neuroblastoma TR 14 cells." J Cell Sci **107 (Pt 12)**: 3379-92.

Cavalcanti-Adam, E. A., P. Tomakidi, M. Bezler and J. P. Spatz (2005). "Geometric organization of the extracellular matrix in the control of integrin-mediated adhesion and cell function in osteoblasts." Prog Orthod **6**(2): 232-7.

Cukierman, E., R. Pankov, D. R. Stevens and K. M. Yamada (2001). "Taking cell-matrix adhesions to the third dimension." Science **294**(5547): 1708-1712.

Cukierman, E., R. Pankov and K. M. Yamada (2002). "Cell interactions with three-dimensional matrices." Curr Opin Cell Biol **14**(5): 633-639.

Cullen, D. K. and M. C. LaPlaca (2006). "Neuronal response to high rate shear deformation depends on heterogeneity of the local strain field." Journal Of Neurotrauma **23**(9): 1304-1319.

Cullen, D. K., M. C. Lessing and M. C. LaPlaca (2007). "Collagen-dependent neurite outgrowth and response to dynamic deformation in three-dimensional neuronal cultures." Annals Of Biomedical Engineering **35**(5): 835-46.

Danen, E. H. and A. Sonnenberg (2003). "Integrins in regulation of tissue development and function." J Pathol **201**(4): 632-41.

Dash, P. K., S. A. Mach and A. N. Moore (2002). "The role of extracellular signal-regulated kinase in cognitive and motor deficits following experimental traumatic brain injury." Neuroscience **114**(3): 755-67.

De Arcangelis, A. and E. Georges-Labouesse (2000). "Integrin and ECM functions: roles in vertebrate development." Trends Genet **16**(9): 389-95.

Dillon, G. P., X. Yu, A. Sridharan, J. P. Ranieri and R. V. Bellamkonda (1998). "The influence of physical structure and charge on neurite extension in a 3D hydrogel scaffold." J Biomater Sci Polym Ed **9**(10): 1049-69.

Dodla, M. C. and R. V. Bellamkonda (2006). "Anisotropic scaffolds facilitate enhanced neurite extension in vitro." Journal of Biomedical Materials Research Part A **78A**(2): 213-221.

Dolz, R., J. Engel and K. Kuhn (1988). "Folding of collagen IV." Eur J Biochem **178**(2): 357-66.

Eddleman, C. S., M. E. Smyers, A. Lore, H. M. Fishman and G. D. Bittner (1998). "Anomalies associated with dye exclusion as a measure of axolemmal repair in vertebrate axons." Neuroscience Letters **256**(3): 123-126.

Ellis, E. F., J. S. McKinney, K. A. Willoughby, S. Liang and J. T. Povlishock (1995). "A new model for rapid stretch-induced injury of cells in culture: characterization of the model using astrocytes." J Neurotrauma **12**(3): 325-339.

Evans, M. S., M. A. Collings and G. J. Brewer (1998). "Electrophysiology of embryonic, adult and aged rat hippocampal neurons in serum-free culture." Journal Of Neuroscience Methods **79**: 37-46.

Fawcett, J. W., R. A. Barker and S. B. Dunnett (1995). "Dopaminergic neuronal survival and the effects of bFGF in explant, three dimensional and monolayer cultures of embryonic rat ventral mesencephalon." Exp Brain Res **106**(2): 275-282.

Fitzpatrick, M. O., D. Dewar, G. M. Teasdale and D. I. Graham (1998). "The neuronal cytoskeleton in acute brain injury." Br J Neurosurg **12**(4): 313-7.

Flanagan, L. A., Y. E. Ju, B. Marg, M. Osterfield and P. A. Janmey (2002). "Neurite branching on deformable substrates." Neuroreport **13**(18): 2411-5.

Geddes, D. M. and R. S. Cargill, 2nd (2001). "An in vitro model of neural trauma: device characterization and calcium response to mechanical stretch." J Biomech Eng **123**(3): 247-255.

Geddes, D. M., R. S. Cargill, 2nd and M. C. LaPlaca (2003a). "Mechanical stretch to neurons results in a strain rate and magnitude-dependent increase in plasma membrane permeability." Journal Of Neurotrauma **20**(10): 1039-49.

Geddes, D. M., M. C. LaPlaca and R. S. Cargill (2003b). "Susceptibility of hippocampal neurons to mechanically induced injury." Experimental Neurology **184**(1): 420-427.

Gefen, A., N. Gefen, Q. Zhu, R. Raghupathi and S. S. Margulies (2003). "Age-dependent changes in material properties of the brain and braincase of the rat." J Neurotrauma **20**(11): 1163-77.

Genis, L., Y. Chen, E. Shohami and D. M. Michaelson (2000). "Tau hyperphosphorylation in apolipoprotein E-deficient and control mice after closed head injury." J Neurosci Res **60**(4): 559-64.

Granet, C., N. Laroche, L. Vico, C. Alexandre and M. H. Lafage-Proust (1998). "Rotating-wall vessels, promising bioreactors for osteoblastic cell culture: comparison with other 3D conditions." Med Biol Eng Comput **36**(4): 513-519.

Gumbiner, B. M. and K. M. Yamada (1995). "Cell-to-cell contact and extracellular matrix." Curr Opin Cell Biol **7**(5): 615-8.

Hamill, O. P. and B. Martinac (2001). "Molecular basis of mechanotransduction in living cells." Physiol Rev **81**(2): 685-740.

Hoffman, R. M. (1993). "To do tissue culture in two or three dimensions? That is the question." Stem Cells **11**(2): 105-11.

Huh, J. W., H. L. Laurer, R. Raghupathi, M. A. Helfaer and K. E. Saatman (2002). "Rapid loss and partial recovery of neurofilament immunostaining following focal brain injury in mice." Exp Neurol **175**(1): 198-208.

Ingber, D. E. (1997). "Tensegrity: the architectural basis of cellular mechanotransduction." Annu Rev Physiol **59**: 575-99.

Jin, H. and J. Varner (2004). "Integrins: roles in cancer development and as treatment targets." Br J Cancer **90**(3): 561-5.

Kamm, R. D. and M. R. Kaazempur-Mofrad (2004). "On the molecular basis for mechanotransduction." Mech Chem Biosyst **1**(3): 201-9.

Kleinman, H. K., M. L. McGarvey, J. R. Hassell, V. L. Star, F. B. Cannon, G. W. Laurie and G. R. Martin (1986). "Basement membrane complexes with biological activity." Biochemistry **25**(2): 312-8.

Ko, K. S. and C. A. McCulloch (2001). "Intercellular mechanotransduction: cellular circuits that coordinate tissue responses to mechanical loading." Biochem Biophys Res Commun **285**(5): 1077-83.

Krewson, C., S. Chung, W. Dai and W. Saltzman (1994). "Cell-aggregation and neurite growth in gels of extracellular-matrix molecules." Biotechnology and Bioengineering **43**(7): 555-562.

Langlois, J., W. Rutland-Brown and K. Thomas (2004). "Traumatic brain injury in the United States: emergency department visits, hospitalizations, and deaths."

LaPlaca, M. C., D. K. Cullen, J. J. McLoughlin and R. S. Cargill II (2005). "High Rate Shear Strain of Three-Dimensional Neural Cell Cultures: A New In Vitro Traumatic Brain Injury Model." J Biomech **38**(-): 1093-1105.

LaPlaca, M. C., V. M. Lee and L. E. Thibault (1997). "An in vitro model of traumatic neuronal injury: loading rate-dependent changes in acute cytosolic calcium and lactate dehydrogenase release." J Neurotrauma **14**(6): 355-68.

Li, B. S., L. Zhang, J. Gu, N. D. Amin and H. C. Pant (2000). "Integrin alpha(1) beta(1)-mediated activation of cyclin-dependent kinase 5 activity is involved in neurite outgrowth and human neurofilament protein H Lys-Ser-Pro tail domain phosphorylation." J Neurosci **20**(16): 6055-62.

Margulies, S. S. and L. E. Thibault (1992). "A proposed tolerance criterion for diffuse axonal injury in man." J Biomech **25**(8): 917-23.

Masi, L., A. Franchi, M. Santucci, D. Danielli, L. Arganini, V. Giannone, L. Formigli, S. Benvenuti, A. Tanini, F. Beghe and et al. (1992). "Adhesion, growth, and matrix production by osteoblasts on collagen substrata." Calcif Tissue Int **51**(3): 202-12.

Mori, T., X. Wang, J. C. Jung, T. Sumii, A. B. Singhal, M. E. Fini, C. E. Dixon, A. Alessandrini and E. H. Lo (2002). "Mitogen-activated protein kinase inhibition in traumatic brain injury: in vitro and in vivo effects." J Cereb Blood Flow Metab **22**(4): 444-52.

Nakayama, Y., Y. Aoki and H. Niitsu (2001). "Studies on the mechanisms responsible for the formation of focal swellings on neuronal processes using a novel in vitro model of axonal injury." J Neurotrauma **18**(5): 545-54.

O'Connor, S. M., J. D. Andreadis, K. M. Shaffer, W. Ma, J. J. Pancrazio and D. A. Stenger (2000). "Immobilization of neural cells in three-dimensional matrices for biosensor applications." Biosens Bioelectron **14**(10-11): 871-81.

O'Connor, S. M., D. A. Stenger, K. M. Shaffer and W. Ma (2001). "Survival and neurite outgrowth of rat cortical neurons in three-dimensional agarose and collagen gel matrices." Neurosci Lett **304**(3): 189-93.

Povlishock, J. T. and D. I. Katz (2005). "Update of neuropathology and neurological recovery after traumatic brain injury." J Head Trauma Rehabil **20**(1): 76-94.

Raghupathi, R. (2004). "Cell death mechanisms following traumatic brain injury." Brain Pathol **14**(2): 215-22.

Roskelley, C. D., P. Y. Desprez and M. J. Bissell (1994). "Extracellular matrix-dependent tissue-specific gene expression in mammary epithelial cells requires both physical and biochemical signal transduction." Proc Natl Acad Sci U S A **91**(26): 12378-82.

Schense, J. C. and J. A. Hubbell (2000). "Three-dimensional migration of neurites is mediated by adhesion site density and affinity." J Biol Chem **275**(10): 6813-8.

Schmeichel, K. L. and M. J. Bissell (2003). "Modeling tissue-specific signaling and organ function in three dimensions." J Cell Sci **116**(Pt 12): 2377-88.

Sjaastad, M. D., B. Angres, R. S. Lewis and W. J. Nelson (1994). "Feedback regulation of cell-substratum adhesion by integrin-mediated intracellular Ca2+ signaling." Proc Natl Acad Sci U S A **91**(17): 8214-8.

Smith, D. H., J. A. Wolf, T. A. Lusardi, V. M. Lee and D. F. Meaney (1999). "High tolerance and delayed elastic response of cultured axons to dynamic stretch injury." J Neurosci **19**(11): 4263-9.

Thurman, D. J., C. Alverson, K. A. Dunn, J. Guerrero and J. E. Sniezek (1999). "Traumatic brain injury in the United States: A public health perspective." J Head Trauma Rehabil **14**(6): 602-15.

Tomaselli, K. J. (1991). "Beta 1-integrin-mediated neuronal responses to extracellular matrix proteins." Ann N Y Acad Sci **633**: 100-4.

Volbracht, C., B. T. Chua, C. P. Ng, B. A. Bahr, W. Hong and P. Li (2005). "The critical role of calpain versus caspase activation in excitotoxic injury induced by nitric oxide." J Neurochem **93**(5): 1280-92.

Wehrle-Haller, B. and B. A. Imhof (2003). "Integrin-dependent pathologies." J Pathol **200**(4): 481-7.

Willits, R. K. and S. L. Skornia (2004). "Effect of collagen gel stiffness on neurite extension." J Biomater Sci Polym Ed **15**(12): 1521-31.

Woerly, S., G. W. Plant and A. R. Harvey (1996). "Cultured rat neuronal and glial cells entrapped within hydrogel polymer matrices: a potential tool for neural tissue replacement." Neurosci Lett **205**(3): 197-201.

Yamada, K. M., R. Pankov and E. Cukierman (2003). "Dimensions and dynamics in integrin function." Braz J Med Biol Res **36**(8): 959-66.

Yu, T. T. and M. S. Shoichet (2005). "Guided cell adhesion and outgrowth in peptide-modified channels for neural tissue engineering." Biomaterials **26**(13): 1507-14.

Yu, X. and R. V. Bellamkonda (2001). "Dorsal root ganglia neurite extension is inhibited by mechanical and chondroitin sulfate-rich interfaces." J Neurosci Res **66**(2): 303-10.

CHAPTER 3

SUBREGIONAL VULNERABILITY OF HIPPOCAMPAL NEURONS TO PLASMA MEMBRANE DAMAGE AND DEGENERATION FOLLOWING CONTROLLED CORTICAL IMPACT IN RATS

3.1 Abstract

Recent efforts to characterize TBI on the cellular level show that a mechanical insult to the brain results in increases in cellular plasma membrane permeability. Membrane damage, whether transient or persistent, allows non-specific flux of ions and other molecules across the plasma membrane, and these events triggered by membrane damage may ultimately lead to cell dysfunction or death. The goal of this study was to examine the spatial distribution and coincidence of plasma membrane damage and neuronal degeneration in the rat hippocampus following brain injury. Adult male rats received an intrathecal injection of permeability marker (rhodamine-conjugated 3 kDa dextran) followed by controlled cortical impact (3 m/s velocity, 2 mm depth) over the left frontoparietal cortex, and animals were sacrificed at either 10 min or 24 hr after injury. Immunostaining for neuronal nuclei suggests permeable cells were predominately of neuronal phenotype. Permeable cells were located primarily in the dentate gyrus subregion of the ipsilateral hippocampus of injured rats at 10 minutes post-injury; however by 24 hours there was a significant increase in the number of permeable cells in the same subregions of the contralateral hippocampus of injured rats as well. Within the hippocampus cellular uptake of permeability marker was heterogeneous as adjacent cells

exhibited different levels of marker uptake, suggesting different thresholds for membrane breaches, or alternatively, local heterogeneous strains. Fluoro-Jade B staining revealed degenerating neurons in the same subregions of the hippocampus in which permeable cells were identified. Analysis of colocalization of permeability marker uptake and Fluoro-Jade staining revealed only a subset of permeable cells showed signs of degeneration at 24 hours. Conversely, plasma membrane damage was evident in most degenerating cells. Current finite element models of the injured brain predict the ipsilateral CA3 and dentate gyrus subregions receive higher strains than the other subregions, suggesting the increased plasma membrane damage observed in these subregions may be due to specific vulnerability of these subregions to deformation. Together these results indicate that the response is complex, both spatially within the brain and over time, suggesting that membrane permeability may partially contribute to cell death but is likely part of a multifaceted, dynamic course of events contributing to secondary injury.

3.2 Introduction

Traumatic brain injury (TBI) results in memory and learning deficits that can limit short- and long-term recovery from the injury (Levin 1990; Zec et al. 2001). Memory loss is partially attributed to damage to the hippocampus, and hippocampal atrophy is observed clinically by magnetic resonance imaging after TBI (Bigler et al. 1997; Tomaiuolo et al. 2004). Similar observations are seen in experimental models of TBI. Several studies have investigated the vulnerability of different regions of the brain to mechanical injury, finding the hippocampus to be particularly susceptible to injury despite its location beneath the cortical layers. Damage to the hippocampus characterized

by neuronal degeneration and cell loss has been observed in fluid percussion (Hicks et al. 1996; Sato et al. 2001; Grady et al. 2003) and cortical contusion (Colicos et al. 1996; Anderson et al. 2005; Hall et al. 2008) rat brain injury models. Specifically, cell damage or death has been noted in all the subregions of the hippocampus, including the hilus (Lowenstein et al. 1992; Grady et al. 2003; Hall et al. 2008), dentate gyrus (Colicos et al. 1996; Sato et al. 2001; Anderson et al. 2005; Hellmich et al. 2007; Hall et al. 2008), CA1 (Colicos et al. 1996; Sato et al. 2001; Hellmich et al. 2007; Hall et al. 2008), and CA3 (Colicos et al. 1996; Dash et al. 2001; Grady et al. 2003; Anderson et al. 2005; Hellmich et al. 2007; Hall et al. 2008). Some of these studies have shown preferential cell death in the CA3 and dentate gyrus subregions (Grady et al. 2003; Anderson et al. 2005), suggesting these regions may be uniquely vulnerable to injury.

The plasma membrane is the first line of defense for a cell, and it can fail under mechanical loading resulting in holes and tears that may allow a non-specific flux of ions and molecules into and out of the cell. An example of the deleterious effects of plasma membrane damage is disruption of intracellular calcium homeostasis. The intracellular concentration of ionic calcium is tightly regulated as it is involved in numerous biochemical pathways. Plasma membrane damage allows an unregulated influx of calcium which is then available to activate proteolytic enzymes that initiate cell death. Furthermore the energy required to repair damaged membranes and reestablish ion homeostasis is significant, and the resulting energy depletion may be beyond recovery and lead to cell death. Membrane integrity assays evaluating dye exclusion (horseradish peroxidase (HRP) and dextrans) or molecule release (lactate dehydrogenase (LDH)) have been used to identify this type of damage to neuronal plasma membranes after

deformation *in vitro* (LaPlaca et al. 1997; Geddes et al. 2003) and *in vivo* (Pettus et al. 1994; Pettus and Povlishock 1996; Singleton and Povlishock 2004; Stone et al. 2004; Farkas et al. 2006).

Several studies have investigated the use of membrane resealing agents following neural injury, and the success of some of these suggests that prevention of plasma membrane damage may be a possible therapeutic target. Polyethylene glycol (PEG) is a hydrophilic polymer that is capable of fusing cell membranes (Davidson et al. 1976). PEG treatment has been shown to restore compound action potentials, re-establish cellular dye exclusion, and reduce reactive oxygen species production and lipid peroxidation in an *ex vivo* spinal cord injury model (Shi and Borgens 1999; Shi and Borgens 2000; Luo et al. 2002); brain injured animals have also shown reduced cell loss and improved recovery on an open-field locomotor task after treatment with PEG (Koob et al. 2005; Koob et al. 2008). Another membrane sealing agent is Poloxamer-188 (P188 or Pluronic F68), a triblock copolymer consisting of a hydrophobic polypropylene oxide core flanked by two hydrophilic PEG blocks; its chemical structure allows it to insert directly into lipid membranes (Maskarinec et al. 2002). *In vitro* P188 delivery reduces plasma membrane damage and axonal beading (Kilinc et al. 2008), prevents neuronal cell death, limits LDH release, and inhibits proapoptotic p38 activation after a mechanical injury (Serbest et al. 2005; Serbest et al. 2006). Furthermore it reduces plasma membrane damage (Curry et al. 2004) and cell loss (Frim et al. 2004) after excitotoxic insults *in vivo*. If restoration of plasma membrane integrity so significantly improves cell outcome, these data suggest that plasma membrane damage may be an underlying cause of neuronal death and dysfunction following injury.

In this study, plasma membrane damage was measured in the rat hippocampus following a controlled cortical impact injury in rats. Plasma membrane damage was restricted to neurons in the dentate gyrus subregion of the hippocampus with fewer damaged cells observed in the CA1/CA2 subregion. Fluoro-Jade staining identified degenerating neurons, revealing most degenerating neurons in the hippocampus exhibited plasma membrane damage. However of all neurons in the hippocampus with plasma membrane damage, only a subset showed evidence of degeneration. While other factors likely contribute to neuronal outcome, thus study suggests there may exist local differences in susceptibility to plasma membrane damage and that plasma membrane damage may be a critical factor in determining neuronal survival following traumatic brain injury.

3.3 Materials and methods

All animal procedures were approved by the Institutional Animal Care and Use Committee at Georgia Institute of Technology.

3.3.1 Permeability marker injection

Adult male Sprague Dawley rats (n=24, 275-325 g; Charles River Laboratories Inc., Wilmington, MA) were anesthetized with 50 mg/kg Nembutal, positioned on a stereotactic frame, and permeability marker (3000 Da dextran-tetramethylrhodamine; Molecular Probes, Eugene, OR) was delivered into the cerebrospinal fluid (CSF) via intrathecal injection. To perform this injection, the musculature at the base of the skull was dissected to reveal the atlantooccipital membrane. The dura mater was exposed and punctured, and a catheter was inserted into the subdural spinal canal. A small volume (15

μL) of permeability marker (25 mg/mL) in sterile physiological saline was slowly injected through the catheter into the CSF. Following the injection, the surgery site was closed and the rats were returned to their cages.

3.3.2 Controlled cortical impact

Permeability marker was allowed to diffuse through the CSF and into the brain tissue for 2 hours before surgery. Rats were re-anesthetized and again positioned on a stereotactic frame. A midline incision was performed on the scalp to reveal the skull, and connective tissue and muscle were removed from the top and left side of the skull. A 7 mm craniectomy was performed tangent to the sagittal and coronal sutures, exposing the left fronto-parietal cortex. Injured animals (n=12) received a controlled cortical impact (3 m/s velocity, 2 mm depth, 250 ms dwell time) from a pneumatic piston with a 6 mm impact tip (Pittsburgh Precision Instruments, Pittsburgh, PA). Sham animals (n=12) received all surgical procedures including craniectomy but were not injured. Following surgery or injury the scalp was closed.

Animals were sacrificed at 10 minutes (n=12) or 24 hours (n=12) post-injury. The 10 minute time point was chosen because it captures the cells that are permeable in the immediate acute post-injury period; this allows sufficient permeability marker to diffuse into cells with membrane damaged caused by the primary mechanical insult while minimizing the number of cells with delayed permeability marker uptake. However Fluoro-Jade B staining (discussed in the next section) requires time before staining of degenerating cells becomes apparent, so few cells stain with Fluoro-Jade at 10 minutes post-injury. Thus because the permeability marker is delivered before injury, the 24 hour time point captures all cells that are permeable in the immediate acute post-injury period

(the same cells that are identified at the 10 minute time point) and permeable cells with delayed plasma membrane damage (although the permeability marker should clear from the CSF with time, limiting the presence of marker for identification of cells with delayed plasma membrane damage); the 24 hour time point allows for Fluoro-Jade staining of cells degenerating within this time period.

3.3.3 Histology

At sacrifice animals received a Nembutal overdose and were perfused transcardially with phosphate buffered saline (PBS) followed by 4% paraformaldehyde with 0.1% glutaraldehyde in PBS. Brain tissue was removed following perfusion, post-fixed overnight at 4 °C in 4% paraformaldehyde with 0.1% glutaraldehyde in PBS, and soaked in 30% sucrose at 4 °C for 2-3 days for cryoprotection. Tissue was then frozen in OCT cryoembedding compound (Tissue-Tek, Torrance, CA) and 20 µm thick coronal sections were collected using a cryostat (Leica CM3050S, Wetzlar, Germany). Neurons and astrocytes were identified with immunohistochemistry using monoclonal antibodies against NeuN (1:500 dilution; Millipore, Billerica, MA) and GFAP (1:500 dilution, Millipore) respectively.

Degenerating neurons were identified with Fluoro-Jade B staining (Millipore, Billerica, MA) as described previously (Schmued and Hopkins 2000). Slides were first thawed and rinsed to remove cryoembedding compound and then heated to 50 °C for 30 minutes. Slides were then soaked in 100% ethanol for 3 minutes, 70% ethanol for 1 minute, and deionized water for 1 minute. Fluoro-Jade staining solution (0.0001% Fluoro-Jade B in 0.1% acetic acid with 0.00001% DAPI to visualize cell nuclei) was made immediately before staining, and slides were submerged in the solution for 1 hour

in the dark at 4 °C. Slides were then rinsed 3 times in deionized water, dried, rinsed in xylene, and coverslipped. A background quenching step was eliminated from the procedure to minimize the reduction of permeability marker fluorescence.

3.3.4 Microscopy

Stained tissue sections were visualized on a Nikon Eclipse 80i upright microscope (Nikon Instruments Inc., Melville, NY) with fluorescein and Texas red filters. The Texas red filter was required for imaging to eliminate bleed through of Fluoro-Jade signal into the red channel. Neurolucida software (MBF Bioscience, Williston, VT) was used to obtain montage images of the ipsilateral and contralateral sides of the hippocampus. Neurolucida was also used to map the boundaries and measure the area of the the CA1/CA2, CA3, and dentate gyrus subregions of the hippocampus and count the cells in those subregions that were dextran positive, Fluoro-Jade positive, or showed evidence of colocalized dextran and Fluoro-Jade staining. Cell counts were normalized to the area of the subregion in which they were counted. Matlab software (The MathWorks, Natick, MA) was used to transform and plot the Cartesian XY coordinates of permeable cells.

3.3.5 Statistics

Cell counts were analyzed for statistical significance using SigmaStat software (Systat Software Inc., San Jose, CA). Two-way repeated measures ANOVAs were performed with injury group and subregion as factors followed by Tukey test pairwise comparisons. All data are presented as mean values with standard error of the mean indicated.

3.4 Results

3.4.1 Plasma membrane damage following injury

The morphology of permeable cells combined with immunostaining for cell phenotype revealed that in the cortex and in the hippocampus most cells that exhibited permeability marker uptake were neurons (Figures 3.1 and 3.2). No astrocytes were observed flooded with permeability marker (not shown). In animals sacrificed 10 minutes following injury, plasma membrane damage (indicated by cellular uptake of the fluorescent permeability marker) was observed in the hippocampus (Figures 3.3A and 3.4A), while in sham animals few cells contained permeability marker (Figure 3.3B). The 10 minute time point captures plasma membrane damage resulting from the primary mechanical insult while allowing sufficient time for permeability marker to diffuse into damaged cells. While the permeability marker was introduced into the CSF two hours before injury, many cells still contained permeability marker 24 hours post-injury (Figure 3.4D). The intracellular presence of permeability marker at 10 minutes was very clearly observed within both the somata and neurites of cells, and by 24 hours the permeability marker began to appear splotchy or punctuate in and around cells. Cellular uptake of the permeability marker was heterogeneous within the hippocampus, with permeable cells appearing adjacent to non-permeable cells and different fluorescence intensities among permeable cells.

Quantification revealed that at 10 minutes post-injury there were statistically more permeable cells in the subregions of the ipsilateral hippocampus compared to the same subregions in shams (Figure 3.5). Furthermore, there were more permeable cells in the ipsilateral dentate gyrus compared to the ipsilateral CA1/CA2 subregion as well as

compared to the subregions of the contralateral hippocampus in injured brains. With the exception of the contralateral CA1/CA2 and dentate gyrus subregions, there were more permeable cells in all hippocampal subregions compared to shams at 24 hours post-injury (Figure 3.5). Additionally the number of permeable cells in the CA3 subregion of the contralateral hippocampus in injured brains increased significantly compared to the ipsilateral CA3 subregion as well as the other contralateral subregions at 24 hours.

3.4.2 Locations of permeable cells

The boundaries of the CA1/CA2, CA3, and dentate gyrus subregions were traced, and the Cartesian coordinates of permeable cells within these subregions were collected manually. These points were plotted in two-dimensions, revealing differences in the spatial distribution of permeable cells. Few permeable cells were identified in sham brains. Permeable cells were clustered in high densities within the CA3 and dentate gyrus subregions, while few clusters of cells were identified in the CA1/CA2 subregion (Figure 3.8).

3.4.3 Fluoro-Jade staining following injury

Fluoro-Jade staining identifies degenerating neurons. Faint Fluoro-Jade staining was present in a few cells in the hippocampus 10 minutes post-injury (Figure 3.4B). However Fluoro-Jade staining was greatly increased 24 hours post-injury, indicating neuronal degeneration, and Fluoro-Jade stained cells were easily distinguished from background (Figure 3.4E). Few cells stained with Fluoro-Jade in sham animals.

Quantification of Fluoro-Jade stained cells revealed statistically more cells in the CA1/CA2 and dentate gyrus subregions of the ipsilateral hippocampus at 10 minutes

post-injury compared to the same subregions in shams (Figure 3.6). With the exception of the contralateral CA1/CA2 subregion, the increase in the number of Fluoro-Jade stained cells on both sides of the injured hippocampus compared to shams at 24 hours was significant (Figure 3.6). There were also more permeable cells in the contralateral CA3 subregion compared to the CA1/CA2 subregion at 24 hours.

3.4.4 Colocalization of plasma membrane damage and Fluoro-Jade staining

Permeability marker and Fluoro-Jade staining overlapped in many cells, and this was especially evident at 24 hours post-injury (Figure 3.4F). Nearly all cells that were FluoroJade positive also contained permeability marker; however only a subset of cells containing permeability marker also exhibited FluoroJade staining. Within the injured brain the percentage of permeable cells that also stained with Fluoro-Jade (Dextran with Fluoro-Jade) was only statistically increased in the contralateral hippocampus at 24 hours compared to 10 minutes (Figure 3.7A). These averages also suggest that by 24 hours post-injury less than half of all permeable cells show signs of degeneration. Comparing all Fluoro-Jade stained cells a greater percentage contained dextran (Fluoro-Jade with Dextran) at 10 minutes in the ipsilateral hippocampus compared to the contralateral hippocampus (Figure 3.7B). At 24 hours post-injury most Fluoro-Jade stained cells also contained permeability marker.

3.5 Discussion

This study shows that traumatic brain injury causes damage to neuronal plasma membranes. Plasma membrane damage was identified by cellular uptake of a membrane impermeable molecule and was limited to neuronal cell types, and neuronal degeneration

was identified using Fluoro-Jade B staining. This data also suggests cells in adjacent subregions within the same brain structure have different susceptibilities to plasma membrane damage during injury, and that the dentate gyrus may be particularly susceptible to damage. While most degenerating neurons exhibited plasma membrane damage, only a subset of the damaged cells showed signs of degeneration. These findings suggest a complex role for plasma membrane damage in determining neuronal outcome following traumatic brain injury.

This study is significant in that it is shows that plasma membrane permeability leads to cell death in only some cells. Singleton and Povlishock reported a similar observation using horseradish peroxidase as a permeability marker in the cortex following a fluid percussion injury (Singleton and Povlishock 2004). With less than half of permeable cells showing signs of degeneration 24 hours post-injury in this study, questions remain about the remaining population of permeable cells. Some of these cells may have repaired their plasma membranes and recovered from the primary mechanical insult. Other cells may have initiated failed attempts at plasma membrane repair, buying some survival time but causing the first signs of degeneration or death to appear more than 24 hours post-injury. Cells that exhibit delayed onset permeability also may not show signs of degeneration or death within the first 24 hours post injury. These latter explanations are supported by observations by Whalen et al. that permeable cells take up to 7 days to die and clear from the brain (Whalen et al. 2007). However the use of propidium iodide, a DNA binding molecule, as a permeability marker may have contributed to cell death in that study. It is unlikely that our dextran-based permeability

marker is cytotoxic given its use as a cell tracer and our observation that only a subset of cells containing the permeability exhibit signs of degeneration.

Among permeable cells, different fluorescent intensities of permeability marker were observed. The dynamic nature of plasma membrane damage makes it difficult to draw inferences about the extent of plasma membrane damage based on fluorescent intensity of the permeability marker. Farkas previously observed three categories of permeable cells (Farkas et al. 2006): cells that were permeable but resealed, cells that were permeable and stayed permeable, and cells that showed a delayed onset of permeability following injury (Figure 1.4). Given these three possibilities, there are also several explanations for the differences in fluorescent intensities: if a cell reseals quickly, only a small amount of dye is allowed into the cell before resealing leading to a dimmer fluorescence; if a cell reseals slowly, dye accumulates and is retained within the cell leading to brighter fluorescence; if a cell does not reseal, dye accumulates within the cell but some may leak back out leading to either brighter or dimmer fluorescence.

Within 10 minutes of injury cellular damage was observed in the ipsilateral hippocampus directly beneath the injury site. However after 24 hours the unilateral mechanical insult resulted in a bilateral injury response, with the number of permeable cells increasing in the ipsilateral hippocampus as well as the contralateral hippocampus distant from the site of injury. This was especially evident in the CA3 subregion of the contralateral hippocampus of the injured brain. Little evidence of contralateral plasma membrane damage was apparent at 10 minutes, suggesting that the increase in the number of permeable cells in the contralateral hippocampus is due to secondary events rather than the initial mechanical insult.

The brain is a mechanically complex tissue. It consists of multiple structures arranged in three-dimensions, each of which has a unique composition and organization of cells and matrix. The bulk mechanical properties of the brain have been characterized previously (Gefen et al. 2003), and a recent studies has shown sub-regional differences in the mechanical properties of the hippocampus of the juvenile rat (Elkin et al. 2007; Elkin et al. 2008). This group has also found in the adult rat that the CA3 subregion of the hippocampus is significantly stiffer than the dentate gyrus subregion, and the CA1 subregion is stiffer than both the CA3 and dentate gyrus subregions (Elkin et al. 2008). A finite element model of the rat brain under deformation has been developed, and it predicts higher lower maximum principal strains in the stiffer hippocampal subregions (Mao et al. 2006; Zhang and Mao 2008). In the context of this work, it is possible that during a mechanical insult the stiffer CA1 and CA3 subregions experience smaller deformations (and therefore fewer cells with plasma membrane damage) than the less stiff dentate gyrus subregion (where more plasma membrane damage and permeability marker uptake is observed).

These results are also complimentary to current attempts to use finite element (FE) modeling to predict subregional strains in the brain during a mechanical insult. An accurate FE model relies on accurate assumptions including spatial organization (including mesh construction) and mechanical properties, and an FE model of the rat brain under deformation have been developed (Mao et al. 2006; Zhang and Mao 2008). Zhang has reported that predictions of maximum principal strain for CA1, CA3, and dentate gyrus subregions differ in a heterogeneous FE model (with different mechanical properties for each of the CA1, CA3, and dentate gyrus subregions) compared to a

homogeneous model (with the same mechanical properties for each of the subregions) (Zhang and Mao 2008). Modifications to the axis of mechanical loading in the FE model results in differences in the strain profiles of the hippocampus subregions, further suggesting that the heterogeneity of subregional mechanical properties may be responsible for the differential predictions of maximum principal strain.

Thus three datasets exist: subregional measurements of the mechanical properties of the hippocampus, FE model with an enhanced resolution mesh of the hippocampus that incorporates tissue heterogeneity, and our observations of post-injury plasma membrane damage within the hippocampus. Predictions of maximum principal strain by the current FE model closely overlap with our subregional observations of plasma membrane damage (Figure 3.9). Furthermore by incorporating the newest measurements of the subregional mechanical properties, we may be able to more accurately predict which regions of the hippocampus receive the highest strains and are most susceptible to damage after an injury of a particular severity or at a particular location. By serving as a cell-level strain gauge, our experimental permeability data will then be used to validate the FE model predictions.

It is of interest whether the profile of cell damage and degeneration in the hippocampus following controlled cortical impact is similar to other brain pathologies. It has been shown previously in experimental models that CA1 neurons are acutely unaffected by transient ischemia but exhibit a delayed cell death in the days and weeks following the ischemic insult (Nitatori et al. 1995). In fact, while CA1, CA2, and CA4 neuronal cell death is evident following ischemia, the CA3 and dentate gyrus subregions appear to be less susceptible to ischemic injury (Kirino and Sano 1984). Expression of

bcl-2 family pro-survival genes is greater in the dentate gyrus and CA3 subregions, while the pro-apoptotic gene *bax* is expressed in the CA1 subregion (Graham and Chen 2001). These observations of cell damage and degeneration in the hippocampus following ischemia are, at first consideration, contradictory to the profile observed here after a traumatic brain injury. However although dentate gyrus neurons appear to most vulnerable to plasma membrane damage immediately following injury, by 24 hours there was no difference in the numbers of degenerating neurons in the subregions of the ipsilateral injured hippocampus. Other studies have also shown delayed cell loss in the CA1 subregion following controlled cortical impact (Colicos et al. 1996; Hall et al. 2008) and lateral fluid percussion injury (Sato et al. 2001). This suggests that other factors in addition to initial plasma membrane damage contribute to cellular outcome in the traumatically injured brain.

Subregional differences in hippocampal mechanical properties and injury-induced plasma membrane damage may be due to multiple factors, including the variety of cell types located in the different regions. Cell phenotype determines plasma membrane composition, including different receptor and ion channel densities, which consequently can affect the mechanical properties of the cell (Mohandas and Evans 1994). Phenotype also determines cytoskeletal composition and organization; these can also affect cell stiffness. The geometry of cells, including morphological features such as axons and dendrites, and their orientation within the tissue can contribute to the overall mechanical properties of the tissue. Finally cell-cell interactions, cell-matrix interactions, and the composition of the extracellular matrix itself within a tissue can all also improve the ability of the tissue to resist deformation.

In conclusion, traumatic brain injury causes mechanical disruptions to cell membranes that closely associate with signs of cell degeneration. With only a subset of permeable cells staining positive with Fluoro-Jade, the dynamics of plasma membrane damage and resealing may be important to understanding neuronal dysfunction and death following injury. Further investigation of the mechanisms of cell damage and repair may identify therapeutic targets and enable improved predictions of injuries and outcomes after traumatic brain injury.

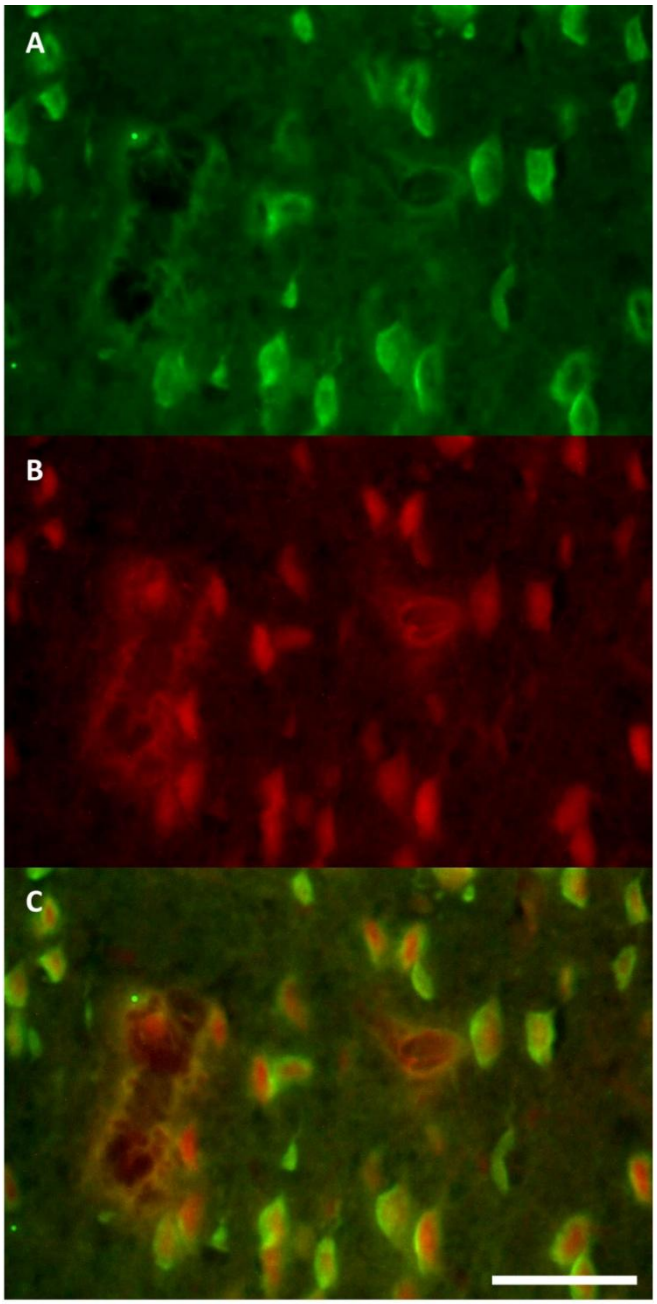

Figure 3.1: Phenotype of permeable cells in the cortex

In the cortex adjacent to the site of injury 10 minutes following injury, neuronal nuclei were identified with NeuN staining (green, A). Cells in the same region contain permeability marker (red, B). An overlay of the images reveals that permeable cells in the cortical neurons (C). (scale bar = 50 µm)

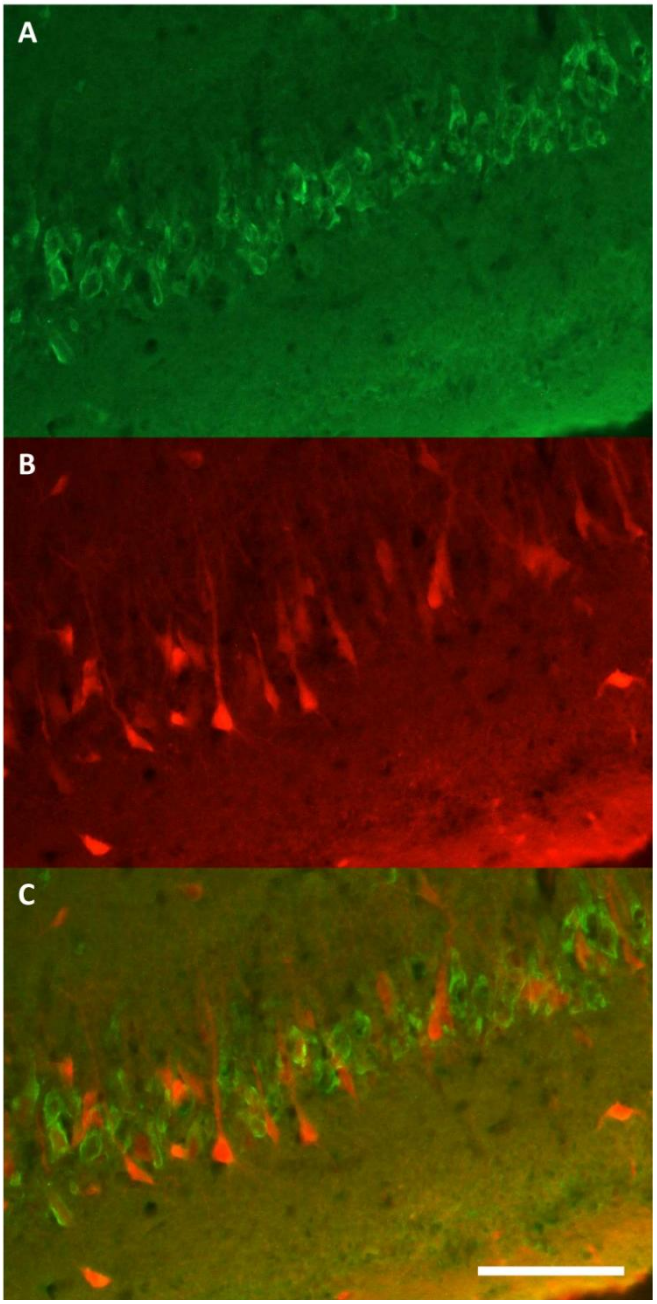

Figure 3.2: Phenotype of permeable cells in hippocampus

In the CA3 subregion of the hippocampus 10 minutes following injury, neuronal nuclei were identified with NeuN staining (green, A). Cells in the same region contain permeability marker (red, B). Permeable cells have a distinct neuronal morphology and stain positive for NeuN (C). (scale bar = 100 μm)

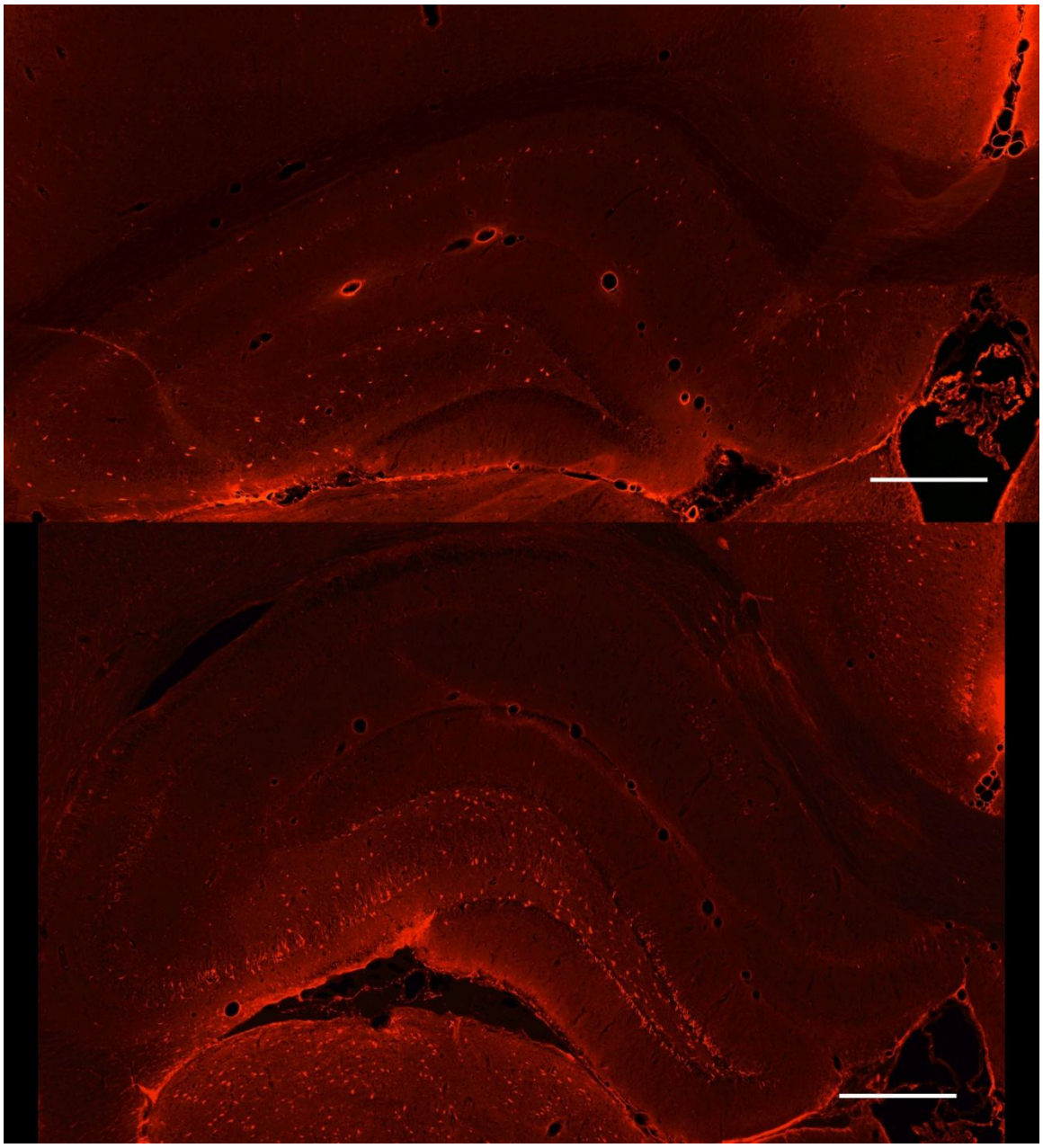

Figure 3.3: Pattern of plasma membrane permeability in the hippocampus

Permeability marker was injected into the CSF of rats 2 hours before surgery, and rats were sacrificed 10 minutes after sham surgery (A) or injury (B). Few permeable cells were identified in the ipsilateral hippocampus of sham surgery rats. However in injured rats, most permeable cells were located in the CA3 and dentate gyrus subregions of the ipsilateral hippocampus. (scale bar = 500 µm)

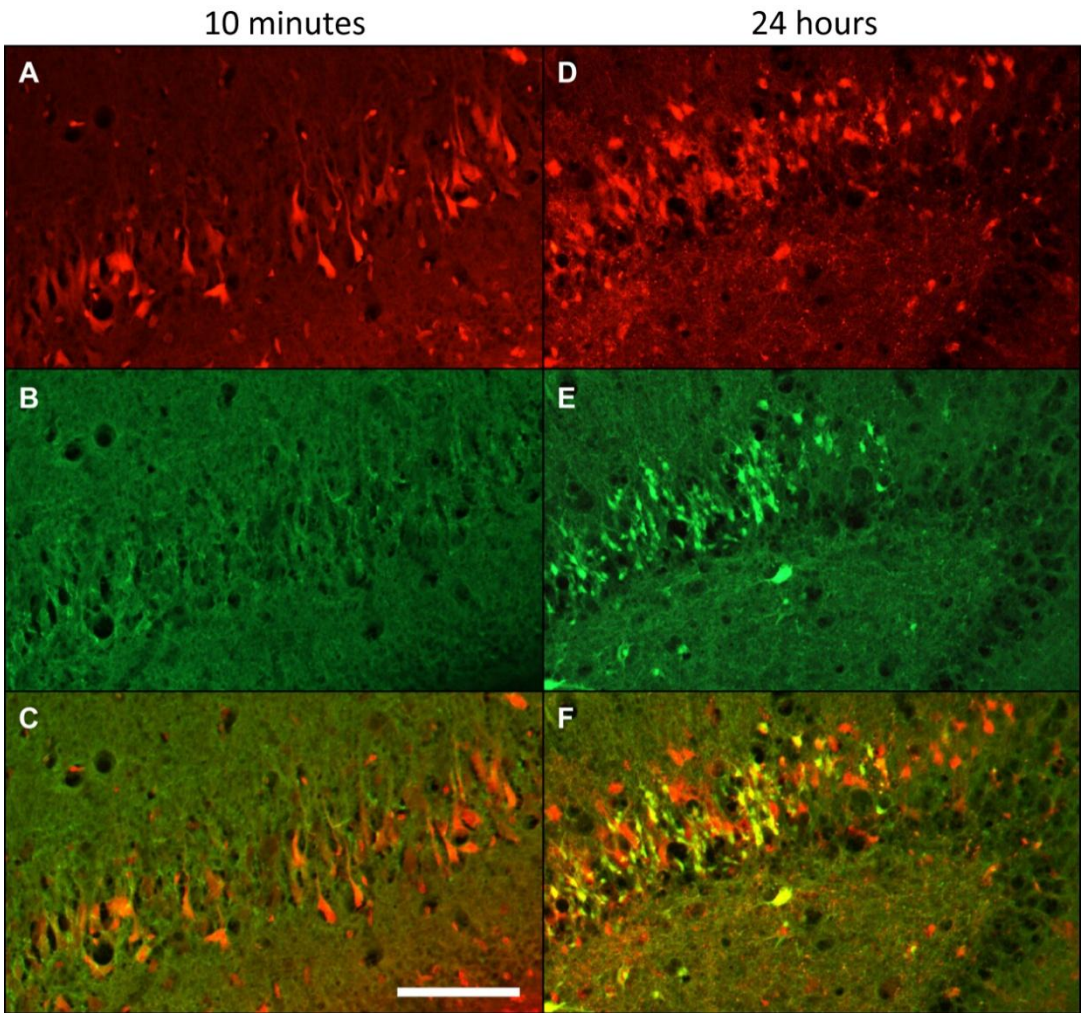

Figure 3.4: Plasma membrane permeability and cell death in the hippocampus at 10 minutes and 24 hours post-injury

Permeability marker uptake (A, D) indicates which cells in the CA3 (A-C) and dentate gyrus (D-F) subregions of the ipsilateral hippocampus sustained plasma membrane damage by the mechanical insult. Fluoro-Jade staining shows degenerating neurons in the same tissue sections at 10 minutes (B) and 24 hours (C) post-injury, with more intense Fluoro-Jade staining evident at the later time point. Overlays of these photomicrographs (C, F) reveals nearly complete colocalization of Fluoro-Jade staining with permeability marker uptake, whereas only a subset of permeable cells are Fluoro-Jade positive. (scale bar = 100 µm)

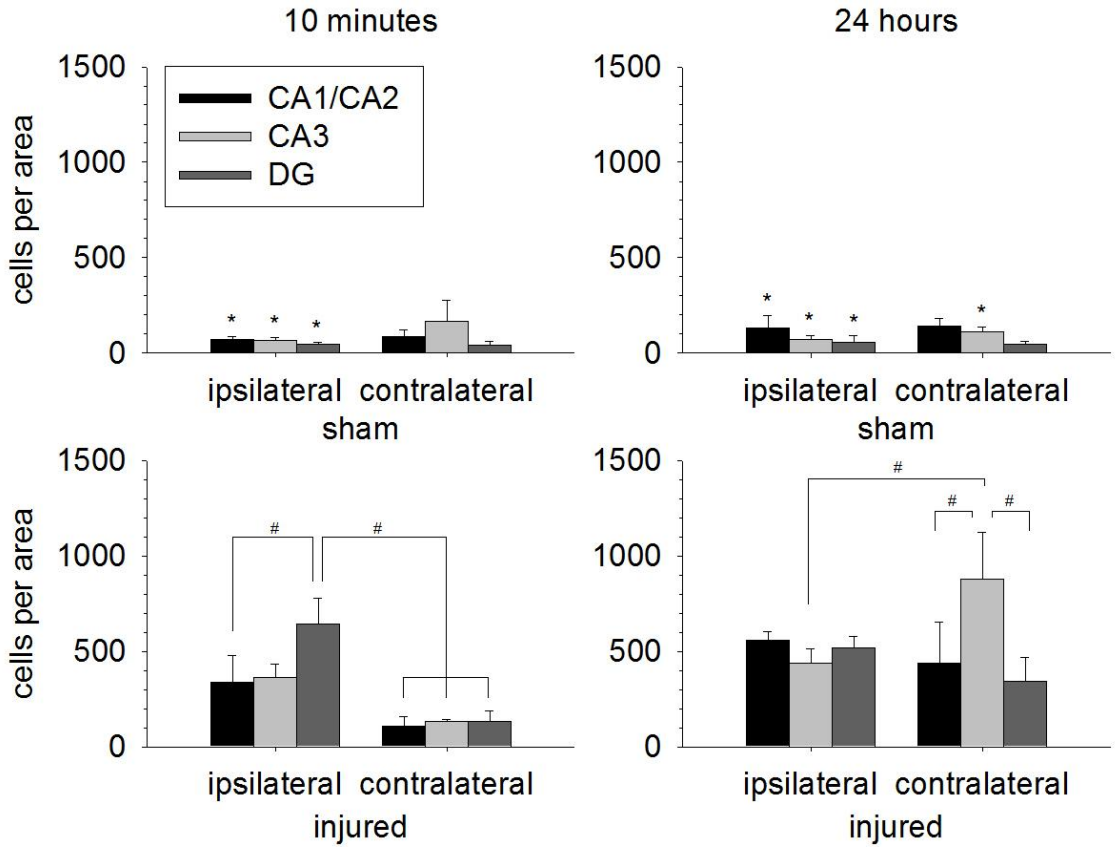

Figure 3.5: Plasma membrane permeability increases in the hippocampus following injury

Cells in the pyramidal (CA1/CA2 and CA3 subregions) and granule (dentate gyrus subregion) cell body layers of the hippocampus were examined for the presence of permeability marker. Few permeable cells were identified in sham animals. At 10 minutes post-surgery, more permeable cells were identified in the ipsilateral hippocampus in injured animals compared to the contralateral hippocampus in injured animals as well as compared to the ipsilateral hippocampus in sham animals. At 24 hours post injury, the ipsilateral and contralateral hippocampi in injured animals contained significantly more permeable cells than the same regions in sham animals. In addition, the contralateral hippocampus in injured animals exhibited a significant increase in the

number of permeable cells from 10 minutes to 24 hours post-surgery. Data graphed as mean ± standard error. (* $p < 0.05$ compared to injured, # $p < 0.05$ as indicated)

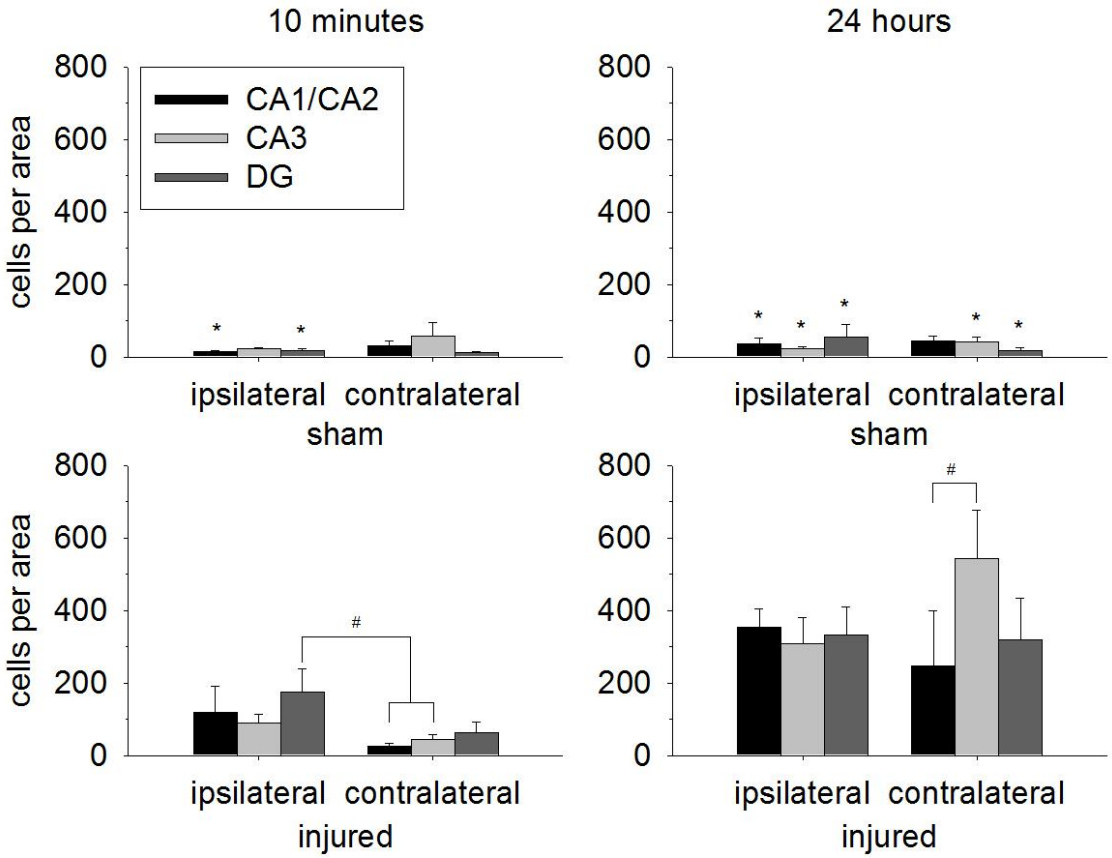

Figure 3.6: Cell death increases in the hippocampus following injury

Fluoro-Jade staining was used to identify degenerating neurons in the cell body layers of the hippocampus following injury. Few Fluoro-Jade positive cells were identified in sham animals. At 10 minutes post-surgery, significantly more Fluoro-Jade positive cells were identified in the ipsilateral hippocampus of injured animals compared to the contralateral hippocampus in injured animals as well as compared to the ipsilateral hippocampus in sham animals. At 24 hours post injury, both the ipsilateral and contralateral hippocampi in injured animals contained significantly more Fluoro-Jade positive cells than the same regions in sham animals. In addition, the contralateral and ipsilateral hippocampi in injured animals exhibited a significant increase in the number of permeable cells in the same regions from 10 minutes to 24 hours post-surgery. Data

graphed as mean ± standard error. (* $p < 0.05$ compared to injured, # $p < 0.05$ as indicated)

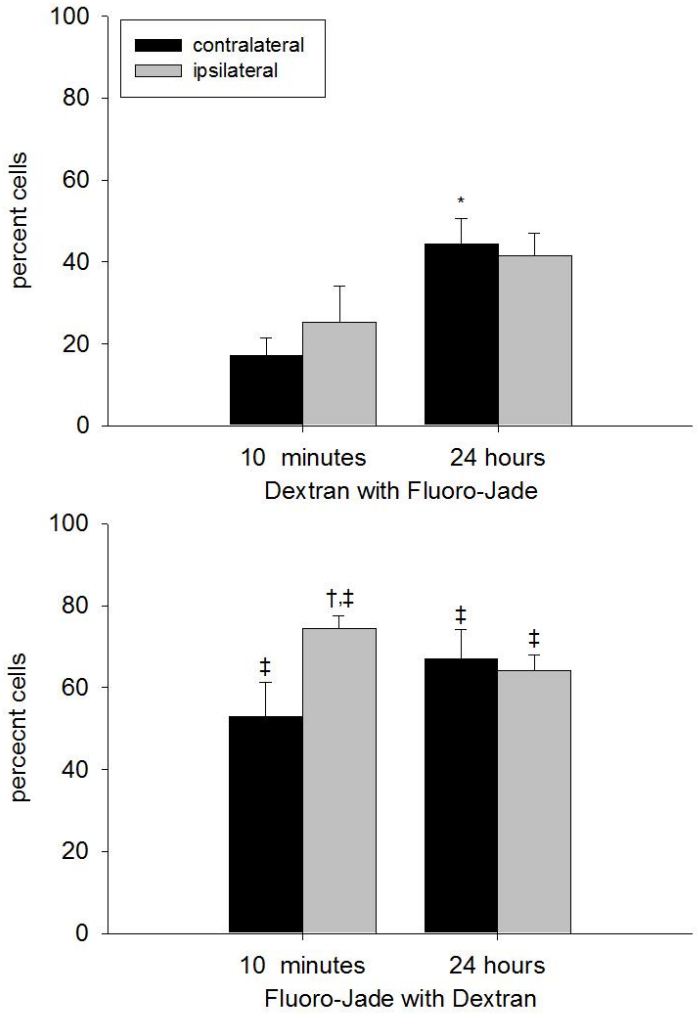

Figure 3.7: Heterogeneity of cellular response to plasma membrane damage

In injured brains most cells that were Fluoro-Jade positive also contained dextran (Fluoro-Jade with dextran), while a smaller percentage of cells that contained dextran became Fluoro-Jade positive (Dextran with Fluoro-Jade). (* compared to 10 minute, † compared to contralateral, ‡ compared to Dextran with Fluoro-Jade) (mean ± standard error)

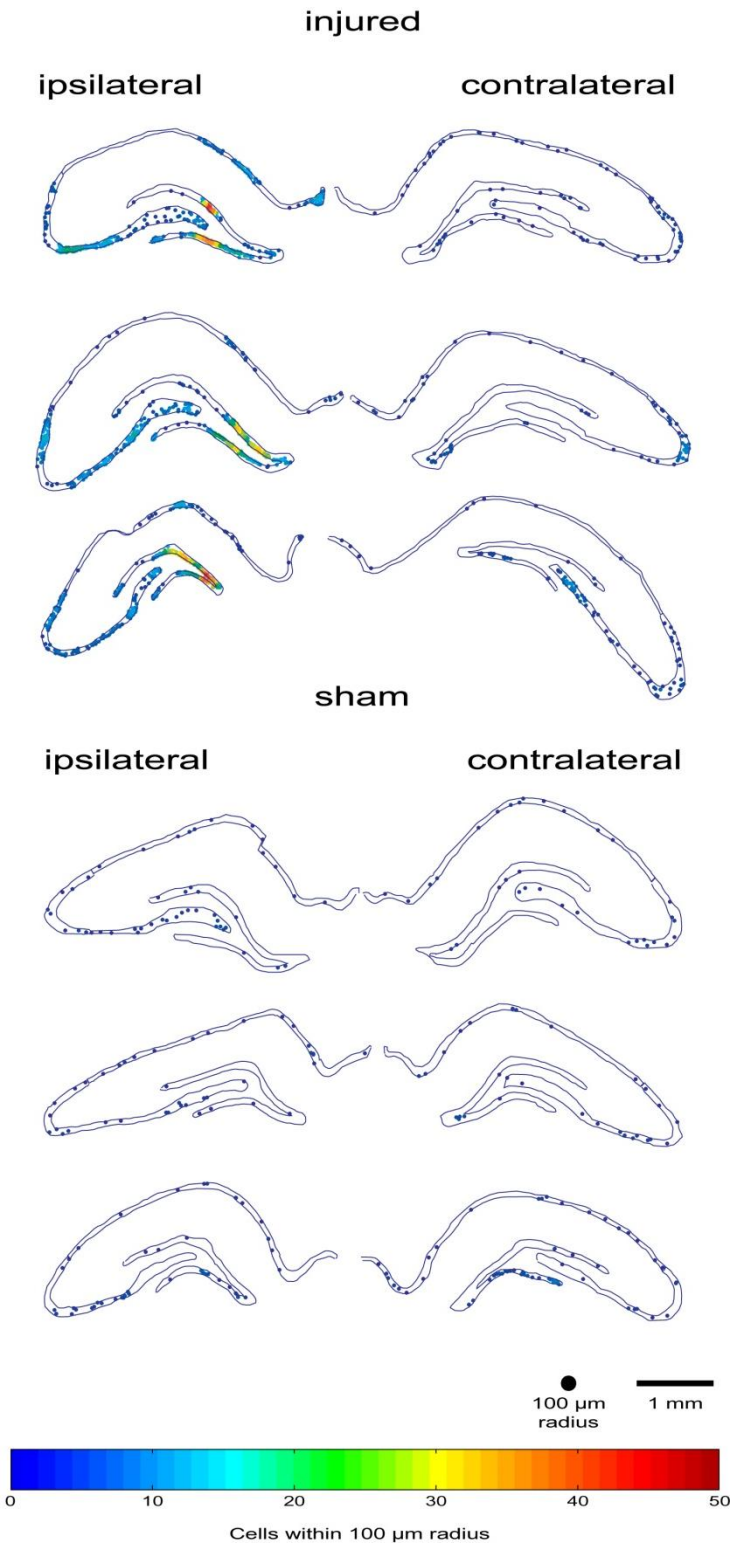

Figure 3.8: Locations of permeable cells in the hippocampus

The Cartesian coordinates of the locations of permeable cells in the cell body layers of the hippocampus of injured sham brains were collected and plotted. Each point represents the location of a permeable cell, and the color of the point represents the density of permeable cells within a 100 μm radius. Representative hippocampi (located at approximately bregma -3.3 mm) are shown.

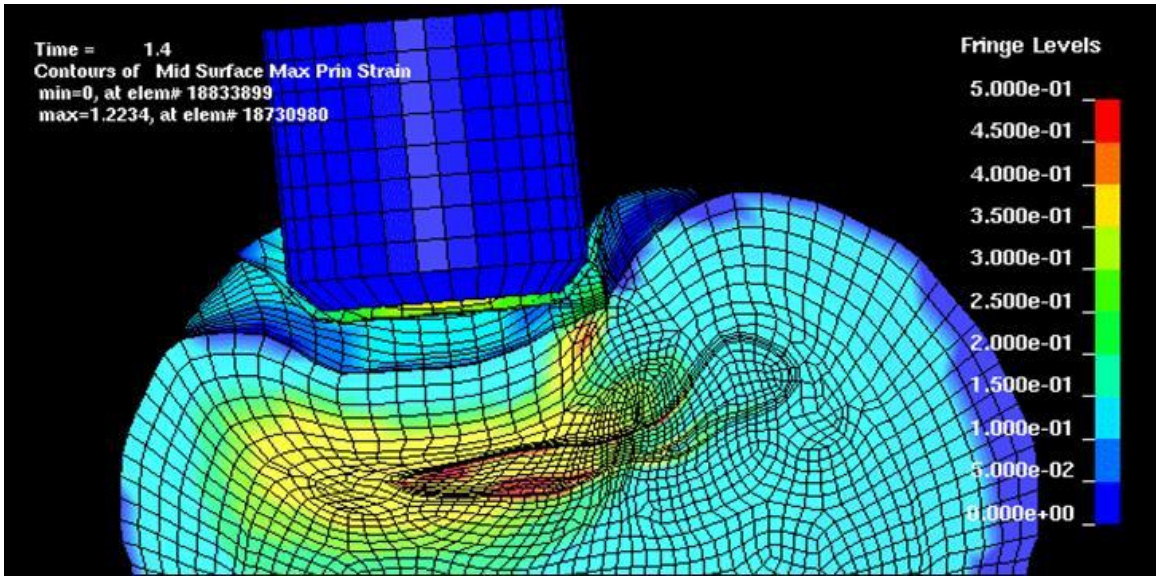

Figure 3.9: Finite element model of brain during injury

Finite element analysis of the rat brain receiving a controlled cortical impact injury predicts the CA3 and dentate gyrus subregions of the ipsilateral hippocampus receive the highest maximum principal strains. Finite element model constructed and provided by Liying Zhang at Wayne State University (Zhang and Mao 2008).

3.6 Works citied

Anderson, K. J., K. M. Miller, I. Fugaccia and S. W. Scheff (2005). "Regional distribution of Fluoro-Jade B staining in the hippocampus following traumatic brain injury." Experimental Neurology 193(1): 125-130.

Bigler, E. D., D. D. Blatter, C. V. Anderson, S. C. Johnson, S. D. Gale, R. O. Hopkins and B. Burnett (1997). "Hippocampal volume in normal aging and traumatic brain injury." AJNR Am J Neuroradiol 18(1): 11-23.

Colicos, M. A., C. E. Dixon and P. K. Dash (1996). "Delayed, selective neuronal death following experimental cortical impact injury in rats: possible role in memory deficits." Brain Research 739(1-2): 111-119.

Curry, D. J., D. A. Wright, R. C. Lee, U. J. Kang and D. M. Frim (2004). "Poloxamer 188 volumetrically decreases neuronal loss in the rat in a time-dependent manner." Neurosurgery 55(4): 943-8; discussion 948-9.

Dash, P. K., S. A. Mach and A. N. Moore (2001). "Enhanced neurogenesis in the rodent hippocampus following traumatic brain injury." Journal Of Neuroscience Research 63(4): 313-9.

Davidson, R. L., K. A. O'Malley and T. B. Wheeler (1976). "Polyethylene glycol-induced mammalian cell hybridization: effect of polyethylene glycol molecular weight and concentration." Somatic Cell Genetics 2(3): 271-80.

Elkin, B. S., E. U. Azeloglu, K. D. Costa and B. Morrison, 3rd (2007). "Mechanical heterogeneity of the rat hippocampus measured by atomic force microscope indentation." Journal Of Neurotrauma 24(5): 812-22.

Elkin, B. S., E. U. Azeloglu, K. D. Costa and B. Morrison, 3rd (2008). Developmental changes in regional mechanical properties of the rat hippocampus and cortex. National Neurotrauma Symposium. Orlando, FL.

Farkas, O., J. Lifshitz and J. T. Povlishock (2006). "Mechanoporation induced by diffuse traumatic brain injury: an irreversible or reversible response to injury?" The Journal Of Neuroscience: The Official Journal Of The Society For Neuroscience 26(12): 3130-40.

Frim, D. M., D. A. Wright, D. J. Curry, W. Cromie, R. Lee and U. J. Kang (2004). "The surfactant poloxamer-188 protects against glutamate toxicity in the rat brain." Neuroreport 15(1): 171-4.

Geddes, D. M., R. S. Cargill, 2nd and M. C. LaPlaca (2003). "Mechanical stretch to neurons results in a strain rate and magnitude-dependent increase in plasma membrane permeability." Journal Of Neurotrauma 20(10): 1039-49.

Gefen, A., N. Gefen, Q. Zhu, R. Raghupathi and S. S. Margulies (2003). "Age-dependent changes in material properties of the brain and braincase of the rat." Journal Of Neurotrauma 20(11): 1163-77.

Grady, M. S., J. S. Charleston, D. Maris, B. M. Witgen and J. Lifshitz (2003). "Neuronal and glial cell number in the hippocampus after experimental traumatic brain injury: analysis by stereological estimation." Journal Of Neurotrauma 20(10): 929-41.

Graham, S. H. and J. Chen (2001). "Programmed Cell Death in Cerebral Ischemia." Journal Of Cerebral Blood Flow And Metabolism: Official Journal Of The International Society Of Cerebral Blood Flow And Metabolism 21(2): 99-109.

Hall, E. D., Y. D. Bryant, W. Cho and P. G. Sullivan (2008). "Evolution of post-traumatic neurodegeneration after controlled cortical impact traumatic brain injury in mice and rats as assessed by the de Olmos silver and fluorojade staining methods." Journal Of Neurotrauma 25(3): 235-47.

Hellmich, H. L., K. A. Eidson, B. A. Capra, J. M. Garcia, D. R. Boone, B. E. Hawkins, T. Uchida, D. S. DeWitt and D. S. Prough (2007). "Injured Fluoro-Jade-positive hippocampal neurons contain high levels of zinc after traumatic brain injury." Brain Research 1127(1): 119-126.

Hicks, R., H. Soares, D. Smith and T. McIntosh (1996). "Temporal and spatial characterization of neuronal injury following lateral fluid-percussion brain injury in the rat." Acta Neuropathologica 91(3): 236-246.

Kilinc, D., G. Gallo and K. A. Barbee (2008). "Mechanically-induced membrane poration causes axonal beading and localized cytoskeletal damage." Experimental Neurology 212(2): 422-30.

Kirino, T. and K. Sano (1984). "Selective vulnerability in the gerbil hippocampus following transient ischemia." Acta Neuropathologica 62(3): 201-208.

Koob, A. O., J. M. Colby and R. B. Borgens (2008). "Behavioral recovery from traumatic brain injury after membrane reconstruction using polyethylene glycol." Journal Of Biological Engineering 2(1): 9.

Koob, A. O., B. S. Duerstock, C. F. Babbs, Y. Sun and R. B. Borgens (2005). "Intravenous Polyethylene Glycol Inhibits the Loss of Cerebral Cells after Brain Injury." Journal Of Neurotrauma 22(10).

LaPlaca, M. C., V. M. Y. Lee and L. E. Thibault (1997). "An in vitro model of traumatic neuronal injury: Loading rate-dependent changes in acute cytosolic calcium and lactate dehydrogenase release." Journal of Neurotrauma 14(6): 355-368.

Levin, H. S. (1990). "Memory deficit after closed-head injury." Journal of Clinical and Experimental Neuropsychology 12(1): 129 - 153.

Lowenstein, D. H., M. J. Thomas, D. H. Smith and T. K. McIntosh (1992). "Selective vulnerability of dentate hilar neurons following traumatic brain injury: a potential mechanistic link between head trauma and disorders of the hippocampus." The Journal Of Neuroscience: The Official Journal Of The Society For Neuroscience 12(12): 4846-53.

Luo, J., R. Borgens and R. Shi (2002). "Polyethylene glycol immediately repairs neuronal membranes and inhibits free radical production after acute spinal cord injury." J Neurochem 83(2): 471-80.

Mao, H., L. Zhang, K. H. Yang and A. I. King (2006). "Application of a finite element model of the brain to study traumatic brain injury mechanisms in the rat." Stapp Car Crash Journal 50: 583-600.

Maskarinec, S. A., J. Hannig, R. C. Lee and K. Y. Lee (2002). "Direct observation of poloxamer 188 insertion into lipid monolayers." Biophysical Journal 82(3): 1453-9.

Mohandas, N. and E. Evans (1994). "Mechanical Properties of the Red Cell Membrane in Relation to Molecular Structure and Genetic Defects." Annual Review of Biophysics and Biomolecular Structure 23(1): 787-818.

Nitatori, T., N. Sato, S. Waguri, Y. Karasawa, H. Araki, K. Shibanai, E. Kominami and Y. Uchiyama (1995). "Delayed neuronal death in the CA1 pyramidal cell layer of the gerbil hippocampus following transient ischemia is apoptosis." J. Neurosci. 15(2): 1001-1011.

Pettus, E. H., C. W. Christman, M. L. Giebel and J. T. Povlishock (1994). "Traumatically induced altered membrane permeability: its relationship to traumatically induced reactive axonal change." Journal Of Neurotrauma 11(5): 507-22.

Pettus, E. H. and J. T. Povlishock (1996). "Characterization of a distinct set of intra-axonal ultrastructural changes associated with traumatically induced alteration in axolemmal permeability." Brain Research 722(1-2): 1-11.

Sato, M., E. Chang, T. Igarashi and L. J. Noble (2001). "Neuronal injury and loss after traumatic brain injury: time course and regional variability." Brain Research 917(1): 45-54.

Schmued, L. C. and K. J. Hopkins (2000). "Fluoro-Jade B: a high affinity fluorescent marker for the localization of neuronal degeneration." Brain Research 874(2): 123-130.

Serbest, G., J. Horwitz and K. Barbee (2005). "The effect of poloxamer-188 on neuronal cell recovery from mechanical injury." J Neurotrauma 22(1): 119-32.

Serbest, G., J. Horwitz, M. Jost and K. Barbee (2006). "Mechanisms of cell death and neuroprotection by poloxamer 188 after mechanical trauma." The FASEB Journal 20(2): 308-310.

Shi, R. and R. B. Borgens (1999). "Acute repair of crushed guinea pig spinal cord by polyethylene glycol." Journal Of Neurophysiology 81(5): 2406-14.

Shi, R. and R. B. Borgens (2000). "Anatomical repair of nerve membranes in crushed mammalian spinal cord with polyethylene glycol." Journal Of Neurocytology 29(9): 633-43.

Singleton, R. H. and J. T. Povlishock (2004). "Identification and characterization of heterogeneous neuronal injury and death in regions of diffuse brain injury: evidence for multiple independent injury phenotypes." The Journal Of Neuroscience: The Official Journal Of The Society For Neuroscience 24(14): 3543-53.

Stone, J. R., D. O. Okonkwo, A. O. Dialo, D. G. Rubin, L. K. Mutlu, J. T. Povlishock and G. A. Helm (2004). "Impaired axonal transport and altered axolemmal permeability occur in distinct populations of damaged axons following traumatic brain injury." Experimental Neurology 190(1): 59-69.

Tomaiuolo, F., G. A. Carlesimo, M. Di Paola, M. Petrides, F. Fera, R. Bonanni, R. Formisano, P. Pasqualetti and C. Caltagirone (2004). "Gross morphology and morphometric sequelae in the hippocampus, fornix, and corpus callosum of patients with severe non-missile traumatic brain injury without macroscopically detectable lesions: a T1 weighted MRI study." J Neurol Neurosurg Psychiatry 75(9): 1314-1322.

Whalen, M., T. Dalkara, Z. You, J. Qiu, D. Bermpohl, N. Mehta, B. Suter, P. Bhide, E. Lo, M. Ericsson and M. Moskowitz (2007). "Acute plasmalemma permeability and protracted clearance of injured cells after controlled cortical impact in mice." J Cereb Blood Flow Metab 28(3): 490-505.

Zec, R. F., D. Zellers, J. Belman, J. Miller, J. Matthews, D. Ferneau-Belman and R. Robbs (2001). "Long-Term Consequences of Severe Closed Head Injury on Episodic Memory." Journal of Clinical & Experimental Neuropsychology 23(5): 671.

Zhang, L. and H. Mao (2008). Subregional mechanical properties contribute to local biomechanical response following traumatic brain injury. National Neurotrauma Symposium. Orlando, FL.

CHAPTER 4

CATWALK ASSESSMENT OF LOCOMOTOR DEFICITS FOLLOWING CORTICAL CONTUSION INJURY IN RATS

4.1 Abstract

Traumatic brain injury (TBI) is a leading cause of disability, resulting in altered gait and motor function in humans. Altered locomotor function is also commonly assessed in experimental models of traumatic brain injury. A variety of tests, including beam walk, grid walk, footprint analysis, and open field testing, have been used to assess locomotor deficits after experimental brain injury, but these assessments only provide relatively crude qualitative and semi-quantitative measurements. The objective of this study was to find a more sensitive and quantitative method for measuring alterations in locomotor deficits following brain injury in rats. Adult male rats received a unilateral cortical contusion injury or sham operation and were tested daily on the beam walk and CatWalk on the day of injury and for the following six days. Injured rats showed a sustained increased latency to cross the beam walk and decreased beam walk scores compared to shams through the end of the 6 day testing period, with a trend toward recovery consistent with previous reports. Performance on the CatWalk task generally showed altered motor function for all limbs on the day of injury and the first two days post-injury for the following parameters: stride length, swing speed, base of support, stand phase duration, duty cycle, and stand index. Within three to four days post-injury some of these parameters were no longer statistically different from shams. Remarkably

the unilateral injury resulted in bilateral changes in limb function that were detectable by the CatWalk system. These findings are significant as they demonstrate the CatWalk gait analysis system can provide a sensitive and accurate method of detecting locomotor deficits after cortical contusion injury in rats.

4.2 Introduction

Traumatic brain injury (TBI) is a leading socieoeconomic concern in the United States, with nearly 1.4 million people annually receiving emergency department treatment or hospitalization for a TBI (Langlois et al. 2006). While the initial clinical manifestations vary depending on the type and extent of injury, more than 5 million people live with long-term impairments resulting from TBI including altered motor function (Thurman et al. 1999). Gait-related motor impairments observed clinically following TBI include reduced walking speeds and shorter stride lengths (McFadyen et al. 2003), as well as increased variability in these gait parameters (Niechwiej-Szwedo et al. 2007).

Gait-related motor impairments have also been observed following experimental brain injury, and several methods are used to measure these alterations in motor function. (For review, see (Fujimoto et al. 2004)). Open field locomotor tests, whether manually or automatically observed and scored, allow for both quantitative or qualitative measurements of movement and exploratory behavior (Koob et al. 2006). The rotarod (Hamm et al. 1994), beam walk (Dixon et al. 1999), and grid walk (Baskin et al. 2003) tasks can be used to assess motor coordination and balance following TBI, while footprint analysis (Gonzalez-Pina et al. 2005) allows measurement of locomotor parameters including stride width and length. The beam walk task provides a crude

assessment of motor function by measuring the amount of time an animal takes to cross a narrow elevated beam and qualitatively scoring its hind limb performance and coordination as it completes the task. The equipment required for the task can be fashioned from common materials, so the task is inexpensive to set up (Gerfen 2006); as such the procedure is frequently used and referenced in the literature. Training animals for the task is straightforward, as the animals are motivated to not fall off the beam and to enter the darkened goal box at the end of the beam. Despite its simplicity and widespread use, the beam walk task does not allow for quantitative measurements of gait parameters.

Additionally an automated gait analysis system (CatWalk™ system, Noldus Information Technology, Inc., Leesburg, VA) is commercially available. In addition to quantitative spatial measurements afforded by the traditional ink and paper footprint analysis method, the CatWalk system also allows quantitative measurements of temporal differences in gait including step sequences and durations. This system has been successfully implemented in several studies characterizing locomotor deficits resulting from spinal cord injury (Koopmans et al. 2005; Gensel et al. 2006; Hamers et al. 2006), pain (Gabriel et al. 2007; Angeby-Moller et al. 2008), Parkinson's disease (Vlamings et al. 2007), and peripheral nerve injury (Deumens et al. 2007; Bozkurt et al. 2008).

The goal of this study was to determine whether the CatWalk system can detect locomotor deficits that result from controlled cortical impact in rats. The CatWalk may be a valuable tool for future research aimed at determining the mechanisms or treating gait impairments in the rat model of TBI. Therefore, the objective of this study was to characterize the TBI-induced gait alterations. Rats received a moderate/severe unilateral cortical contusion injury and behavioral outcomes were measured using both beam walk

and CatWalk analyses. While traditional locomotor tasks such as the beam walk provide only crude assessments of motor function, the CatWalk system allows for quantitative and sensitive measurements of multiple gait parameters in a single test. This study is the first reported use of the CatWalk gait analysis system to evaluate locomotor deficits following experimental brain injury.

4.3 Materials and methods

All surgical and behavioral procedures were approved by the Institutional Animal Care and Use Committee at the Georgia Institute of Technology.

4.3.1 Animal procedures and experimental injury model

In total, 15 adult male Sprague Dawley rats (400-500 g; Charles River Laboratories, Wilmington, MA) were anesthetized with Nembutal (50 mg/kg). Fur was shaved from the head which was then immobilized in a stereotactic frame. A midline incision was made into the scalp to reveal the skull, and a 7 mm diameter craniectomy was performed over the left fronto-parietal cortex centered 3.5 mm posterior to the bregma and 3.5 mm lateral to the midline. After removal of the skull flap, the 6 mm diameter impactor tip of the controlled cortical impact device (Pittsburgh Precision Instruments, Pittsburgh, PA) was positioned over the craniectomy site at a 15 degree angle from vertical and the zero distance of the impactor tip was set. Injured animals (n=9) received an impact to the brain with velocity 4.5 m/s to a depth of 2.7 mm; sham animals (n=6) received the same craniectomy surgery but no impact. Immediately following surgery, the scalp was closed and cleaned.

Beginning at pre-surgery training and throughout the course of the study, rats were individually housed in a 12 hour light/dark environment and received food *ad libitum*. All animals maintained their pre-surgical weight within 10% and showed no signs of infection following surgery.

4.3.2 Beam walk behavioral assessment

The method for measuring performance on a beam walk test was adapted from previously described methods (Gerfen 2006). A beam 1.25 m long by 2.5 cm wide was supported 30 cm above the surface of a table. A darkened goal box (25 cm deep by 20 cm wide by 15 cm tall) with a small entrance (10 cm wide by 9 cm high) was placed at one end of the beam. The time required to cross the middle 80 cm segment of the beam between the start line and the goal box was measured, and score was given to the animal based on their performance on the beam (Table 4.1, adapted from (Gerfen 2006)). A maximum latency to cross the beam of 60 s was allowed. Pre-surgery training required animals to complete three successful crossings of the beam on two consecutive days. Beam walk assessment was performed at the end of the light cycle on the surgery day (day 0) 6 to 8 hours following completion of the surgical procedure and then daily for six days. Performance from three successive trials on each day was averaged.

4.3.3 CatWalk behavioral assessment

The CatWalk system and animal training protocol has been described previously (Hamers et al. 2001). Animals were trained to traverse a 1.25 m long by 7 cm wide glass walkway that uses a video camera to digitally capture footprints as the rat crosses the middle 80 cm of the walkway. Footprint information was then analyzed using the

CatWalk software to determine timing and spacing between individual footprints. Thus the CatWalk system was sensitive to the velocity of the moving animal, and the pre-surgery training required animals to complete 10 passes of the walkway without hesitation in less than 5 seconds. To motivate the animals to cross, a small food treat (fruit cereal) and the home cage of the animal were placed at the end of the walkway. CatWalk assessment was performed at the beginning of the dark cycle on the surgery day (day 0) 6 to 8 hours following completion of the surgical procedure and then daily for six days. Performance from three successive crosses on each day was averaged.

4.3.4 Histological analysis

At the completion of the behavioral assessments (7 days post-surgery), animals were sacrificed and brain tissue was analyzed to confirm that injuries were consistent with previous studies. Rats were deeply anesthetized with Nembutal and perfused transcardially with ice cold saline followed by 4 % paraformaldehyde with 0.01 % glutaraldehyde. The brain was removed and post-fixed in paraformaldehyde with glutaraldehyde for 24 hr at 4 °C. The tissue was then submerged in 30 % sucrose at 4 °C for 3 days. The tissue was frozen in cryoembedding compound, sectioned at 20 µm thickness on a cryostat (Leica CM3050S, Wetzlar, Germany), and mounted on gelatin-coated slides. Tissue sections were Nissl stained with cresyl violet, and image montages were collected using Neurolucida software (MBF Bioscience, Williston, VT) on a Nikon 80i upright microscope (Nikon Instruments Inc., Melville, NY).

4.3.5 Statistical analysis

Comparisons of sham and injured animals at each time point were performed using two-way repeated-measures ANOVA followed by the Student-Newman-Keuls test. All data are represented as mean ± standard error with significance marked when $p < 0.05$.

4.4 Results

4.4.1 Experimental injury model

Histological analysis at 7 days post-surgery revealed a cavity at the injury site that extended through the cortex and subcortical white matter (Figure 4.1). This lesion extended into the hippocampus of some brains, and all brains exhibited Nissl loss in the ipsilateral CA3 subregion. Sham brains did not contain a cavity at the craniectomy site or damage to the ipsilateral hippocampus.

4.4.2 Beam walk behavioral assessment

Animals receiving sham surgery showed no significant changes in the latency to cross the beam or the beam walk score in the hours and days following surgery (Figure 4.2). However among the injured animals no animals were able to cross the beam on the day of surgery and the day after surgery. Although latency times and scores remained statistically lower than sham animals at the end of the testing period, the injured group showed a trend toward recovery. A summary of the statistical comparisons between sham and injured animals for the beam walk measurements is presented in Table 4.2. Within the injured population some animals recovered on the task and received scores and

latencies similar to uninjured animals but others never regained the ability to traverse the beam (data not shown).

4.4.3 CatWalk behavioral assessment

The following gait parameters were measured using the CatWalk system: stride length, swing speed, base of support, stand, duty cycle, and stand index. The step cycle, which is referenced in the calculations of some of these parameters, consists of two parts for each step: the stand phase and the swing phase. A summary of the statistical comparisons between sham and injured animals for each of these parameters is also presented in Table 4.2.

4.4.3.1 Stride length

Stride length, which is the distance between successive placements of the same paw, was significantly reduced compared to shams in all limbs on the day of and the first day following injury (Figure 4.3). A reduced stride length was also observed in injured animals on the right front limb on day 2 and on the right front and hind limbs on day 3.

4.4.3.2 Swing speed

With the exception of the left hind limb, all limbs showed a statistically reduced swing speed compared to shams on the day of and the first day following injury (Figure 4.4). Swing speed, which is the speed of the limb during the swing phase of the step cycle, was also reduced in injured animals in the left front limb on day 2, in the right front limb and the right and left hind limbs on day 3, and the right front limb on day 4.

4.4.3.3 Base of support

The distance between the hind paws or the paws, or the stride width, is referred to as the base of support. The base of support was greater on the day of injury compared to shams for the hind paws, on the day following injury for the front paws and the hind paws, and the second day following injury for the hind paws (Figure 4.5).

4.4.3.4 Stand

The stand phase duration is the amount of time each paw spends in contact with the floor. The stand phase duration was statistically increased for all limbs on the day of and on the first and second days following injury compared to shams (Figure 4.6).

4.4.3.5 Duty cycle

The duty cycle is the percentage of the step cycle that a paw is in contact with the floor. The duty cycle is increased following injury compared to shams on the day of injury in all limbs except the right hind limb (Figure 4.7). Duty cycle is also statistically increased in the left front and hind limbs on the first day following injury and in all limbs except the right hind limb on the second day following injury. Both front limbs are statistically increased on day 5, and the left hind limb is statistically increased on day 6. The difference for the right hind limb was not significant on any testing day.

4.4.3.6 Stand index

The stand index represents the speed at which the paw looses contact with the glass floor by measuring the area of the paw print. Stand index was statistically increased on the day of injury for both front paws and on the left hind paw (Figure 4.8). Stand

index was also statistically increased for right front and left hind paws on the first day following injury and for the left hind paw on days 4 and 6.

4.5 Discussion

This study is the first to use the CatWalk system to measure locomotor changes in rats following cortical contusion injury. Brain injury caused changes in motor function in all four limbs that could be measured by the CatWalk system, and the measures tested were only statistically different compared to shams within the first few days post surgery (days 0 through day 2). These locomotor changes were in agreement with the deficits observed on the beam walk task, suggesting the CatWalk system may be suitable for assessing multiple modes of motor deficits in rats resulting from brain injury.

The injury velocity and depth were selected to match injury severity to a previous study that used beam walk performance as an outcome measure (Dixon et al. 1999). The results of the previous study and the present study are similar, with rats showing improvement on beam walk performance by the end of the testing period. However unlike the previous study, the injured population in the present study did not show a complete recovery perhaps due to a difference in injury location

Within the context of studies characterizing locomotor deficits following brain injury, it should be noted that the type and duration of deficits are dependent on the injury model. A summary of these studies is provided by Fujimoto et al. (Fujimoto et al. 2004). For example beam walk deficits were shown to last up to three days in previous studies of controlled cortical impact in rats (Dixon et al. 1999), whereas deficits have persisted through 9 weeks after the same injury in mice (Tate et al. 2007). Furthermore, beam walk deficits have been shown to persist through 6 weeks in rat fluid percussion injury model

(Lyeth et al. 2001). While the present study matches the injury velocity and depth of the study performed by Dixon et al. in 1999, the differences in behavioral outcome between these two studies may be due to small differences in the location of the injury. Thus model selection is an important factor in determining locomotor outcome. The changes in neurological motor function observed after brain injury in rats may be different in mice, in an injury model other than controlled cortical impact (such as fluid percussion or impact acceleration injury), or even in the same injury model with different injury parameters.

While the CatWalk system provides a plethora of data and measurements for each experimental trial, we found that care must be taken when interpreting the data. The CatWalk is sensitive for some measurements, including the ones presented in this study. However other measurements provided by the device where differences were expected showed no statistical difference. An example of this is the print position, or the difference in position of a hind paw compared to the previously placed corresponding front paw. An uninjured rat will place its hind foot very close to where its front foot was previously placed whereas the foot placement of an injured rat will deviate from this placement; however we observed variability of the print position measurement within both the sham and injured groups, preventing statistical significance despite a qualitative observed change from normal. While increasing the statistical power of the experimental design may resolve this, it is possible that the CatWalk system may not be suitable for determining subtle differences or increased variability in print position (and other parameters as well) after brain injury.

The general observations of this study support clinical observations of human patients recovering from a brain injury. Walking velocity is reduced in patients with a brain injury (Ochi et al. 1999) (McFadyen et al. 2003), and during the experimental period it was observed that injured rats generally crossed the CatWalk at a slower speed than sham rats (data not shown). Ochi et al. suggest this reduced velocity in patients may be related to a reduced step length, which was also observed in rats in this study (Ochi et al. 1999). They also note that in brain injured patients the unaffected limb has a longer stance time, allowing for increased stability as the affected limb swings and enters its stance. Similarly we find a significant increase in the duty cycle in the left front and hind unaffected limbs of the injured rat.

Adding to the complexity of the data, other factors may affect the performance of the rat on the CatWalk. Rats on the beam walk have two incentives to complete the crossing task: to not fall off the beam and to enter the darkened goal box at the end of the beam. However the CatWalk task is performed in the dark and rats have no risk of falling; their only motivation to complete the task is their pre-injury training and their home cage positioned with a food treat at the end of the platform. Several injured rats had difficulty completing the CatWalk task, walking slowly and sometimes stopping halfway across the platform. McFadyen et al. cite clinical studies where brain injured patients suffer from anxiety and that anxiety can affect motor function, suggesting that anxiety and fear may have a negative effect on locomotor function (McFadyen et al. 2003). These effects may be more pronounced on rats freely walking on the CatWalk apparatus compared to the beam walk.

In conclusion, the CatWalk system is complementary to other testing methods and may be a useful tool for quantitatively assessing different types of and treatments for TBI-related locomotor deficits in rats. It provides consistent and quantifiable data that complement other assessment methods. Testing trials take about as long to perform as the beam walk but much more time is required for data analysis. However the extra time spent on analysis may yield results that could reveal subtle locomotor changes undetectable by other methods. This sensitivity may be an asset for future studies of brain injury induced motor deficits and may provide useful information for investigations of potential rehabilitative strategies.

Table 4.1: Beam walk scoring system (adapted from Gerfen 2006)

Score	Performance on the beam
1	Unable to cross beam and cannot place right hind limb on beam
2	Unable to cross beam but places right hind limb on beam, maintains balance ≥ 5 s
3	Crosses beam by dragging right hind limb
4	Crosses beam and places right hind limb on beam at least once
5	Crosses beam but uses right hind limb in < 50 % of steps
6	Crosses beam but uses right hind limb in > 50 % of steps
7	Crosses beam normally with no more than 2 foot falls of the right hind limb

Rats were given a score of 1 to 7 based on their performance on the beam walk task. Three trials were collected and averaged for each animal to determine the score at each time point.

Table 4.2: Summary of behavior assessment statistics

		Time point							
Parameter	Limb	baseline	day 0	day 1	day 2	day 3	day 4	day 5	day 6
Latency to cross			*	*	*	*	*	*	*
Beam walk score	H		*	*	*	*	*	*	*
Stride length	LF		*	*					
	RF		*	*	*	*			
	LH		*	*					
	RH		*	*		*			
Swing speed	LF		*	*	*				
	RF		*	*		*	*		
	LH			*		*			
	RH		*	*		*			
Base of support	F			*					
	H		*	*	*				
Stand	LF		*	*	*				
	RF		*	*	*				
	LH		*	*	*				
	RH		*	*	*				
Duty cycle	LF		*	*	*			*	
	RF		*		*			*	
	LH		*	*	*				*
	RH								
Stand index	LF		*						
	RF		*	*					
	LH		*	*			*		*
	RH								

L = left, R = right, F = front, H = hind, * indicates $p < 0.05$ (injured vs. sham)

Locomotor parameters were measured on the beam walk (latency to cross and score) and on the CatWalk (stride length, swing speed, base of support, stand, duty cycle, and stand index) before injury (baseline), on the day of injury (day 0), and following injury on days 1 through 6. (* indicates $p < 0.05$ comparing injured to sham at a time point)

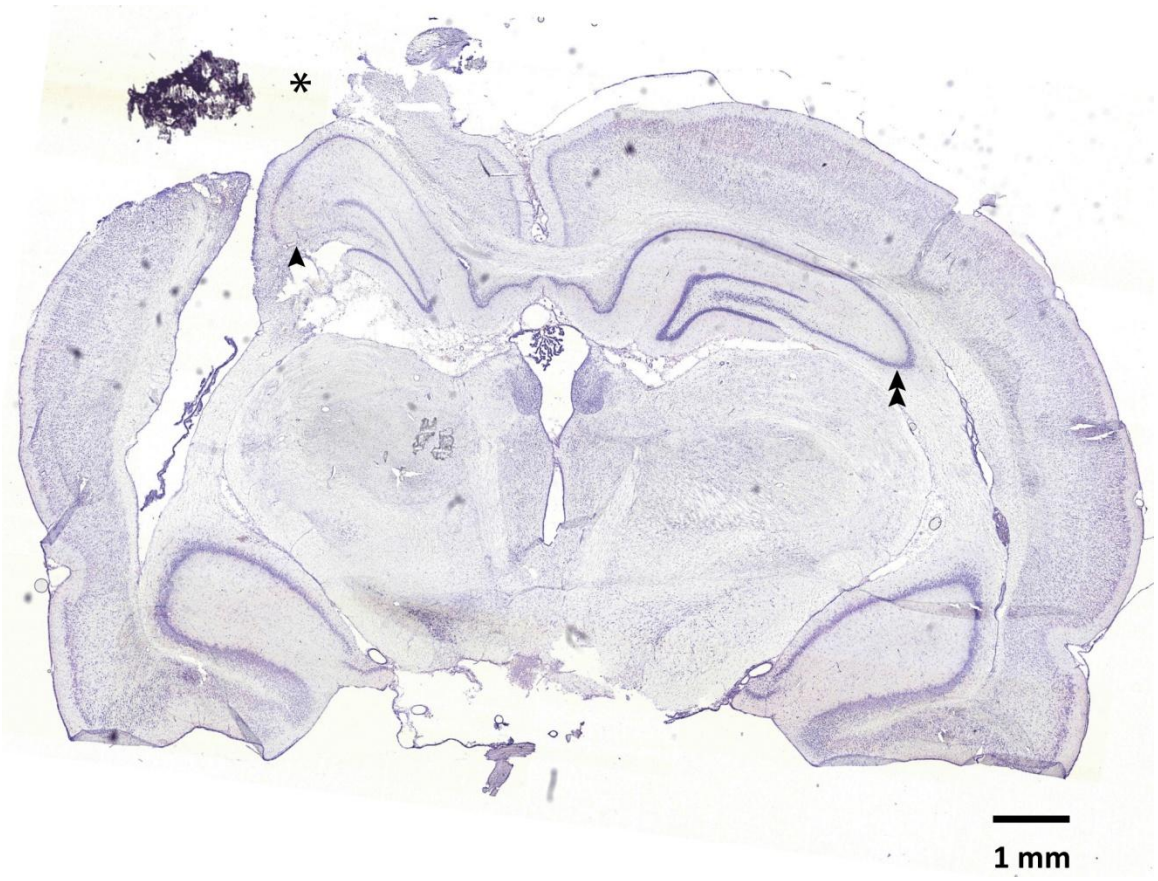

Figure 4.1: Representative tissue damage 7 days post-injury

Rough endoplasmic reticulum, also known as the Nissl substance, can be identified using a Nissl stain such as cresyl violet, and neuronal degeneration is characterized by loss of Nissl stain (Young et al. 2000). Cresyl violet staining of the injured brain at 7 days post-injury reveals tissue loss forming an injury cavity in the ipsilateral sensorimotor cortex and the corpus callosum (*). Nissl loss is evident in the CA3 subregion of the ipsilateral hippocampus (arrowhead) compared to the contralateral hippocampus (double arrowhead). (scale bar = 1 mm)

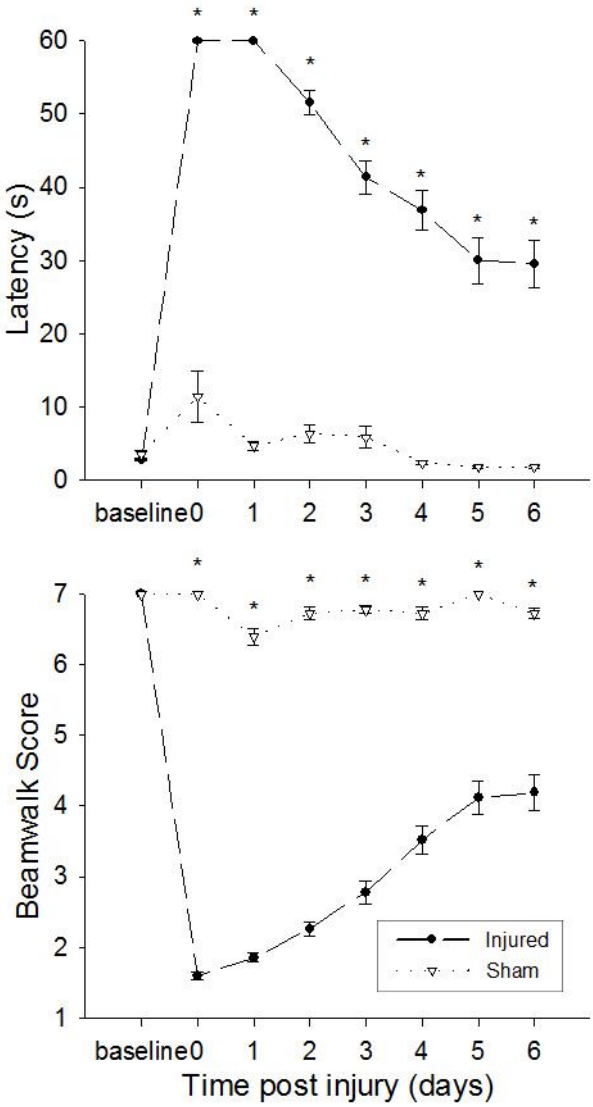

Figure 4.2: Beam walk behavioral assessment

The latency to cross the beam was significantly increased compared to shams at all measured time points post-injury. The beam walk score was also significantly reduced compared to shams at all measured time points post-injury. (* $p < 0.05$)

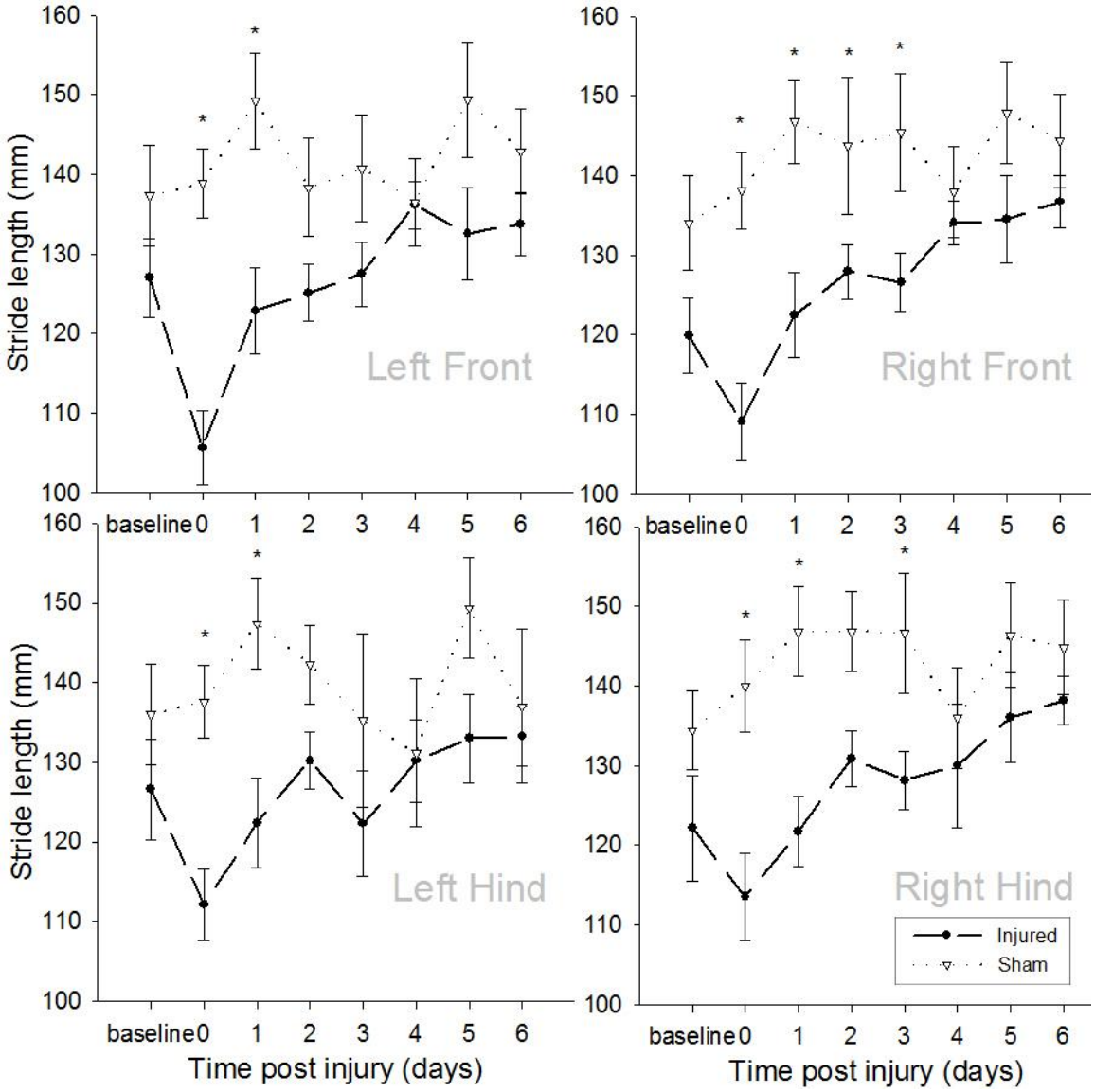

Figure 4.3: Stride length

The distance between successive placements of the same paw, or stride length, was measured before injury (baseline), 6 to 8 hours following injury (day 0), and daily for six days (days 1-6). (* $p < 0.05$)

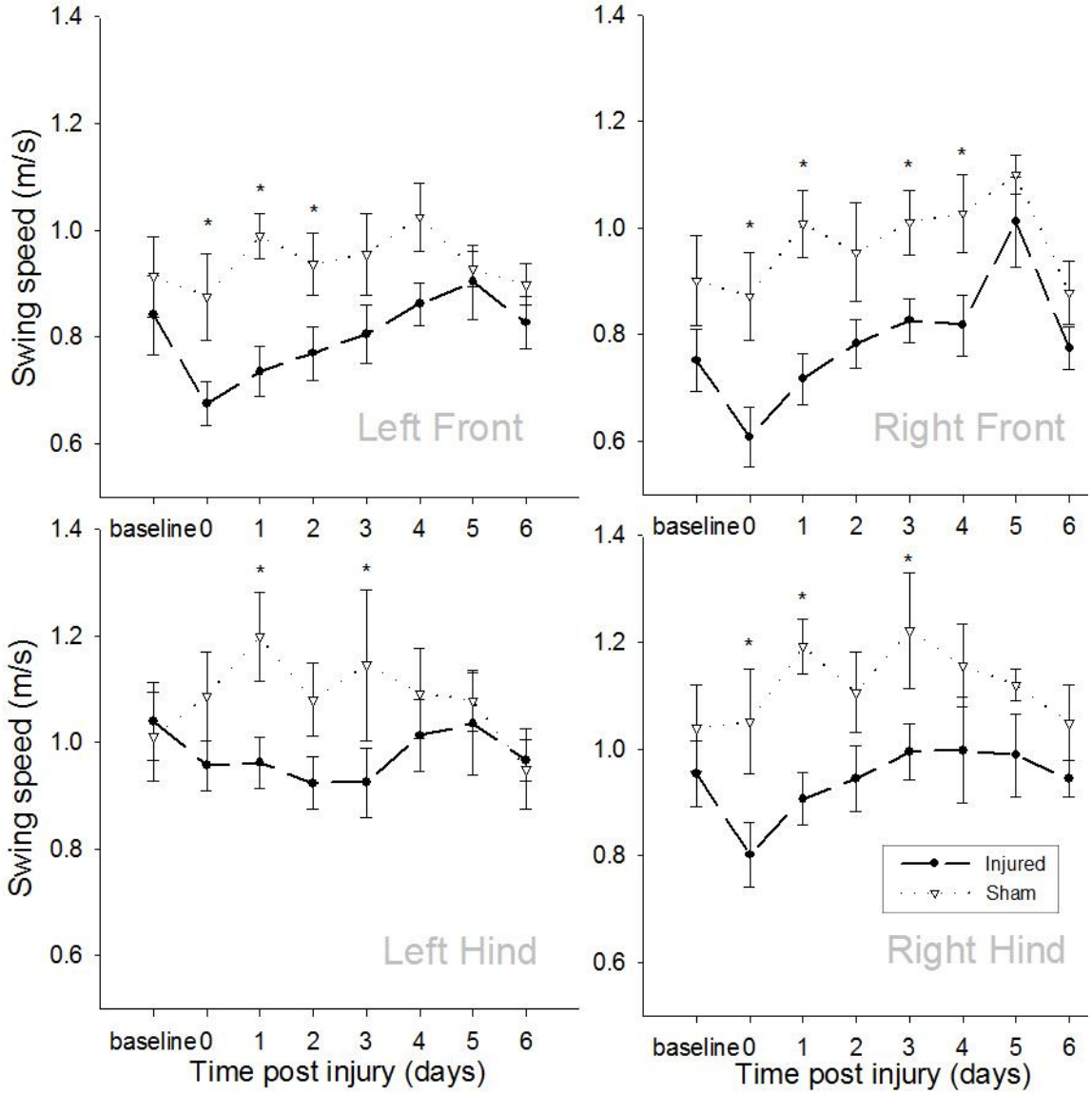

Figure 4.4: Swing speed

Swing speed, or the speed of the limb during the swing phase of the step cycle, was measured before injury (baseline), 6 to 8 hours following injury (day 0), and daily for six days (days 1-6). (* $p < 0.05$)

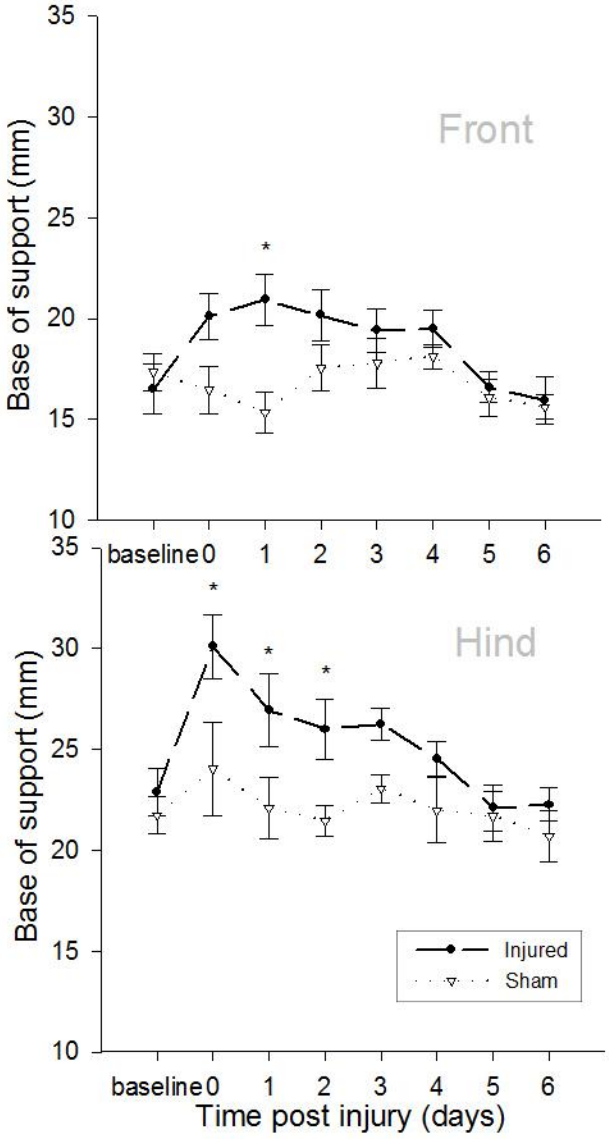

Figure 4.5: Base of support

Base of support, or the distance between the paws, was measured before injury (baseline), 6 to 8 hours following injury (day 0), and daily for six days (days 1-6). (* $p < 0.05$)

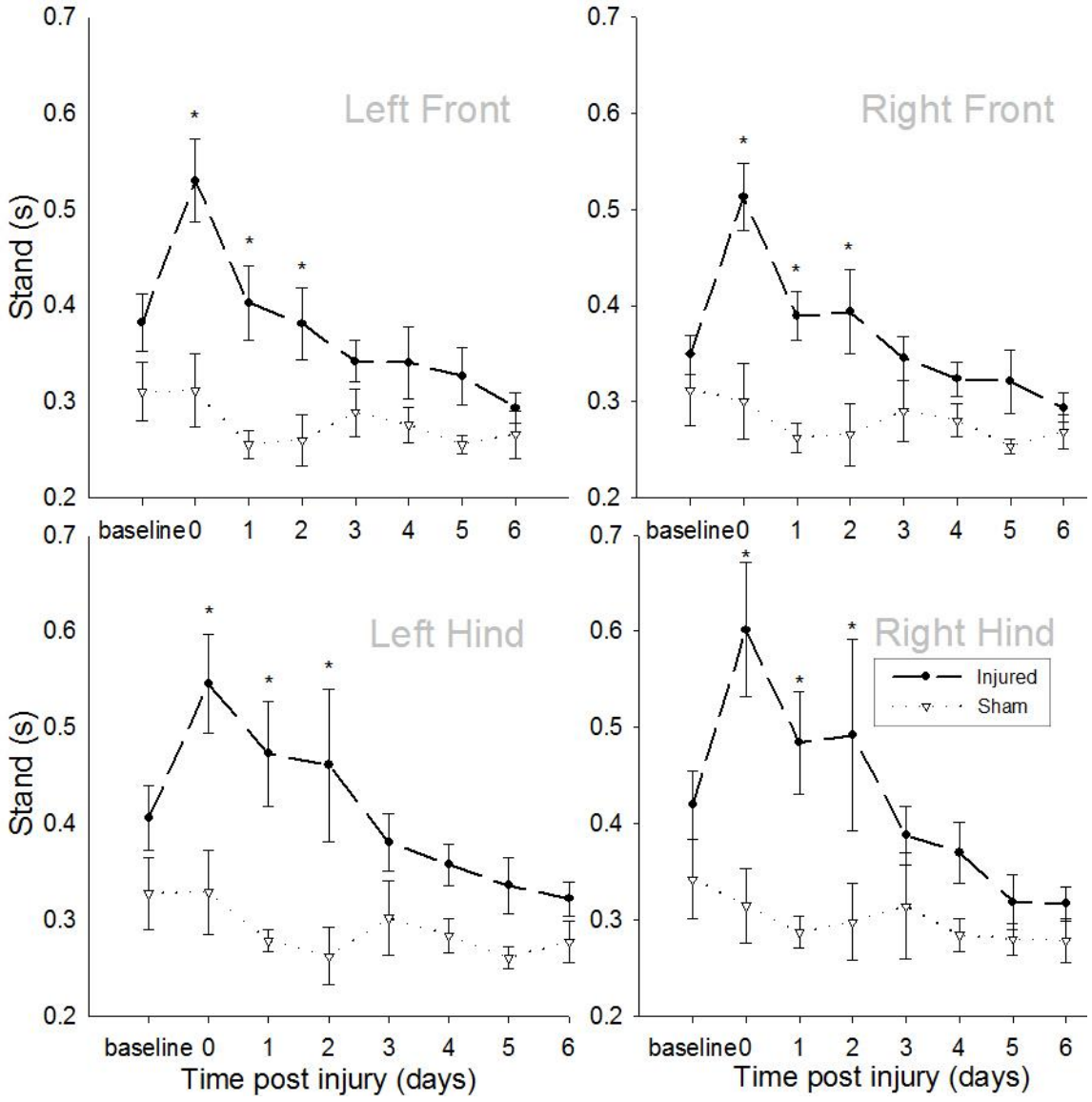

Figure 4.6: Stand

The amount of time each paw spends in contact with the floor, also called stand or the stand phase duration, was measured before injury (baseline), 6 to 8 hours following injury (day 0), and daily for six days (days 1-6). (* $p < 0.05$)

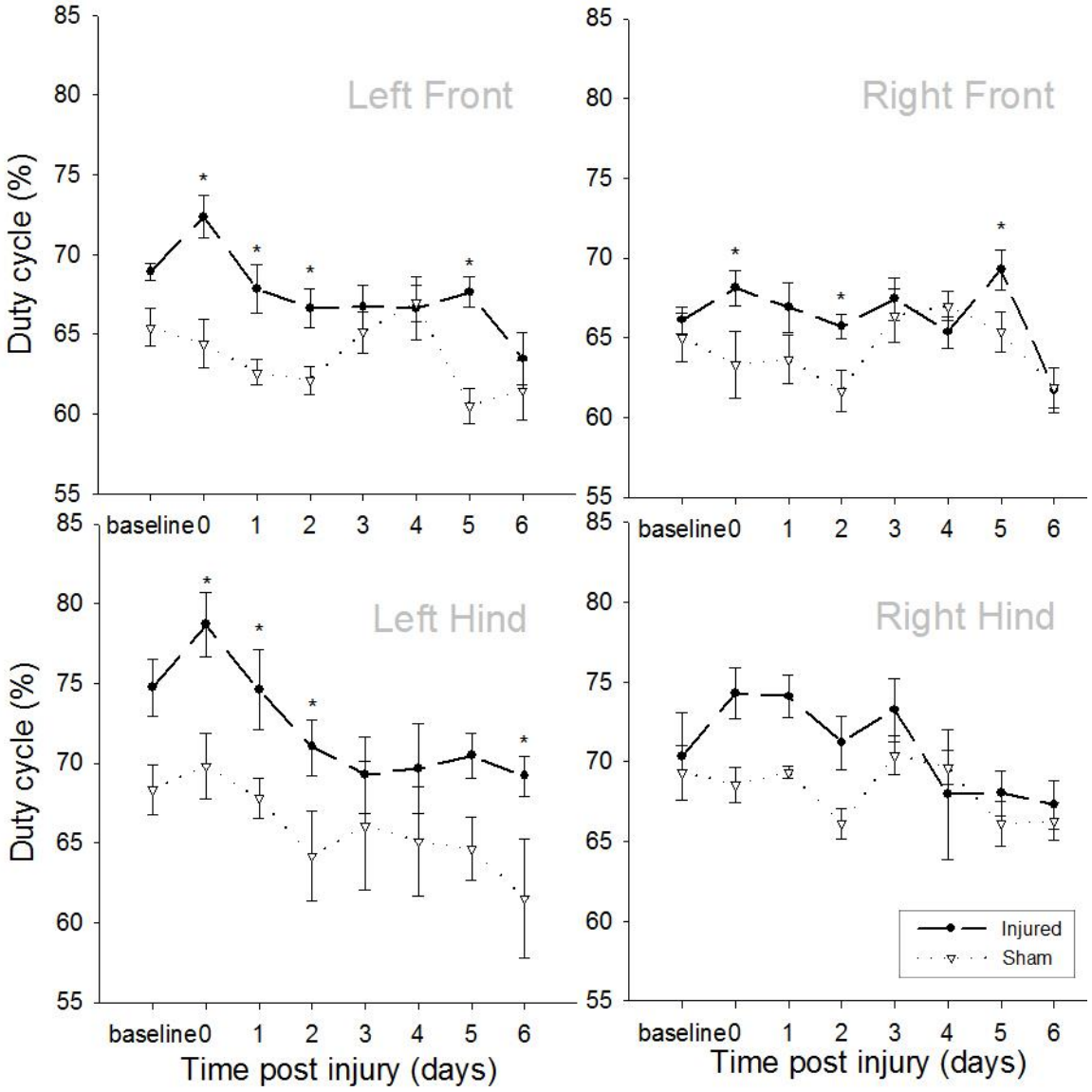

Figure 4.7: Duty cycle

Duty cycle is the percentage of the step cycle that a paw is in contact with the floor. It was calculated before injury (baseline), 6 to 8 hours following injury (day 0), and daily for six days (days 1-6). (* $p < 0.05$)

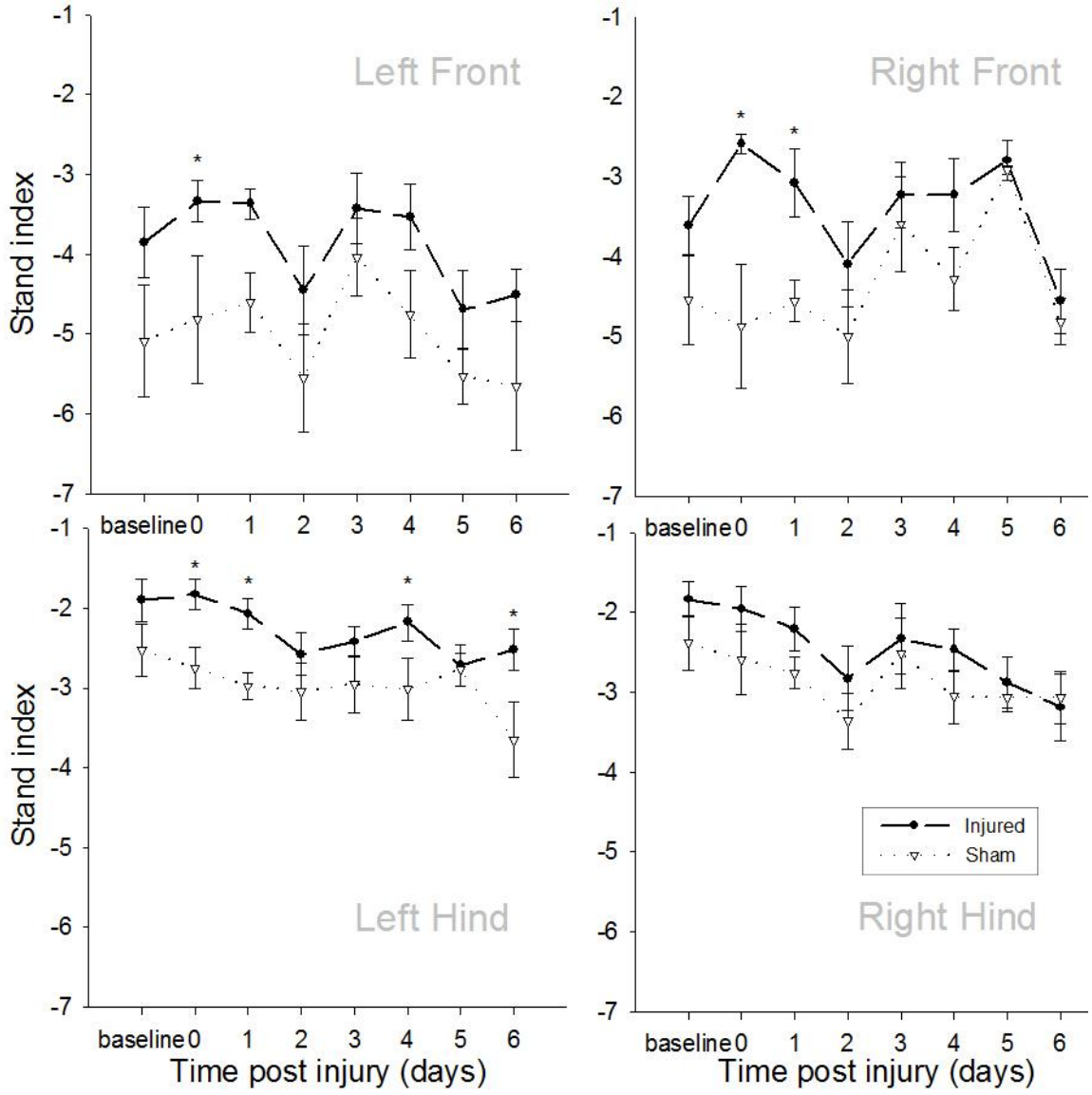

Figure 4.8: Stand index

The stand index represents the speed at which the paw loses contact with the floor. It was measured before injury (baseline), 6 to 8 hours following injury (day 0), and daily for six days (days 1-6). (* $p < 0.05$)

4.6 Works cited

Angeby-Moller, K., O. G. Berge and F. P. Hamers (2008). "Using the CatWalk method to assess weight-bearing and pain behaviour in walking rats with ankle joint monoarthritis induced by carrageenan: effects of morphine and rofecoxib." Journal Of Neuroscience Methods 174(1): 1-9.

Baskin, Y. K., W. D. Dietrich and E. J. Green (2003). "Two effective behavioral tasks for evaluating sensorimotor dysfunction following traumatic brain injury in mice." Journal Of Neuroscience Methods 129(1): 87-93.

Bozkurt, A., R. Deumens, J. Scheffel, D. M. O'Dey, J. Weis, E. A. Joosten, T. Fuhrmann, G. A. Brook and N. Pallua (2008). "CatWalk gait analysis in assessment of functional recovery after sciatic nerve injury." Journal Of Neuroscience Methods 173(1): 91-8.

Deumens, R., R. J. Jaken, M. A. Marcus and E. A. Joosten (2007). "The CatWalk gait analysis in assessment of both dynamic and static gait changes after adult rat sciatic nerve resection." Journal Of Neuroscience Methods 164(1): 120-30.

Dixon, C. E., M. F. Kraus, A. E. Kline, X. Ma, H. Q. Yan, R. G. Griffith, B. M. Wolfson and D. W. Marion (1999). "Amantadine improves water maze performance without affecting motor behavior following traumatic brain injury in rats." Restor Neurol Neurosci 14(4): 285-294.

Fujimoto, S. T., L. Longhi, K. E. Saatman, V. Conte, N. Stocchetti and T. K. McIntosh (2004). "Motor and cognitive function evaluation following experimental traumatic brain injury." Neurosci Biobehav Rev 28(4): 365-78.

Gabriel, A. F., M. A. Marcus, W. M. Honig, G. H. Walenkamp and E. A. Joosten (2007). "The CatWalk method: a detailed analysis of behavioral changes after acute inflammatory pain in the rat." Journal Of Neuroscience Methods 163(1): 9-16.

Gensel, J. C., C. A. Tovar, F. P. Hamers, R. J. Deibert, M. S. Beattie and J. C. Bresnahan (2006). "Behavioral and histological characterization of unilateral cervical spinal cord contusion injury in rats." Journal Of Neurotrauma 23(1): 36-54.

Gerfen, C. R. (2006). Short protocols in neuroscience : systems and behavioral methods. Hoboken, Wiley.

Gonzalez-Pina, R., A. Bueno-Nava, S. Montes, A. Alfaro-Rodriguez, A. Gonzalez-Maciel, R. Reynoso-Robles and F. Ayala-Guerrero (2005). "Pontine norepinephrine content after motor cortical ablation in rats." Proc West Pharmacol Soc 48: 73-6.

Hamers, F. P., A. J. Lankhorst, T. J. van Laar, W. B. Veldhuis and W. H. Gispen (2001). "Automated quantitative gait analysis during overground locomotion in the rat: its

application to spinal cord contusion and transection injuries." J Neurotrauma 18(2): 187-201.

Hamers, F. P. T., G. C. Koopmans and E. A. J. Joosten (2006). "CatWalk-Assisted Gait Analysis in the Assessment of Spinal Cord Injury." Journal Of Neurotrauma 23(3-4): 537-548.

Hamm, R. J., B. R. Pike, D. M. O'Dell, B. G. Lyeth and L. W. Jenkins (1994). "The rotarod test: an evaluation of its effectiveness in assessing motor deficits following traumatic brain injury." Journal Of Neurotrauma 11(2): 187-196.

Koob, A. O., J. Cirillo and C. F. Babbs (2006). "A novel open field activity detector to determine spatial and temporal movement of laboratory animals after injury and disease." Journal Of Neuroscience Methods 157(2): 330-6.

Koopmans, G. C., R. Deumens, W. M. M. Honig, F. P. T. Hamers, H. W. M. Steinbusch and E. A. J. Joosten (2005). "The Assessment of Locomotor Function in Spinal Cord Injured Rats: The Importance of Objective Analysis of Coordination." Journal Of Neurotrauma 22(2): 214-225.

Langlois, J. A., W. Rutland-Brown and K. E. Thomas (2006). "Traumatic brain injury in the United States: emergency department visits, hospitalizations, and deaths." Atlanta (GA): Centers for Disease Control and Prevention, National Center for Injury Prevention and Control: 1–55.

Lyeth, B. G., Q. Z. Gong, S. Shields, J. P. Muizelaar and R. F. Berman (2001). "Group I metabotropic glutamate antagonist reduces acute neuronal degeneration and behavioral deficits after traumatic brain injury in rats." Experimental Neurology 169(1): 191-9.

McFadyen, B. J., B. Swaine, D. Dumas and A. Durand (2003). "Residual effects of a traumatic brain injury on locomotor capacity: a first study of spatiotemporal patterns during unobstructed and obstructed walking." The Journal Of Head Trauma Rehabilitation 18(6): 512-25.

Niechwiej-Szwedo, E., E. L. Inness, J. A. Howe, S. Jaglal, W. E. McIlroy and M. C. Verrier (2007). "Changes in gait variability during different challenges to mobility in patients with traumatic brain injury." Gait & Posture 25(1): 70-7.

Ochi, F., A. Esquenazi, B. Hirai and M. Talaty (1999). "Temporal-spatial feature of gait after traumatic brain injury." The Journal Of Head Trauma Rehabilitation 14(2): 105-15.

Tate, C. C., A. J. Garcia and M. C. LaPlaca (2007). "Plasma fibronectin is neuroprotective following traumatic brain injury." Experimental Neurology 207(1): 13-22.

Thurman, D. J., C. Alverson, K. A. Dunn, J. Guerrero and J. E. Sniezek (1999). "Traumatic brain injury in the United States: A public health perspective." J Head Trauma Rehabil 14(6): 602-15.

Vlamings, R., V. Visser-Vandewalle, G. Koopmans, E. A. Joosten, R. Kozan, S. Kaplan, H. W. Steinbusch and Y. Temel (2007). "High frequency stimulation of the subthalamic nucleus improves speed of locomotion but impairs forelimb movement in Parkinsonian rats." Neuroscience 148(3): 815-23.

Young, B., J. W. Heath, A. Stevens, J. S. Lowe, P. R. Wheater and H. G. Burkitt (2000). Wheater's functional histology : a text and colour atlas. Edinburgh ; New York, Churchill Livingstone.

CHAPTER 5

DISCUSSION

The studies presented in this thesis contribute to the understanding of the mechanisms of acute cell damage that initiate neuronal dysfunction and cell death resulting from traumatic brain injury. Multi-scale experiments were used to demonstrate the utility of a well controlled *in vitro* system as well as more complex animal studies in conjunction with novel analysis techniques.

5.1 *In vitro* neuronal injury model

5.1.1 Conclusions

Using an *in vitro* injury model with a novel cell culture scaffold we found that the mechanical properties and extracellular matrix composition of the injury substrate influence cell survival post-injury (Cullen et al. 2007). This unique injury model serves as a robust platform for future investigations. For example, modification of the ECM motifs presented to neurons in the cultures will facilitate investigation of specific mechanotransduction events in neuronal injury. Different ECM may initiate an alternate receptor-ligand signaling response to injury, allowing us to discern the dominant signaling pathways contributing to cell survival or cell death after mechanical trauma. Additionally, by directly controlling the interactions between cells and the extracellular environment, we will be able to more clearly discern how mechanical forces and deformations are transmitted to and affect cells. This force transfer presumably occurs via cell-cell and cell-ECM interactions and may result in stress concentrations at these

connections rather than as a stress distribution evenly across the cell. Stress concentrations may also develop at the interface between morphological features, such as at the axon hillock or at axonal branches. These stress concentrations on the cell surface may lead to plasma membrane rupture and mechanical failure of the cell.

5.1.2 Significance and contribution to literature

The *in vitro* work presented in this thesis establishes a novel 3-D platform for studying the role cell-ECM interactions and ECM stiffness play in the neuronal injury response. Cell growth, biochemical responses, and gene expression in a 3-D cell culture system are more similar to the *in vivo* situation than 2-D systems (Masi et al. 1992; Hoffman 1993; Fawcett et al. 1995; Granet et al. 1998). Additionally the culture model has three components (cell type and density, agarose substrate stiffness, and ECM composition) that can be independently and systematically varied, providing a level of control unattainable in other *in vitro* and *in vivo* systems.

5.1.3 Implications for therapy

This cell culture system and injury model can be used as a tool to probe the fundamental mechanisms of traumatic brain injury at the cellular level. Additionally it is well suited as a platform for screening potential therapies. Furthermore, while this system was designed and optimized to study neuronal injury, it employs the general tissue engineering strategy of scaffold plus ECM plus cells. As such, it can be readily adapted to investigate neural tissue engineering and regenerative therapies that promote repair.

5.2 Plasma membrane damage and neuronal degeneration

5.2.1 Conclusions

The permeability study is one of the first report of concomitant TBI-induced plasma membrane damage and cell degeneration in the hippocampus, and the mechanisms by which plasma membrane damage leads to cell death appear to be complex. Adjacent permeable cells often had dissimilar fates, with one appearing healthy and the one next to it showing signs of degeneration. If plasma membrane damage alone is not sufficient to cause cell death, then other factors must contribute to cell outcome. Perhaps the size or number of membrane tears or the duration of permeability may determine whether a neuron can recover from a traumatic mechanical insult. Or perhaps the cells experience the same extent and duration of permeability but one cell is energetically or genetically more capable of repair. Finally, it is possible that the non-degenerating cell may appear healthy in the acute timeframe following injury but experience a delayed cell death that occurs outside our 24 hour observation window. While repairing plasma membrane damage after injury may promote cell survival, understanding the injury response of non-degenerating permeable cells may be more beneficial for identifying new therapeutic targets.

Our observations of the subregional differences in plasma membrane damage in the hippocampus have led to an exciting collaboration using finite element analysis of the injured brain to predict locations of cell damage after injury. Using high spatial resolution measurements of the mechanical properties of subregions of the hippocampus obtained by researchers at Columbia University, a more accurate finite element model of the injured brain is being generated at Wayne State University. What is presented here is a

preliminary comparison of our observations of the subregional differences in plasma membrane damage to the predicted strains in the hippocampus, finding that more plasma membrane damage is detected in regions of predicted high strain. Further validation of the finite element model should include manipulation of injury severity and location as well as comparison of the fidelity of the predictive model to observed cell damage. Having a computational model for predicting regional damage after brain injury will be a valuable tool that allows for targeted treatment opportunities determined by the biomechanics of the injury itself.

5.2.2 Significance and contribution to literature

The permeability study is one of the first to show concomitant plasma membrane damage and cell degeneration in neurons following brain injury, addressing the limitations of two previous studies that have attempted to do the same. A 2004 study by Singleton and Povlishock notes incomplete overlap between markers of plasma membrane damage and neuronal degeneration, but these statements were based on qualitative observations of injured tissue (Singleton and Povlishock 2004). The quantified data presented in this thesis substantiates Singleton and Povlishock's report, suggesting that while only some neurons with plasma membrane damage show signs of degeneration, most degenerating neurons in the cell body layers of the hippocampus of the injured brain also show evidence of plasma membrane damage. A 2007 study by Whalen et al. used propidium iodide as a permeability marker to show that all neurons with plasma membranes damaged at the moment of injury are cleared from the brain in the days following injury (Whalen et al. 2007). The authors of that study however do not discuss the potential toxicity of propidium iodide and whether the presence of the marker

itself could play a role in the degeneration, death, and clearance of injured cells from the brain. For our permeability marker we chose dextran, a non-toxic molecule that is commonly used in long-term cell tracer studies (Heinzmann 1980; Condron and Zinn 1994), and thus the marker itself should have no short-term toxicity that would affect the interpretation of our results. Furthermore, its long term stability should also enable the tracking of permeable cells following injury for several days or more, providing more latitude in future studies investigating the time course of neuronal degeneration and death after plasma membrane damage.

5.2.3 Implications for therapy

Previous studies have shown the efficacy of plasma membrane resealing agents like polyethylene glycol and poloxamer-188 for improving cellular and behavioral outcomes in experimental models of neural injury (Shi and Borgens 1999; Shi and Borgens 2000; Marks et al. 2001; Luo et al. 2002; Curry et al. 2004a; Curry et al. 2004b; Laverty et al. 2004; Koob et al. 2005; Serbest et al. 2005; Koob and Borgens 2006; Serbest et al. 2006; Kilinc et al. 2008; Koob et al. 2008). However given the complexity of the brain environment following injury, targeting plasma membrane damage alone may not be sufficient for sustained improved clinical outcomes. As many of the components of the secondary injury response are interrelated, one could address one therapeutic target from multiple approaches. For example, an increase in intracellular calcium after injury may be a primary initiator of cell dysfunction following injury, and this increase may be due to plasma membrane damage, increased NMDA receptor activation, or release from the endoplasmic reticulum. A treatment including a plasma membrane resealing agent like poloxamer-188 (which will inhibit calcium influx through

membrane tears or pores) combined with the NMDA antagonist MK-801 (which will inhibit calcium influx through the NMDA receptor) and an inhibitor of calcium release from the endoplasmic reticulum (such as xestospongin or dantrolene) would address the multiple potential sources of increased intracellular calcium following injury. Such an approach could prove to be more effective than any of these therapies alone. Improved understanding of the role that plasma membrane damage plays in traumatic brain injury may make a compelling case for the investigation of plasma membrane repair as a component of novel clinical therapies.

5.3 Locomotor deficits following brain injury

5.3.1 Conclusions

We are also the first to use the CatWalk gait analysis system for measuring changes in locomotor function following traumatic brain injury. We found that this system has sufficient sensitivity to detect both locomotor deficits and gait adaptations made by the animal to accommodate affected limbs. Combining this system with a cognitive behavior test, such as the Morris water maze, will provide a robust testing battery for measuring injury-induced alterations in behavior as well as the functional efficacy of therapeutic agents.

5.3.2 Significance and contribution to the literature

This study establishes the CatWalk gait analysis system for the study of locomotor changes following traumatic brain injury. This system has been used previously to study locomotor changes in experimental models of spinal cord injury (Koopmans et al. 2005; Gensel et al. 2006; Hamers et al. 2006), sciatic nerve resection

(Deumens et al. 2007; Bozkurt et al. 2008), Parkinson's disease (Vlamings et al. 2007), pain (Gabriel et al. 2007), and arthritis (Angeby-Moller et al. 2008), but this is its first use for TBI. The addition of the CatWalk system to the behavioral analysis toolkit for brain injury researchers will for the first time enable the quantitative simultaneous measurement of multiple spatiotemporal parameters of locomotion, potentially increasing experimental throughput by allowing measurement of several gait parameters from a single test.

5.3.3 Implications for therapy

The strengths of the CatWalk gait analysis system lie in its versatility and its sensitivity, and it will likely serve as an effective platform for screening the locomotor effects of novel therapeutic agents in experimental brain injury models. Its ability to measure multiple related and unrelated gait parameters on each individual testing run give it unmatched versatility compared to other systems, while its real-time digital acquisition capabilities provide a sensitivity for identification of locomotor deficits or improvements that may be undetectable by other methods. As has been shown for studies of spinal cord injury and other pathologies, our data suggest the robustness and ease of use of this system may increase the quantity and quality of data provided while reducing animal testing time for screening potential therapies for traumatic brain injury.

5.4 Summary

In conclusion, characterization of how neurons fail under mechanical deformation may be integral to understanding how they respond to injury. Cell-ECM linkages and scaffold stiffness determine cell viability after injury *in vitro*, and our results suggest

stiffness of the hippocampal subregions may influence the extent of plasma membrane damage in the hippocampus after injury. We know now that most cells that sustain plasma membrane damage show evidence of degeneration and death, but that there also exists a population that is damaged but that survives the injury. A better understanding of the neuronal response to mechanical deformation as well as potential therapeutic targets may come from examining both of these cell populations.

5.5 Works cited

Angeby-Moller, K., O. G. Berge and F. P. Hamers (2008). "Using the CatWalk method to assess weight-bearing and pain behaviour in walking rats with ankle joint monoarthritis induced by carrageenan: effects of morphine and rofecoxib." Journal Of Neuroscience Methods **174**(1): 1-9.

Bozkurt, A., R. Deumens, J. Scheffel, D. M. O'Dey, J. Weis, E. A. Joosten, T. Fuhrmann, G. A. Brook and N. Pallua (2008). "CatWalk gait analysis in assessment of functional recovery after sciatic nerve injury." Journal Of Neuroscience Methods **173**(1): 91-8.

Condron, B. G. and K. Zinn (1994). "The grasshopper median neuroblast is a multipotent progenitor cell that generates glia and neurons in distinct temporal phases." J. Neurosci. **14**(10): 5766-5777.

Cullen, D. K., M. C. Lessing and M. C. LaPlaca (2007). "Collagen-dependent neurite outgrowth and response to dynamic deformation in three-dimensional neuronal cultures." Annals Of Biomedical Engineering **35**(5): 835-46.

Curry, D. J., D. A. Wright, R. C. Lee, U. J. Kang and D. M. Frim (2004a). "Poloxamer 188 volumetrically decreases neuronal loss in the rat in a time-dependent manner." Neurosurgery **55**(4): 943-8; discussion 948-9.

Curry, D. J., D. A. Wright, R. C. Lee, U. J. Kang and D. M. Frim (2004b). "Surfactant poloxamer 188-related decreases in inflammation and tissue damage after experimental brain injury in rats." Journal Of Neurosurgery **101**(1 Suppl): 91-6.

Deumens, R., R. J. Jaken, M. A. Marcus and E. A. Joosten (2007). "The CatWalk gait analysis in assessment of both dynamic and static gait changes after adult rat sciatic nerve resection." Journal Of Neuroscience Methods **164**(1): 120-30.

Fawcett, J. W., R. A. Barker and S. B. Dunnett (1995). "Dopaminergic neuronal survival and the effects of bFGF in explant, three dimensional and monolayer cultures of embryonic rat ventral mesencephalon." Exp Brain Res **106**(2): 275-282.

Gabriel, A. F., M. A. Marcus, W. M. Honig, G. H. Walenkamp and E. A. Joosten (2007). "The CatWalk method: a detailed analysis of behavioral changes after acute inflammatory pain in the rat." Journal Of Neuroscience Methods **163**(1): 9-16.

Gensel, J. C., C. A. Tovar, F. P. Hamers, R. J. Deibert, M. S. Beattie and J. C. Bresnahan (2006). "Behavioral and histological characterization of unilateral cervical spinal cord contusion injury in rats." Journal Of Neurotrauma **23**(1): 36-54.

Granet, C., N. Laroche, L. Vico, C. Alexandre and M. H. Lafage-Proust (1998). "Rotating-wall vessels, promising bioreactors for osteoblastic cell culture: comparison with other 3D conditions." Med Biol Eng Comput **36**(4): 513-519.

Hamers, F. P. T., G. C. Koopmans and E. A. J. Joosten (2006). "CatWalk-Assisted Gait Analysis in the Assessment of Spinal Cord Injury." Journal Of Neurotrauma **23**(3-4): 537-548.

Heinzmann, U. (1980). "FITC-dextrans as fluorescence and electron microscopic tracers in studies on capillary and cell permeability of the CNS." Cellular and Molecular Life Sciences (CMLS) **36**(7): 885-887.

Hoffman, R. M. (1993). "To do tissue culture in two or three dimensions? That is the question." Stem Cells **11**(2): 105-11.

Kilinc, D., G. Gallo and K. A. Barbee (2008). "Mechanically-induced membrane poration causes axonal beading and localized cytoskeletal damage." Experimental Neurology **212**(2): 422-30.

Koob, A. O. and R. B. Borgens (2006). "Polyethylene Glycol Treatment After Traumatic Brain Injury Reduces b-Amyloid Precursor Protein Accumulation in Degenerating Axons." Journal Of Neuroscience Research **83**(8): 1558.

Koob, A. O., J. M. Colby and R. B. Borgens (2008). "Behavioral recovery from traumatic brain injury after membrane reconstruction using polyethylene glycol." Journal Of Biological Engineering **2**(1): 9.

Koob, A. O., B. S. Duerstock, C. F. Babbs, Y. Sun and R. B. Borgens (2005). "Intravenous Polyethylene Glycol Inhibits the Loss of Cerebral Cells after Brain Injury." Journal Of Neurotrauma **22**(10).

Koopmans, G. C., R. Deumens, W. M. M. Honig, F. P. T. Hamers, H. W. M. Steinbusch and E. A. J. Joosten (2005). "The Assessment of Locomotor Function in Spinal Cord Injured Rats: The Importance of Objective Analysis of Coordination." Journal Of Neurotrauma **22**(2): 214-225.

Laverty, P. H., A. Leskovar, G. J. Breur, J. R. Coates, R. L. Bergman, W. R. Widmer, J. P. Toombs, S. Shapiro and R. B. Borgens (2004). "A preliminary study of intravenous surfactants in paraplegic dogs: polymer therapy in canine clinical SCI." J Neurotrauma **21**(12): 1767-77.

Luo, J., R. Borgens and R. Shi (2002). "Polyethylene glycol immediately repairs neuronal membranes and inhibits free radical production after acute spinal cord injury." J Neurochem **83**(2): 471-80.

Marks, J. D., C.-y. Pan, T. Bushell, W. Cromie and R. C. Lee (2001). "Amphiphilic, tri-block copolymers provide potent, membrane-targeted neuroprotection." FASEB J.: 00-0547fje.

Masi, L., A. Franchi, M. Santucci, D. Danielli, L. Arganini, V. Giannone, L. Formigli, S. Benvenuti, A. Tanini, F. Beghe and et al. (1992). "Adhesion, growth, and matrix production by osteoblasts on collagen substrata." Calcif Tissue Int **51**(3): 202-12.

Serbest, G., J. Horwitz and K. Barbee (2005). "The effect of poloxamer-188 on neuronal cell recovery from mechanical injury." J Neurotrauma **22**(1): 119-32.

Serbest, G., J. Horwitz, M. Jost and K. Barbee (2006). "Mechanisms of cell death and neuroprotection by poloxamer 188 after mechanical trauma." The FASEB Journal **20**(2): 308-310.

Shi, R. and R. B. Borgens (1999). "Acute repair of crushed guinea pig spinal cord by polyethylene glycol." Journal Of Neurophysiology **81**(5): 2406-14.

Shi, R. and R. B. Borgens (2000). "Anatomical repair of nerve membranes in crushed mammalian spinal cord with polyethylene glycol." Journal Of Neurocytology **29**(9): 633-43.

Singleton, R. H. and J. T. Povlishock (2004). "Identification and characterization of heterogeneous neuronal injury and death in regions of diffuse brain injury: evidence for multiple independent injury phenotypes." The Journal Of Neuroscience: The Official Journal Of The Society For Neuroscience **24**(14): 3543-53.

Vlamings, R., V. Visser-Vandewalle, G. Koopmans, E. A. Joosten, R. Kozan, S. Kaplan, H. W. Steinbusch and Y. Temel (2007). "High frequency stimulation of the subthalamic nucleus improves speed of locomotion but impairs forelimb movement in Parkinsonian rats." Neuroscience **148**(3): 815-23.

Whalen, M., T. Dalkara, Z. You, J. Qiu, D. Bermpohl, N. Mehta, B. Suter, P. Bhide, E. Lo, M. Ericsson and M. Moskowitz (2007). "Acute plasmalemma permeability and protracted clearance of injured cells after controlled cortical impact in mice." J Cereb Blood Flow Metab **28**(3): 490-505.